FOR FURTHER TRAN

AD A055077

GENERAL ⊛ ELECTRIC

HEAVY MILITARY EQUIPMENT DEPARTMENT

TECHNICAL INFORMATION SERIES

Author	Subject Category	R78EMH5
R. Mann	Solid Mechanics	Date May 1978

Title

IMPACT OF ROCK DEBRIS ON A SIMPLY SUPPORTED BEAM
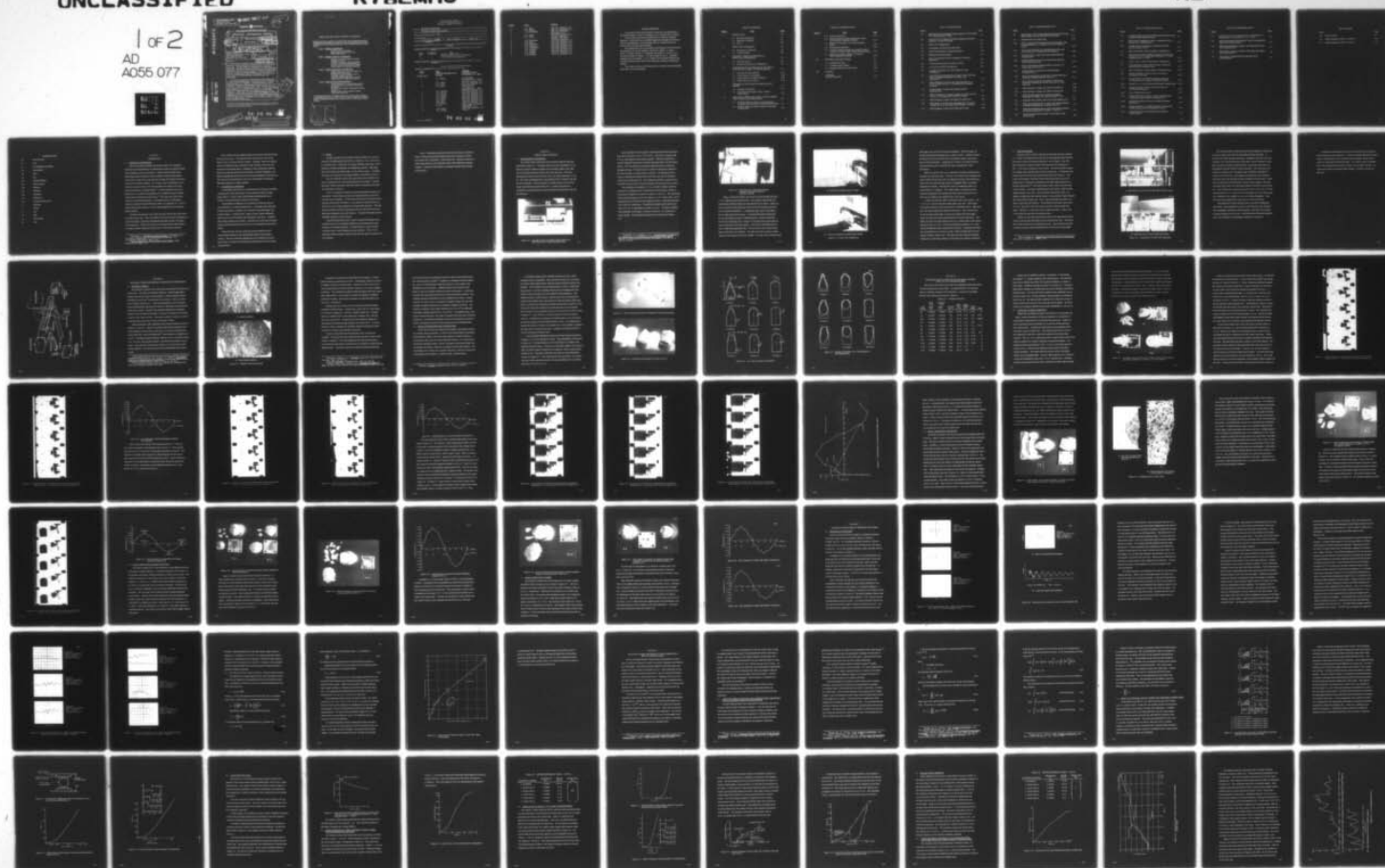
Copies Available at HMED TIS Distribution Center Box 4840 (CSP 4-18) Syracuse, New York 13221	GE Class	1	No. of Pages
	Govt Class	Unclassified	120

Summary

Sedimentary and igneous rock projectiles were fired at the center of a simply supported aluminum beam in a series of impact tests. An experimental investigation was conducted to determine: dynamic response of the beam, localized permanent deformation of the beam in the region of impact, and fracturing behavior of weak and strong sandstone. The experimental results are complemented with the development of analytical impact models for both fracturing and nonfracturing rock projectiles.

An impact apparatus was developed for firing regular and irregular shaped projectiles. The projectiles were partially encapsulated in a 1-in. diameter, cylindrical plaster of Paris housings. Response of strain gages attached to the 0.25 x 1.00 x 18.00 in., 6061T6 aluminum beam, were recorded on a storage oscilloscope and oscillograph recorder. 16-mm high speed films of the impact process, were taken at just under 6000 frames/s. These films provided valuable projectile and beam displacement data both during and after impact. They also provided the means of determining the time duration of impact in the case of single impact, in addition to time between impacts in the case of multiple impact.

78 06 06 020

408 969

Send to _____

GENERAL ELECTRIC COMPANY TECHNICAL INFORMATION

Within the limitations imposed by Government data export regulations and security classifications, the availability of General Electric Company technical information is regulated by the following classifications in order to safeguard proprietary information:

CLASS 1: **GENERAL INFORMATION**

Available to anyone on request.
Patent, legal and commercial review required before issue.

CLASS 2: **GENERAL COMPANY INFORMATION**

Available to any General Electric Company employee on request.
Available to any General Electric Subsidiary or Licensee subject to existing agreements.
Disclosure outside General Electric Company requires approval of originating component.

CLASS 3: **LIMITED AVAILABILITY INFORMATION**

Original Distribution to those individuals with specific need for information.
Subsequent Company availability requires originating component approval.
Disclosure outside General Electric Company requires approval of originating component.

CLASS 4: **HIGHLY RESTRICTED DISTRIBUTION**

Original distribution to those individuals personally responsible for the Company's interests in the subject.
Copies serially numbered, assigned and recorded by name.
Material content, and knowledge of existence, restricted to copy holder.

GOVERNMENT SECURITY CLASSIFICATIONS, when required, take precedence in the handling of the material. Wherever not specifically disallowed, the General Electric classifications should also be included in order to obtain proper handling routines.

HMED 4023B (5-65)

SECTION _Mechanical Engineering_

UNIT _Mechanical Engineering Facilities_

HMED ACCOUNTING REFERENCE _430_

COLLABORATORS _____

APPROVED _C E Hundstad_ TITLE _Mgr., Mech Eng_ LOCATION _CSP 5 - F7_
C. Hundstad

R78EMH5

MINIMUM DISTRIBUTION - <u>Government Unclassified</u> Material (and Title Pages) in G.E. Classes 1, 2, or 3 will be the following.

Copies	Title Page Only	To
0	1	Legal Section, HMED (Syracuse)
0	1	Manager, Technological Planning, HMED (Syracuse)
5	0	G-E Technical Data Center (Schenectady)

MINIMUM DISTRIBUTION - <u>Government Classified</u> Material, Secret or Confidential in G.E. Classes 1, 2, or 3 will be the following.

1	0	Manager, Technological Planning, HMED (Syracuse)

ADDITIONAL DISTRIBUTION (Keep at minimum within intent of assigned G.E. Class.)

COPIES	NAME	LOCATION
5 (CLASS 1 ONLY)	DEFENSE DOCUMENTATION CENTER	CAMERON STATION, ALEXANDRIA, VA. 22314
1	L. I. Chasen	P. O. Box 8555 Philadelphia, Pa., 19101
1	W. E. Abriel	CSP 5-F7, Syracuse, N. Y.
1	R. F. Clark	EP 3-135, Syracuse, N. Y.
1	H. A. Eagle	RESD, Rm 5722 P. O. Box 7722 Philadelphia, Pa., 19101
1	R. E. Edmonds	CSP 5-C3, Syracuse, N. Y.
1	L. J. Fiorito	CSP 5-E4, Syracuse, N. Y.
1	F. F. Ferrara	CSP 5-J2, Syracuse, N. Y.
1	J. R. Golden	CSP 5-F7, Syracuse, N. Y.
1	W. L. Jaynes	EP 3-25A, Syracuse, N. Y.
1	L. J. Hayes	CSP 5-F7, Syracuse, N. Y.
1	D. H. Kuhn	CSP 4-57, Syracuse, N. Y.
1	M. D. Hluchyj	CSP 5-F7, Syracuse, N. Y.
1	S. Levy	CR&D, Bldg. 37, Rm 319 Schenectady, N. Y.
1	P. M. Lucas	FRP 1-E6, Syracuse, N. Y.
1	H. J. Lyness	CSP 5-J2

HMED 4024 REV 3/21/78

Copies	Name	Location
2	R. L. Mann	CSP 5-F7, Syracuse, N.Y.
1	N. J. Manzari	CSP 5-F7, Syracuse, N.Y.
1	J. E. McConnelee	M&P Lab, Building 55 Schenectady, N.Y.
1	D. P. Miller	CSP 5-E4, Syracuse, N.Y.
1	E. L. North	MD K69, Building 500 Evendale, Ohio 45215
1	A. E. Rusmussen	CSP 5-E4, Syracuse, N.Y.
1	J. D. Reale	CSP 5-E2, Syracuse, N.Y.
1	E. R. Ruterman	CSP 5-C3, Syracuse, N.Y.
1	T. W. Starowicz	CSP 5-E4, Syracuse, N.Y.
1	G. F. Trojanowski	EP 3-25A, Syracuse, N.Y.
1	C. E. Titemore	CSP 5-E4, Syracuse, N.Y.
1	F. T. Wenthen	EP 3-135, Syracuse, N.Y.
1	C. R. Womble	CSP 5-F7, Syracuse, N.Y.
1	E. A. Stebbins	CSP 5-F7, Syracuse, N.Y.

ACKNOWLEDGMENTS

TABLE OF CONTENTS

TABLE OF CONTENTS (CONT.)

LIST OF ILLUSTRATIONS

LIST OF ILLUSTRATIONS (CONT.)

LIST OF ILLUSTRATIONS (CONT.)

LIST OF ILLUSTRATIONS (CONT.)

LIST OF TABLES

NOMENCLATURE

dc	Direct Current
ft	Foot
G	Cold Springs Green Gabbro
GL	Glass Sphere
Hz	Hertz
in.	Inch
I. S.	Indiana Sandstone
KE	Kinetic Energy
kHz	Kilohertz
kg	Kilogram
mm	Millimeter
ms	Millisecond
psi	Pounds per Square Inch
S	Sandstone
s	Second
V	Volt
W	Watt
μs	Microsecond
Ω	Ohm

SECTION I

INTRODUCTION

1.1 HISTORICAL BACKGROUND

Many of the radars associated with missile defense are "hardened".
Hardened in the sense that they can withstand the nuclear environment created
by the explosion of a given size weapon. Nuclear explosions differ from
high energy explosive weapons in that in addition to energy being released
in the form of a blast wave, large amounts of energy are released in the form
of thermal and nuclear radiation. For a nuclear weapon classified as a sur-
face burst, large amounts of soil and rock debris are carried up from the
earth's surface into a radioactive cloud.[1] A crater produced in dry soil at
ground zero, as a result of the explosion of a 20 megaton weapon, is approxi-
mately 3000 ft in diameter and 300 ft deep.[2] The crater size will be some-
what less in sandstone and granite. The quantity and size of rock debris
which can rain down from the radioactive cloud, on a hardened radar structure
in the vicinity of the explosion, can be of major significance in the design of
these structures.

During the past decade a new member has been added to the radar family,
the phased array radar. This radar differs from the conventional rotating para-
bolic dish antenna, in that it is electronically steerable and does not require
any moving parts. Phased array radars are characterized by large numbers
of antenna elements mounted to the front face of a flat support structure.

---

[1]Glasstone, S., *The Effects of Nuclear Weapons*, (Washington, D.C.,
U.S. Dept. of Defense and U.S. Atomic Energy Commission, U.S.
Government Printing Office, 1964), p. 33.
[2]*Design of Structures to Resist Nuclear Weapon Effects*, (ASCE
Manual No. 42, 1964), p. 11.

Only a limited amount of debris impact work has been performed during the past several years. The majority of the work has been in the area of failure of antenna element ceramic windows. Presently, there is an interest not only in individual antenna elements, but the response of the array face structure to rock debris impact. Satisfactory radar performance requires that one be concerned with array face vibration, localized indentation, rock debris embedding itself in the array face and total penetration of the structure. The concern of total penetration is due to the vulnerability of the internal electronic equipment to nuclear radiation.

1.2   STATEMENT OF PROBLEM

A rock debris impact study was undertaken for the purpose of providing a starting point and the initial steps of basic research needed to develop design criteria. Criteria which would facilitate predicting the level of damage of structural elements subject to rock impact.

Experimental investigations were performed to study the impact of rock projectiles on a simply supported beam. Projectiles used in the study included sedimentary and igneous rock materials having both regular and irregular shapes. Projectiles had a range of impact velocity sufficiently high to cause severe fracturing to the sedimentary rock group. Projectile initial kinetic energies were limited, so that the beam would only experience localized permanent deformation in the form of an indentation at the point of impact.

High speed film and beam strain gage data provided the crucial measurements necessary to the understanding of this complex impact problem. This data contributed significantly to the development of analytical models, for impact of fracturing and nonfracturing rock with a simply supported beam.

1-2

1.3 SCOPE

An impact apparatus was developed capable of firing 1-in. rock projectiles at velocities greater than 2000 in./s against a 0.25 x 1.00 x 18.00-in. aluminum beam. Strain data, from gages installed on the beam, was recorded on a storage oscilloscope and oscillograph recorder. High speed films of the impact were taken using a 16-mm Fastax camera. A complete discussion of the apparatus and testing methods is presented in Section II.

The rock materials used for the experimental work consisted of two types of sandstone and a coarsed grained igneous rock (gabbro). Physical properties of these materials, along with methods of specimen preparation, are presented in Section III.

Section IV presents a discussion of the phenomenological behavior of rock impact. Several frames of the 16-mm high speed film are given for each type of rock material. The film data was also used to plot the dynamic response of the center of the beam. It was possible to obtain 82 frames of data for one cycle of beam vibration at its fundamental frequency. With this many data points, good beam displacement data was achieved for third and fifth mode contribution to the total vibration. Projectile fracturing and beam indentation behavior is also discussed.

Recorded strain data for beam response during and following impact, revealed that each rock projectile exhibited its own characteristic strain response or mechanical signature. Projectile shape in a given material was found to have a minor influence on beam vibration. Section V discusses the relative energies absorbed by the beam for impact of each type of rock material.

Section VI describes procedures which were developed to predict impulse, localized permanent deformation and dynamic response of a beam upon impact with a fracturing or nonfracturing rock. Dynamic response of a simply supported beam was determined using a finite difference computer program. Analytical model results are compared with the experimentally measured data.

SECTION II

IMPACT TEST APPARATUS

2.1 DESCRIPTION OF APPARATUS

Rock debris impact experiments were conducted using the apparatus illustrated in Figure 2-1. This figure shows an air gun consisting of a 3-in. diameter pressure chamber supplied with air through a fitting at the right and an electrically operated solenoid valve at the other end. This valve separates the pressure vessel from the 25-in. gun barrel which has a 1.0-in. ID. The switch controlling power to the solenoid valve is mounted at the left end of the apparatus. Rock projectiles are loaded in the muzzle end of the barrel and pushed back approximately 24 in. Loading of the barrel is facilitated by pivoting the entire air gun assembly about fixed pins at the left end of the gun.

B6040
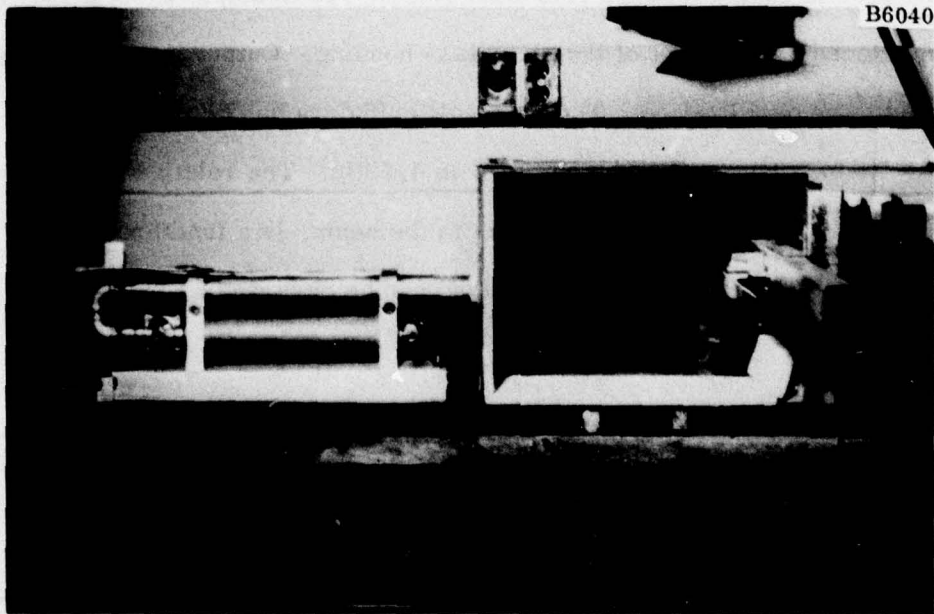
Figure 2-1. Apparatus Used to Investigate Impact Behavior of Rock Debris with a Simply Supported Beam

2-1

Rock projectiles are fired against a simply supported 6061T6 aluminum beam which measures 0.125 x 1.00 x 18.00 in. The beam is supported with 0.015 in. thick stainless steel column supports. This type of support was used by Goldsmith[3] because the connection approaches that of an ideal simple support. The horizontal beam projects through both sides of a protective plexiglass housing. The housing serves a number of functions in addition to the most important one being operator protection. The housing provides a means of capturing all material which may break away from the projectile should severe fracturing occur. The housing also provides a support for two photocells which are used to measure projectile velocity just prior to impact.

The photocells are mounted in 0.50-in. diameter cylinders which are supported by a plexiglass plate mounted directly to the housing. Details of the photocell arrangement are shown in Figures 2-2 and 2-3a. The Hamamatsu silicon photocells having a 14-μs rise time give a 0.10-V output using a 100-W floodlamp placed 3 ft in front of the plexiglass housing. Output from the photocells is fed to an oscilloscope. The photocell cylinders can be placed in as close as 0.75 in. or separated by as much as 4.50 in. The relative position of the photocells to each other, as well as to the beam, is a function projectile velocity. The five photocell positions can be observed in Figure 2-3a.

---

[3]Goldsmith, W., Cunningham, D. M., An Experimental Investigation of The Oblique Impact of Steel Spheres on Simply Supported Steel Beams, "Society of Experimental Stress Analysis Proceedings," Vol. XIV, No. 1, 1955, pp. 171-179.
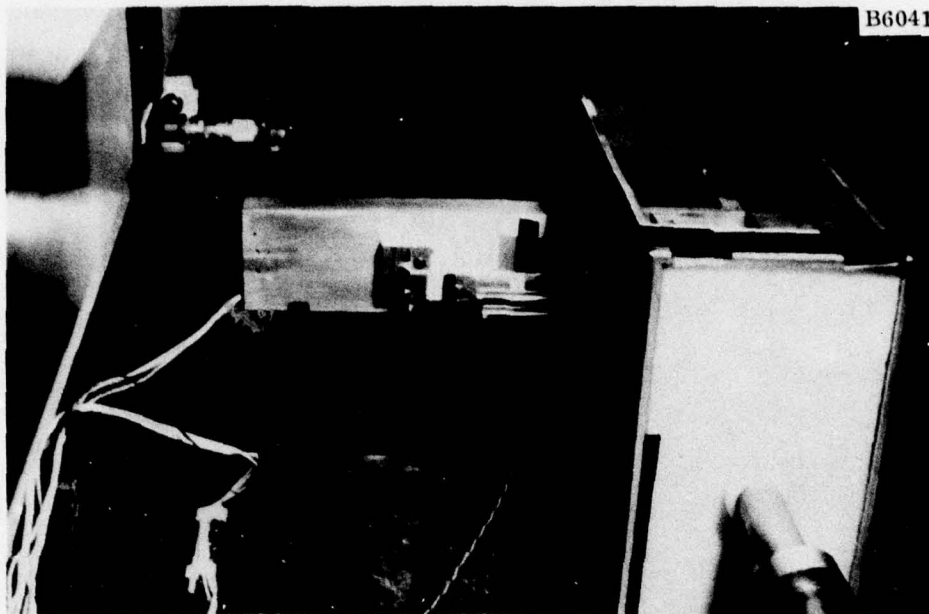
Figure 2-2. Front End View of Apparatus Showing
Adjustable Photocells Mounted to
Protective Housing

Figure 2-1 shows the bottom and air gun end of the housing lined with

0.50-in. thick light polystyrene plastic. This material protects the rock

projectile from further damage upon rebound from beam impact. Figure 2-2

shows an end view of the apparatus where the muzzle of the gun can be ob-

served to enter the enclosure. A polyethylene ring, shown in this figure,

fits over the muzzle end of the gun. It provides the interface between the

gun and the housing serving as a centering device, and also protects the

barrel from rebounding rocks. Figure 2-2 also shows the air hose which is

used to pressurize the air gun cylinder. Also shown in this figure are two

sets of white strain gage lead wires. One set of three wires connect strain

gages on the beam to an amplifier. The other set of wires connect a match-

ing set of dummy gages to the same amplifier. Type ED, Micro-Measurements

B6042
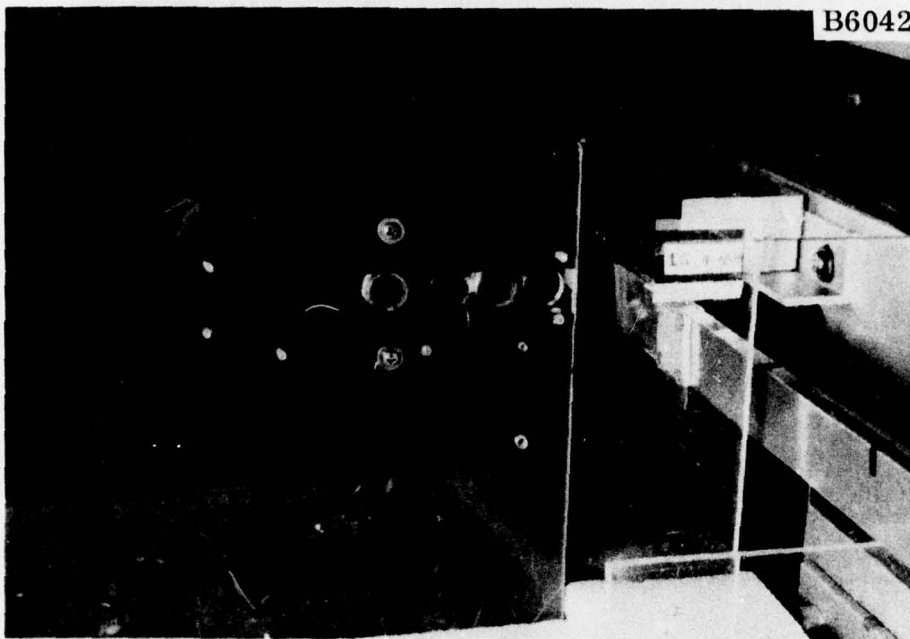
(a) Impact Area During General Testing

B6043
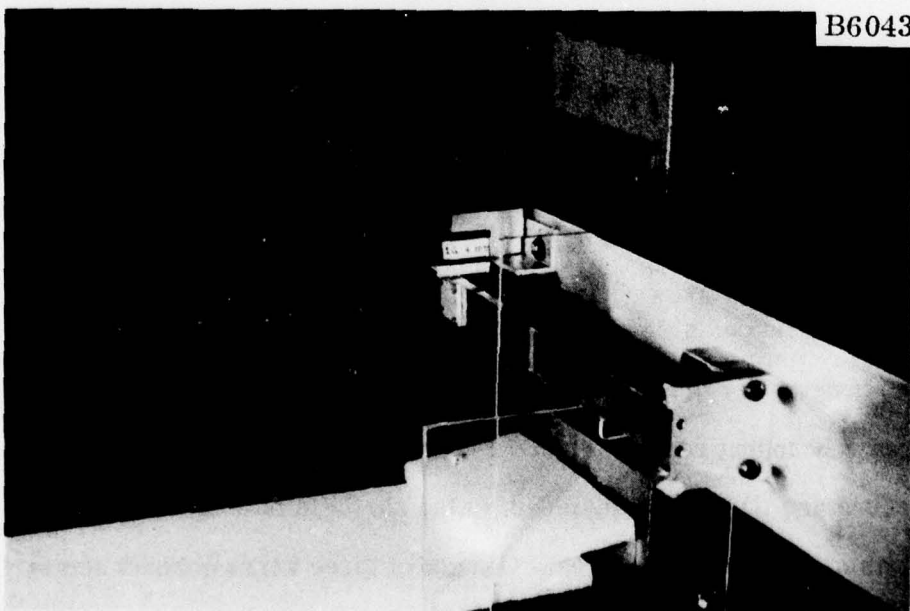
(b) Typical Arrangement for High Speed Filming

Figure 2-3. Impact Test Configuration

strain gages were used for the impact investigation. The 350 Ω gages can operate at temperatures ranging from cryogenic to 500°F. Optimum linearity is achieved at strain levels below 3000 microstrain; however, gage strain limit is 10000 microstrain. Fatigue life is in excess of 10 million cycles at ±2000 microstrain with an indefinite life when operating below ±1800 microstrain.

Figure 2-3a shows cross wires connected to terminals positioned above and below one of the photocells. The lower wire located in the projectile path makes contact with the upper wire and triggers the sweep of the oscilloscope. These wires are extremely light and have a negligible effect on projectile trajectory and velocity. Note that this cross wire triggering switch is in series with two 9 V batteries. This voltage offset is required to prevent premature triggering of the oscilloscope sweep which occasionally occurs when power is applied to the solenoid valve on the air gun.

In order to protect the center of the beam in the contact region, 0.125 x 1.0 x 1.0 in. 6061T6 aluminum contact plates were used. These plates are securely fastened to the beam with four 6-32 flathead screws. After each test, one simply replaces the indented contact plate. This avoids the need for the complete replacement of a beam instrumented with strain gages. Figure 2-3 shows the contact plate fastened to the center of the beam. This figure also shows a bracket attached to the 5-in. channel which is the primary support for the 1-in. beam. The bracket facilitates mounting a 1-in. scale, and test identification data during high speed filming. During high speed filming, the photocells are covered to provide a uniform background for the projectile as shown in Figure 2-3b. This figure also shows that the plexiglass housing has a cutout large enough to accommodate free vibration of the beam.

2.2 TESTING METHODS

Equipment used to acquire projectile and beam data is shown in Figure 2-4. Figure 2-4a illustrates the setup used for obtaining high speed film data. The camera used for the impact studies was a 16-mm Fastax, Type WF3. This camera has a maximum speed of 8000 frames/s upon application of 280 V. The camera contains two drive motors. One drives the film sprocket and rotating prism while the other drives the takeup reel. A Wollensak Goose Control Unit was used for films speeds greater than 4000 frames/s. This control unit contains a time delay circuit which permits the camera to accelerate at low voltage before application of the high voltage required to attain the desired speed.[4] The timing circuits of this control unit were particularly valuable. One timer controlled power to the camera, while the other regulated power to the event. The event being, firing of the air gun. By setting a suitable time delay between timers, it was possible to achieve desired film speed before firing the gun. The majority of the high speed films were taken at just under 6000 frames/s. By having the event lag the camera start by 0.50 s, half of the 100-ft reel of film was used to attain constant film speed. This left 0.3 s and 50 ft of film to capture the event. Kodak, Type 4-X reversal film was used in acquiring all data.

Figure 2-4a also shows the location of the 1000-W high intensity lamps used to provide proper illumination of the enclosed impact area. Both lamps were turned on just prior to starting the camera. This precaution was taken in order to minimize the lamp heating effect on the beam and strain gages.

---

[4]Hyzer, William G., Engineering and Scientific High Speed Photography, (New York: MacMillan Co., 1962), p. 97.

B6044
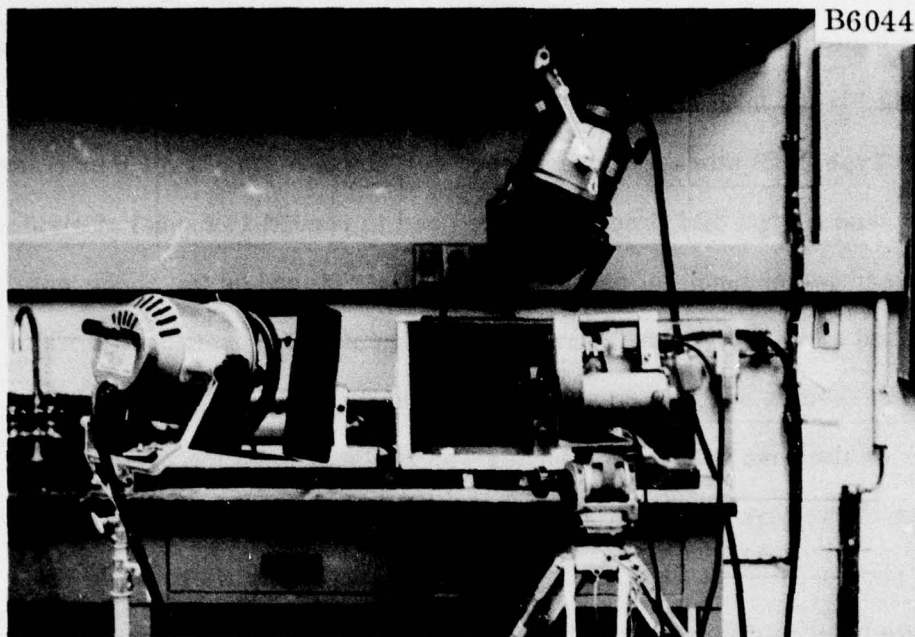
(a) High Speed Camera and Associated High Intensity Lamps

B6045

(b) Equipment Used to Record Strain Gage Output

Figure 2-4. Photographic and Strain Recording Setup

The equipment used to measure and record strain gage and velocity data is shown in Figure 2-4b to the left of the high speed film equipment. A Tektronix Type 564B storage oscilloscope, containing a Type 3A74 four trace amplifier, and a Type 3B4 time base were used to record 1 channel of strain gage data and two channels of photocell data. Data stored on the scope was photographed using the Polaroid camera attachment. The oscilloscope was triggered by feeding an 18-V dc signal to the "EXTERNAL TRIGGER IN" connector on the base unit. This trigger was initiated when the projectile caused the cross wire within the test area enclosure to make contact. Leads from the photocells were fed directly to the four trace amplifier, while the strain gage input to this unit was through Tektronix Type 3C66 Carrier amplifier. This amplifier has a frequency response of dc to 5 kHz, and a rise time of approximately 70 μs. An active 350 Ω strain gage and a 350 Ω dummy gage were connected to the amplifier in a four-arm bridge arrangement. Most strain data was recorded with a sweep rate of 1.0 ms per division.

Strain gage data was also recorded using a Visicorder oscillograph, Model 906B. This equipment was used to record long-time beam response. The oscillograph was fed with a Telex amplifier, model SGA-150, having a frequency response of dc to 10 kHz. The Heiland Type M8000 galvanometers, used in the Visicorder, had a frequency response of 0 to 4800 Hz.

A schematic representation of the impact test apparatus and associated instrumentation is given in Figure 2-5. During a test when high speed film data is taken, the photocells are not required because projectile velocity can accurately be determined from the film speed. The Fastax camera is equipped with a time marking device that puts 120 blips/s on one edge of the film. For impact tests which are conducted without filming, one simply uncovers the photocells.
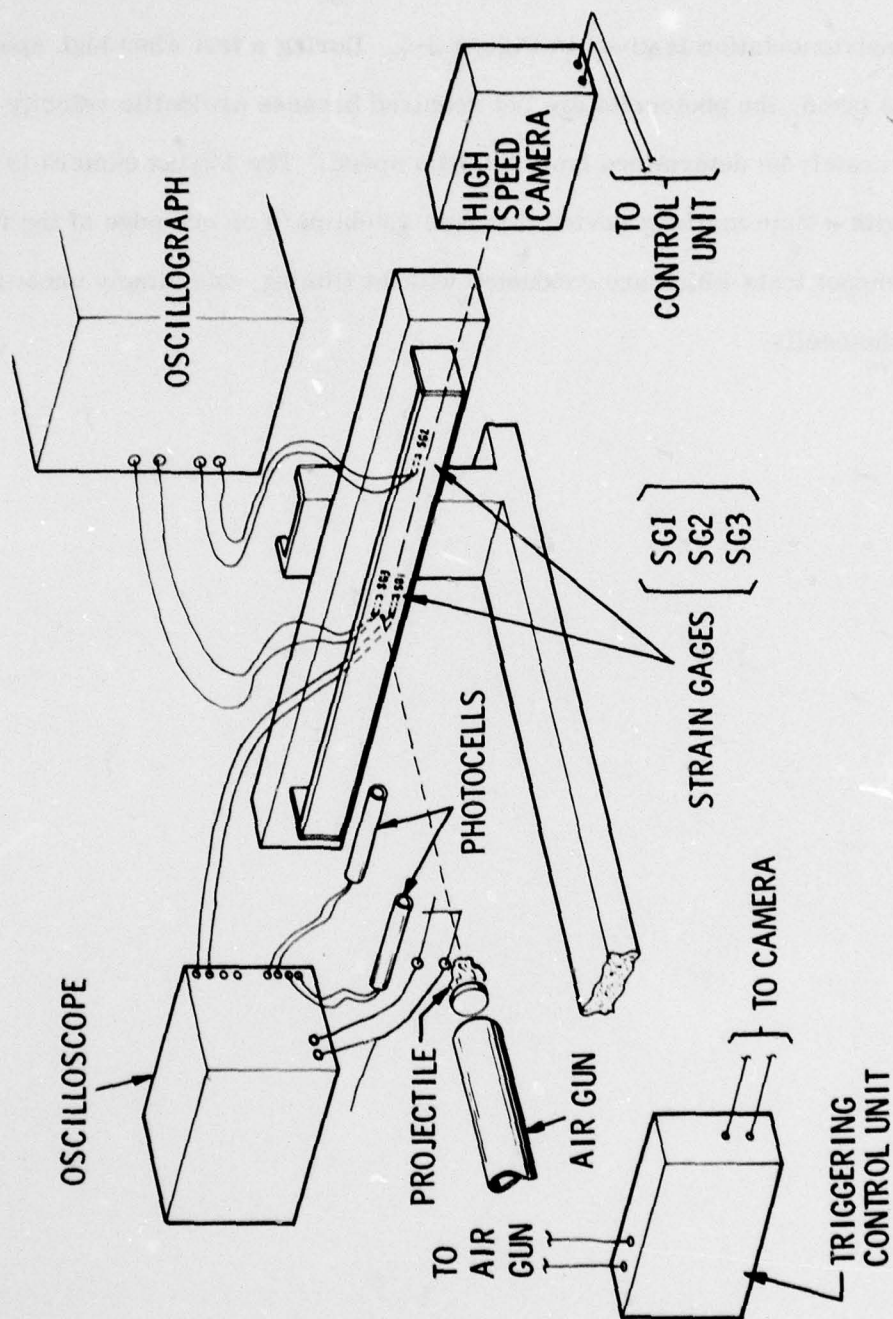
Figure 2-5. Impact Test Apparatus and Instrumentation

SECTION III

MATERIALS TESTED AND METHOD OF PROJECTILE PREPARATION

3.1 MATERIALS TESTED

The materials selected for the impact study included both sedimentary and igneous rock. Two types of fine grained sandstone, a high strength gabbro, and glass spheres were used for the projectiles. Indiana sandstone which is classified as a weak rock[5] was selected for two reasons. First, it is desirable to include rocks in the study which would experience severe fracturing without inducing plastic deformation of the beam, other than local deformation at the point of contact. Secondly, this sandstone exhibited good machining qualities which facilitated the grinding of a number of samples into a grouping having the same shape and mass. This made it possible to conduct a series of controlled impact tests where velocity was the only variable.

Photomacrographs of the sandstones used in the experiments are shown in Figures 3-1a and 3-1b. Figure 3-1a shows that the Indiana sandstone which can be classified as fine grained, quite porous, and not well cemented sandstone bonded with a silica cementing agent.[6] This sandstone is reddish-brown in color. The higher strength sandstone, light tan in color, is shown in Figure 3-1b. It is also a fine grained substance, composed almost entirely of pure quartz. This material is fairly porous; however, it is not as porous as the Indiana sandstone. The quartz grains are also bonded together with a silica cement.

---

[5] Weak being defined as that class of rock having an uniaxial compressive strength less than 10,000 psi. D.F. Coates, R.C. Parsons, *Experimental Criteria for Classification of Rock Substances*, (International Journal of Rock Mechanics and Mining Sciences, Volume 3, 1966), pp. 181-189.

[6] The sandstone and gabbro rocks were analyzed and classified by the Department of Geology, Syracuse University.
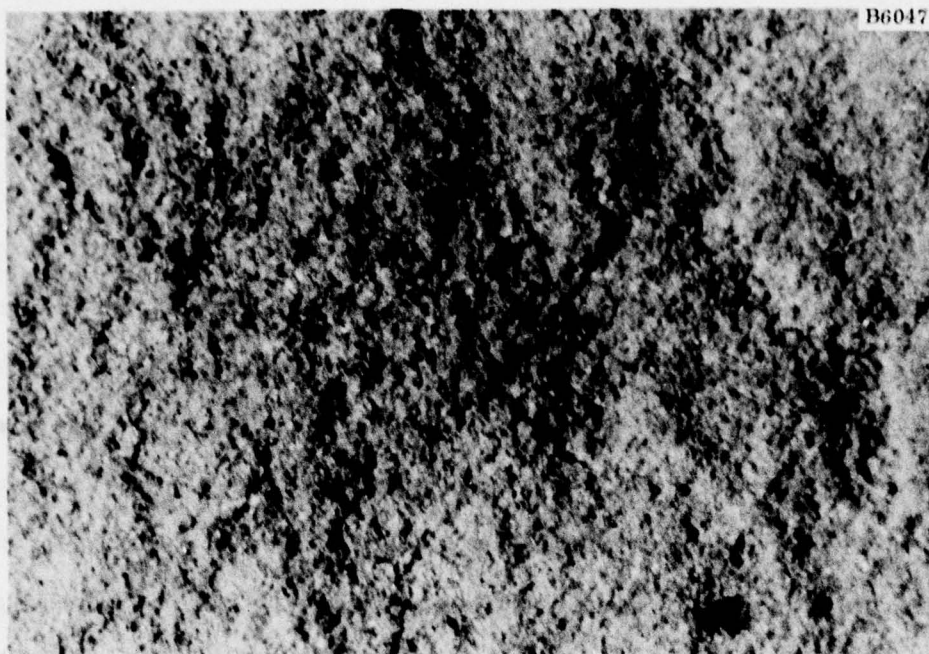
(a) Indiana Sandstone
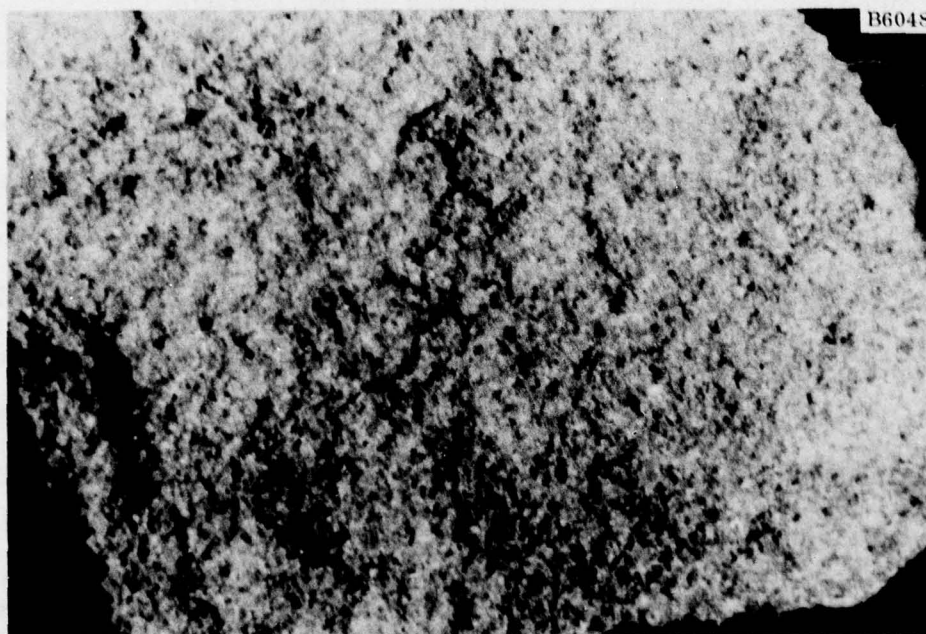
(b) High Strength Sandstone

Figure 3-1. Sandstone Photomacrographs

The igneous rock used in the experimental work is gabbro, a coarse-grained material, greenish black in color. This gabbroic material is primarily feldspar and does not contain quartz. Granite on the other hand is also a coarse grained igneous rock that contains a minimum of 5% quartz in addition to feldspar.[7] The orientation of minerals within the gabbro used in the impact study might result in a 10% variation in modulus of elasticity for different directions of loading. Microscopic examination revealed that gabbroic material had a "weak fabric."

Hardness tests were made on all rock materials using the Rockwell Superficial Hardness Tester. All tests were made on the 15-T scale where a 15 kg load was applied to a 0.0625-in. tungsten carbide ball. The light areas on a polished surface of the gabbro had a hardness of 96, while the dark areas measured 92. The glass sphere had a hardness rating of 99. The hardness of the high strength sandstone was found to be 77. It was not possible to obtain a hardness for the Indiana sandstone because the surface would tend to crumble upon application of the load.

Uniaxial compression tests are frequently used to evaluate rock strength.[8] The standard test uses regular shaped specimens, such as cubes, prisms or cylinders.[9] One of the difficulties with compression testing of rock materials is that friction constrains the rock surfaces in contact with the testing machine. Attempts to reduce the constraint include lubricating the

---

[7]Hurlburt, Cornelius S., Jr., Mineralogy, (New York: John Wiley and Sons, Inc., 1966), pp. 515-518.

[8]Liebowitz, Fracture, (Academic Press, 1972), pp. 104-105.

[9]Protad'yakonov, M.M., Koifman, M.I., Mechanical Properties of Rock, Jerusalem, Israel Program for Scientific Translations, 1968), pp. 76-80.

ends of the specimen or inserting thin layers of a teflon material between the rock specimen and the machine.[8] In addition to reducing the frictional effects, thin layers of a lubricating type material provide for a more uniform load distribution over the specimen. Sandstone samples were prepared in the shape of a cube in accordance with the procedure of reference 9. A thin layer of waxed paper was placed between the rock specimens and the machine. The sandstone specimens experienced an axial splitting mode of failure. Indiana sandstone was found to have a compressive strength of almost 4000 psi while the higher strength sandstone had a compressive strength of 11400 psi. The modulus of elasticity for the Indiana sandstone was 0.58×10^6 psi while that of the higher strength material was 1.03×10^6 psi. Load deflection data, from uniaxial compression tests, were used to calculate the normal stress and strain components. The modulus of elasticity for each of the specimens was then obtained by dividing the maximum normal stress by the corresponding strain.

3.2   SAMPLE PREPARATION AND CLASSIFICATION

Several factors had to be considered in devising an encapsulation scheme for irregular shaped projectiles. In order to have each projectile consistently impact the beam within 0.250 of the center position at a desired velocity, it was necessary that it have an almost perfect fit with the 1.0 in. ID gun barrel. The normal polyethylene sabot, used for a housing on symmetrical bodies such as cylinders and spheres, could not conveniently be used in this instance. The only feasible way to control rock projectile trajectory, motion and velocity was to encapsulate the projectile in a material having a cylindrical base.

---

[8]Liebowitz, Fracture, (Academic Press, 1972), pp. 104-105.

To facilitate potting several projectile specimens at once, a three component mold was fabricated. The mold shown in Figure 3-2 was formed by pouring a heat curable silicone material around accurately machine brass cylinders. These cylinders had an outside diameter 0.002 in. smaller than the gun barrel. A number of potting materials were investigated and tried. Plaster of Paris was found to be most suitable for this application. This potting material is easily prepared, adheres quite well to rock specimens, conforms well with the mold, and provides for minimum friction with the gun barrel. Specimens are prepared by pouring small amounts of plaster of Paris in each cell of the mold, followed by careful placement of each projectile. After 30 minutes, the encapsulated rocks are removed from the mold as shown in Figure 3-3. After 24 hours, any excess plaster of Paris can easily be removed. Following some preliminary projectile firings, it was determined the minimum plaster of Paris length should be 0.300 in. By minimizing the height of the plaster of Paris for each potted rock, it was possible to maximize the rock mass to composite mass ratio. In general, the plaster of Paris is only 20% of the total projectile mass.

A rock projectile classification has been developed which characterizes irregular 1.0 in. rock with regard to shape. This classification is illustrated in Figure 3-4. The ideal boundary shown in this figure is an outline of the desired projectile profiles. A tolerance zone has been applied to the surface to allow for natural surface irregularity and roughness, which is indeed characteristic of rock. Examples of allowable rock shape for each classification are given in Figure 3-5. After conducting several experiments, it was found that some of the projectiles required two shape classifications to completely characterize it; such as A or B.
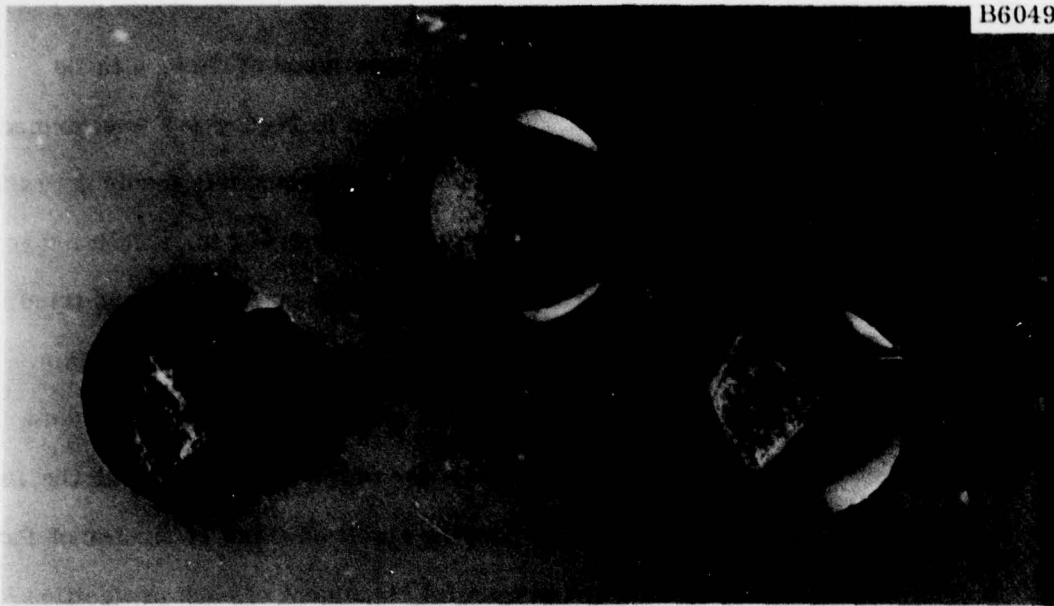
Figure 3-2. Three Compartment Mold for Potting Rock Projectile Specimens
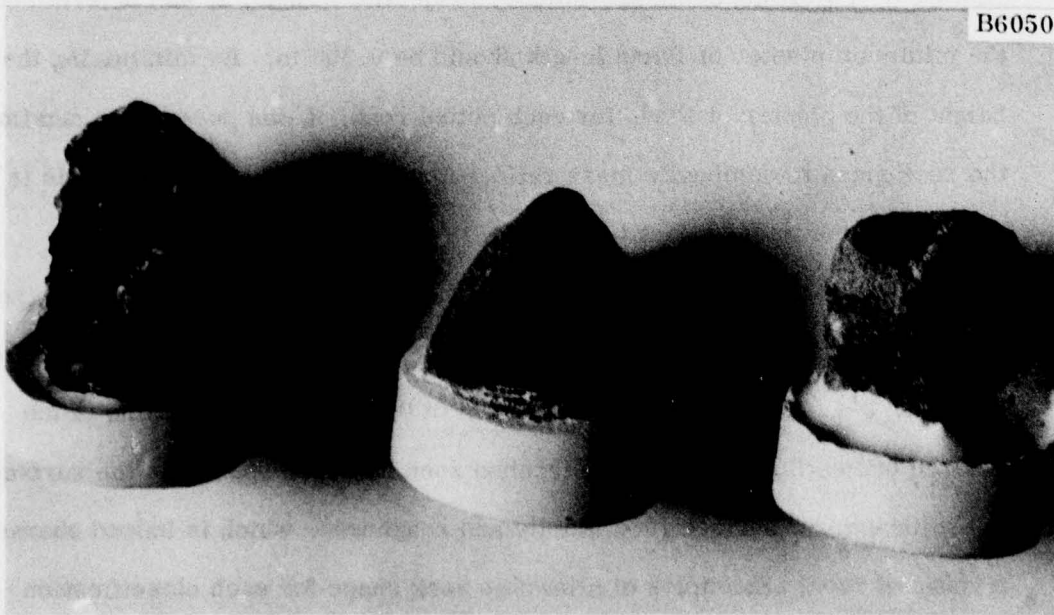
Figure 3-3. Projectiles Encapsulated in Plaster of Paris

Figure 3-4. 1-in. Rock Projectile Classification

B6052
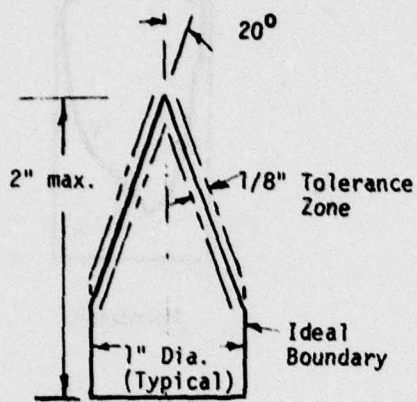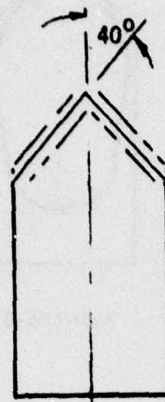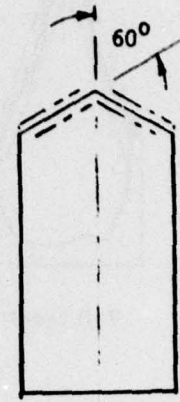
Pointed-A   Pointed-B   Pointed-C
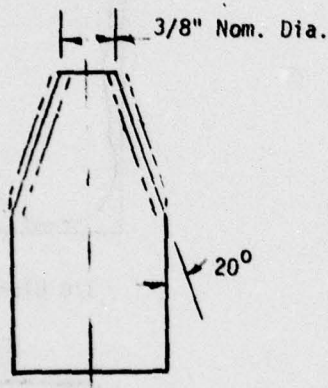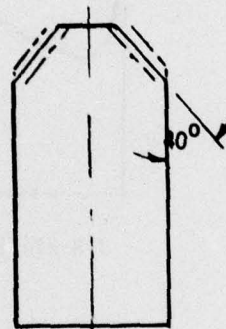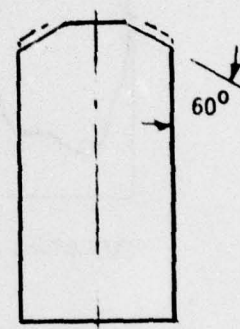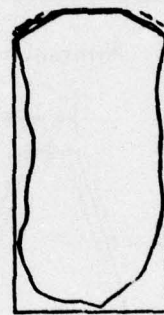
3/8 Blunt-A   3/8 Blunt-B   3/8 Blunt-C
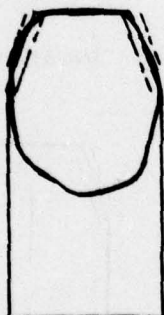
5/8 Blunt-A   5/8 Blunt-B   5/8 Blunt-C

Figure 3-5. Example of Allowable 1-in. Rock Shapes for
              Each Classification

SECTION IV

PHENOMENOLOGICAL BEHAVIOR OF THE IMPACT OF ROCK
WITH A SIMPLY SUPPORTED BEAM

This chapter will present some of the more significant observable results from the experimental impact studies. The salient features of 12 separate tests on 4 different materials will be discussed. A summary of projectile data for each of these tests is given in Table 4-1.

TABLE 4-1. PROJECTILE DATA

Test Sample	Rock Mass $\frac{lb\text{-}s^2}{in.}$	Composite Mass $\frac{lb\text{-}s^2}{in.}$	Velocity (in./s)	Initial KE (in.-lb)	Initial Length (in.)	Final Length	Shape
8S	0.000060	0.000087	1330	76.95	1.18	0.82	B
1G	0.000076	0.000108	720	27.99	1.25	1.25	3/8 A
4GL	0.000076	0.000097	854	35.37	0.82	0.82	Sphere
5S	0.000064	0.000092	1104	56.07	1.18	1.06	A
6S	0.000087	0.000116	1000	58.00	1.18	1.12	3/8 A
4S	0.000063	0.000097	788	30.12	1.38	1.32	A
2G	0.000072	0.000090	868	33.90	0.94	0.94	B/C
3G	0.000072	0.000093	970	43.75	0.975	0.975	B
8 IS	0.000069	0.000088	1184	61.68	1.115	0.905	B
10 IS	0.000067	0.000084	1128	53.44	1.053	0.882	B
11 IS	0.000068	0.000087	1452	91.71	1.10	--	B
12 IS	0.000069	0.000090	1658	123.70	1.083	--	B

Samples can be identified as follows: S-sandstone, G-Cold Springs Green gabbro, IS - Indiana sandstone and GL-glass sphere. The composite mass is the combined mass of the rock specimen imbedded in a plaster of Paris jacket. Projectile velocities vary from 720 to 1658 in./s. Projectile initial kinetic energies were limited based on the yield strength of the 6061T6 aluminum beam. It can be noted that the energies of the sandstones were allowed to exceed 100 in.-lb while the gabbro and glass sphere were limited to below 50 in.-lb. The initial and final length serve to indicate the amount of material which broke away from the main body of the projectile. The shape column is in accordance with the rock geometry classification in Section III.

4.1 OVERVIEW OF IMPACT BEHAVIOR

Rather than immediately focusing on the behavior of each specific rock material, a general discussion will first be presented on a comparison of representative impact behavior of materials from each group. Figure 4-1 shows a grouping of three projectiles 8S, 1G and 4GL and the associated beam contact plates. Projectile 8S experienced severe fracturing and the total intact mass was reduced 23%. This material which broke away from the projectile is in the form of pulverized sandstone and several larger particles. The 1 in. x 1 in. contact plate shows a deposit of fine sand over its surface in addition to a buildup of ingrained compressed sandstone. The buildup measures approximately 0.25 in. x 0.05 in. and projects above the surface 0.04 in. Removal of this ingrained material shows superficial surface indentation. The region under the removed mound of sandstone appears to have negligible depth. However, there appears to be a hundred or so pin point indentations spread over a 0.50 in. diameter area. Evidently, the hard quartz grains have been able to penetrate the surface after breaking

away from the material which cements them together. 1G and 4GL having initial kinetic energies less than 50 percent of 8S experienced no fracturing. They did however leave localized permanent deformations in their respective contact plates. The contact plate for 4GL experienced a spherical indentation of 0.160 in. in diameter and 0.0065 in. deep. The lower edge of the indentation shows a second crater which is the result of multiple impact. The contact plate for 1G shows an irregular shaped indentation, which is approximately the same area and depth as the indentation in 4GL.
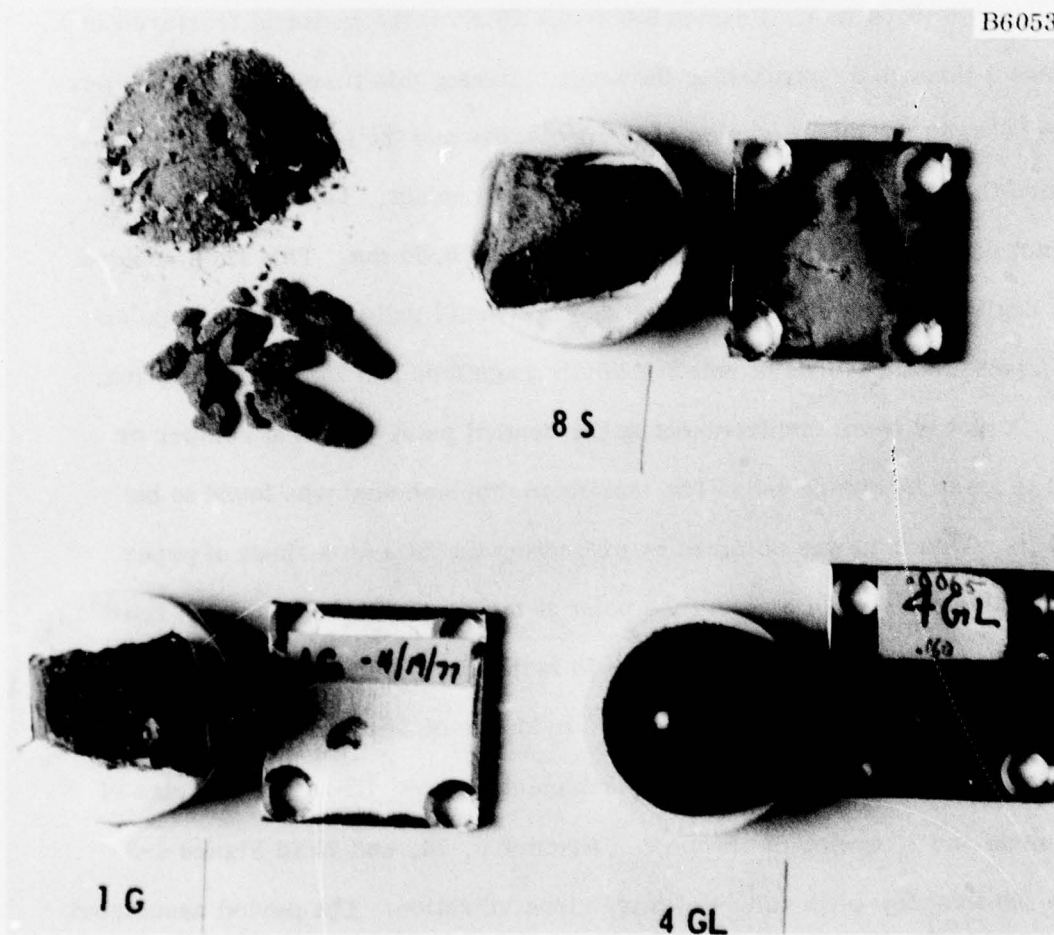
Figure 4-1. Projectiles and Associated Beam Contact Plates Following Impact (8S-Indiana Sandstone, 1G-Gabbro, 4GL-Glass Sphere)

Figure 4-2 shows ten 16-mm frames of the impact process. For this test the film speed was 5760 frames/s. Frame 1 shows the projectile approaching the beam at a velocity of 1330 in./s. Frame 2 shows the projectile making initial contact with the beam impact plate. Frames 3 through 5 are the frames of major contact force between the fracturing projectile and the beam. A measurement of projectile shortening, as a result of loss of material at the contact point, shows the following: frame 3 (0.18 in.), frame 4 (0.12 in.), and frame 5 (0.06 in.). Frames 6 through 10 show the material fractured in frames 3 through 5 approaching the beam. During this time, there is a separation between the intact portion of the projectile and the beam. This film indicates that there are at least three frames of contact. This means that the contact or impulse time for 8S is approximately 0.50 ms. This time coupled with negligible contact plate surface damage would indicate that the impulse has a peak contact force of relative small magnitude and long time duration.

A plot of beam displacement at the contact point vs frame number or time is given in Figure 4-3. The maximum displacement was found to be 0.41 in. This data was obtained by projecting the film on a sheet of paper and plotting the path of a reference point at the center of the beam. A fixed scale was located just above the beam to facilitate calibration of the displacement data. The plotted data also shows evidence of 3rd mode vibration. For each cycle of beam vibration in the fundamental mode, there are 9 cycles of 3rd mode and 25 cycles of 5th mode. Frames 5, 14, and 22 in Figure 4-3 show the first few peak values of third mode vibration. The period associated with the 3rd mode contribution to the total vibration is 1.58 ms. Data points between frames 28 and 33 are missing due to the masking of debris passing over the beam. It should also be noted that a second impact took place at frame 45.
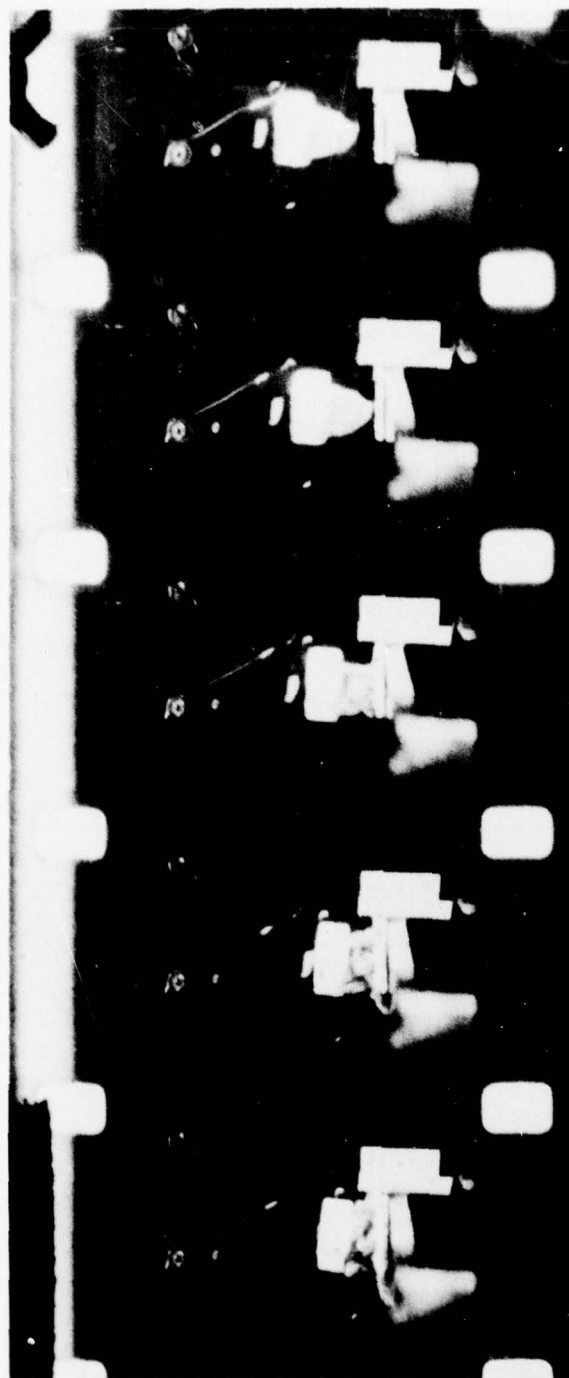
Figure 4-2. Indiana Sandstone Projectile (8S) Impacting Beam (Projectile Velocity 1330 in./s, Film Speed 5760 Frames/s) (Sheet 1 of 2)
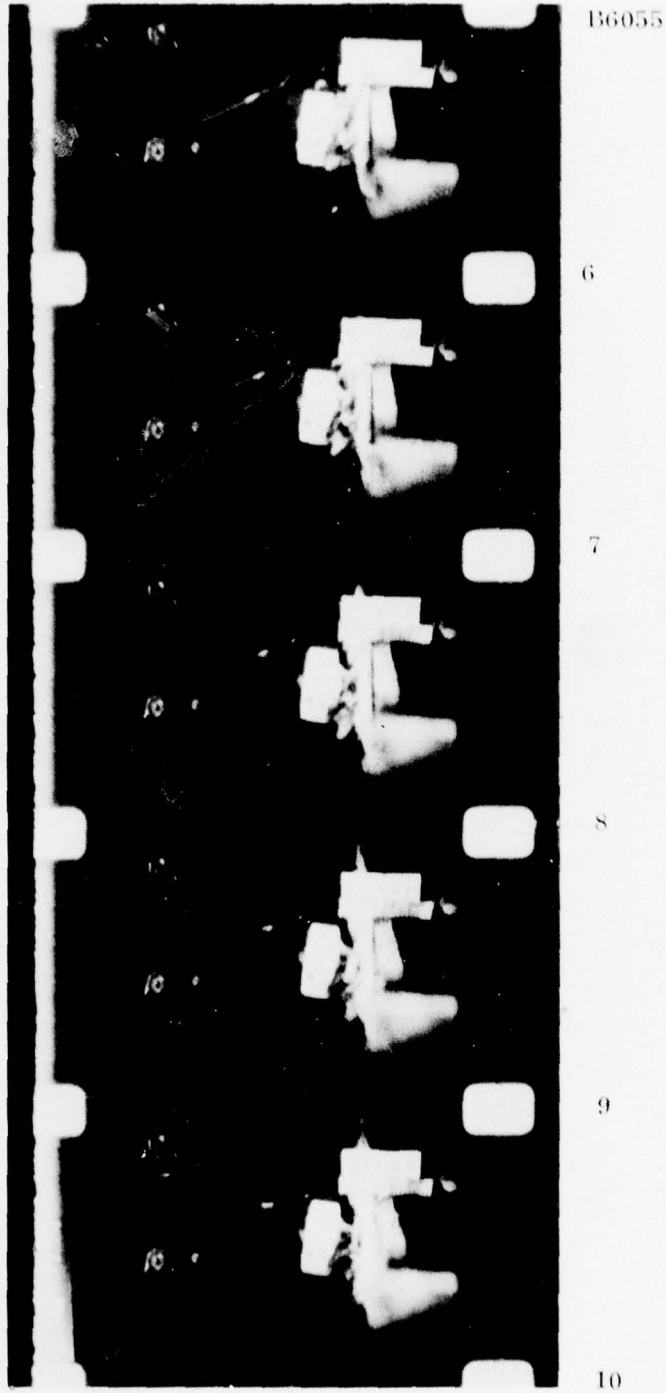
Figure 4-2. Indiana Sandstone Projectile (8S) Impacting Beam (Projectile Velocity 1330 in./s, Film Speed 5760 Frames/s (Sheet 2 of 2)
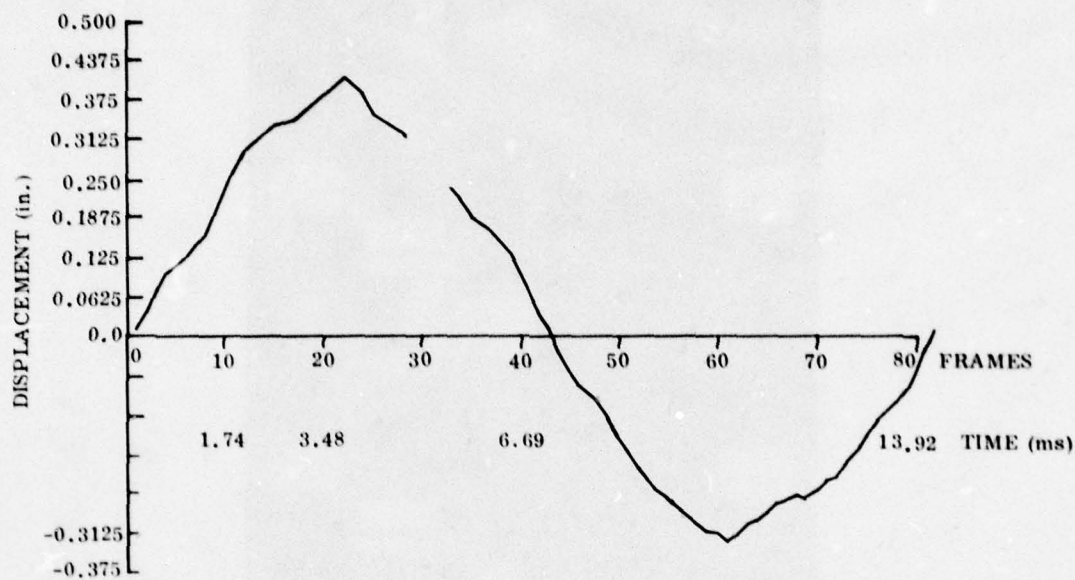
Figure 4-3. Beam Response to Impact with Indiana Sandstone
Projectile (8S)

Figure 4-4 shows ten frames of the impact process for 1G. Frames 1
and 2 show the projectile approaching the beam at 720 in./s. There appears
to be between 5-1/2 to 6 frames of contact before separation at frame 9. It is
difficult to accurately detect separation in this test because the front end of
this projectile was very dark and the background is black. Based on results of
other tests, it is probable that two impacts take place during the apparent six
frames of contact. The maximum center deflection of the beam for 1G was
found to be 0.31 in. as shown in Figure 4-5.
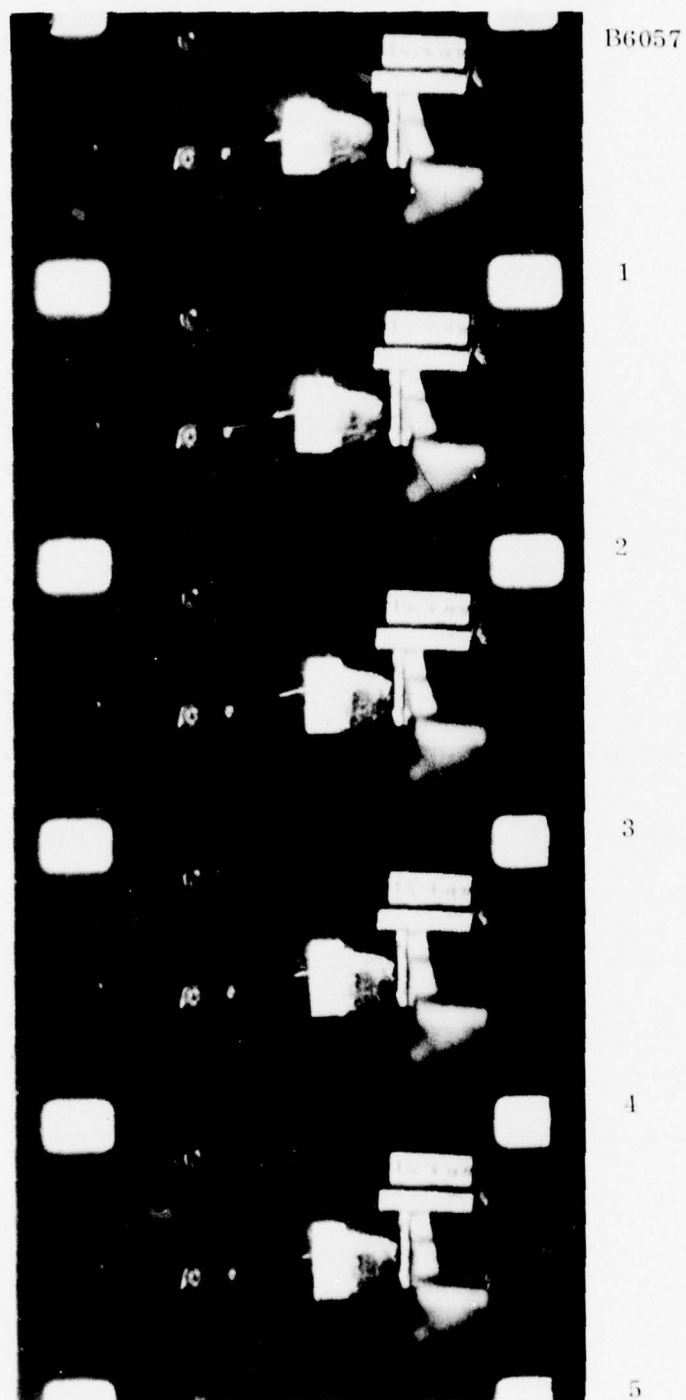
B6057

Figure 4-4. Gabbro Projectile (1G) Impacting Beam (Projectile Velocity 720 in./s, Film Speed 5760 Frames/s (Sheet 1 of 2)
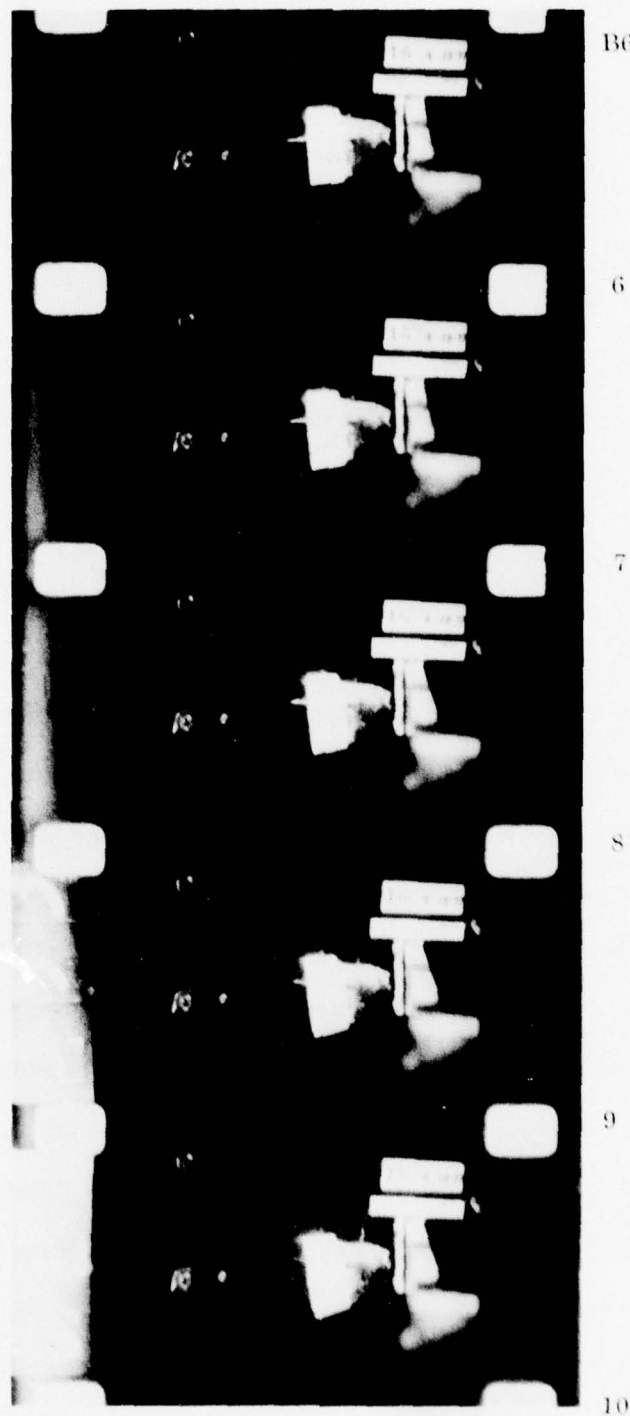
Figure 4-4. Gabbro Projectile (1G) Impacting Beam (Projectile Velocity 720 in./s, Film Speed 5760 Frames/s (Sheet 2 of 2)
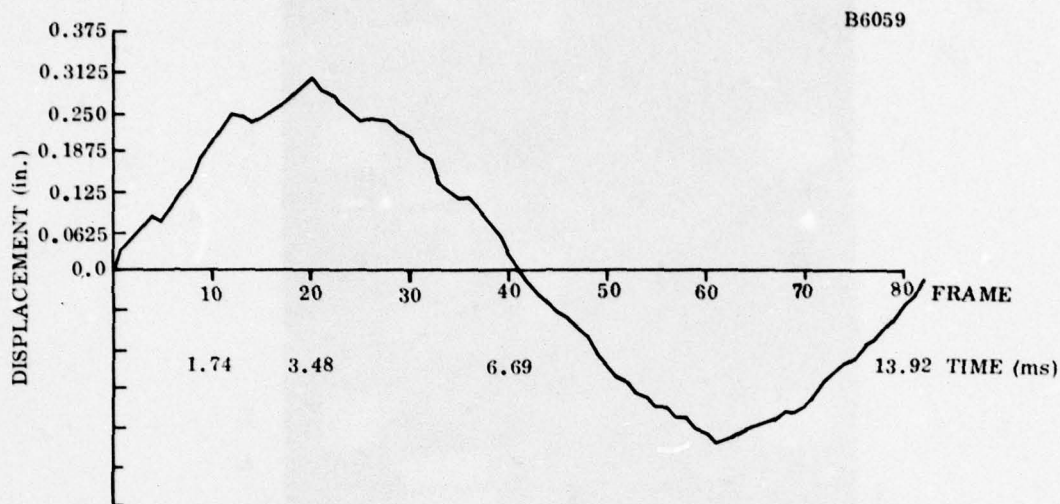
Figure 4-5. Beam Response to Impact with Gabbro Projectile (1G)

The impact behavior of the 0.859 in. diameter glass sphere 4GL is presented in Figure 4-6. For this test, a white background was used to provide the necessary contrast required to detect separation of the colliding bodies. Frames 1-3 show the projectile moving at a constant velocity of 854 in./s. Midway between frames 3 and 4, initial contact is made. There is apparent contact between frames 4 and 9. Separation of the bodies can clearly be observed in frame 10. Frames 11 through 15 show an increasing separation with the projectile essentially moving horizontally at -33 in./s. Figure 4-7 gives the beam as well as the projectile displacement for 4GL. This plot was made to a larger scale by projecting the film a distance of 20 ft. Examination of the projectile motion clearly shows that three separate impacts have taken place. Note first that frame numbers 0-6 in Figure 4-7 correspond to frames 3-9 in Figure 4-6. In Figure 4-7, initial contact is made midway between frame numbers 0 and 1. It is during this time that the major impulse occurs where the projectile velocity is rapidly reduced from 854 to 140 in./s. From
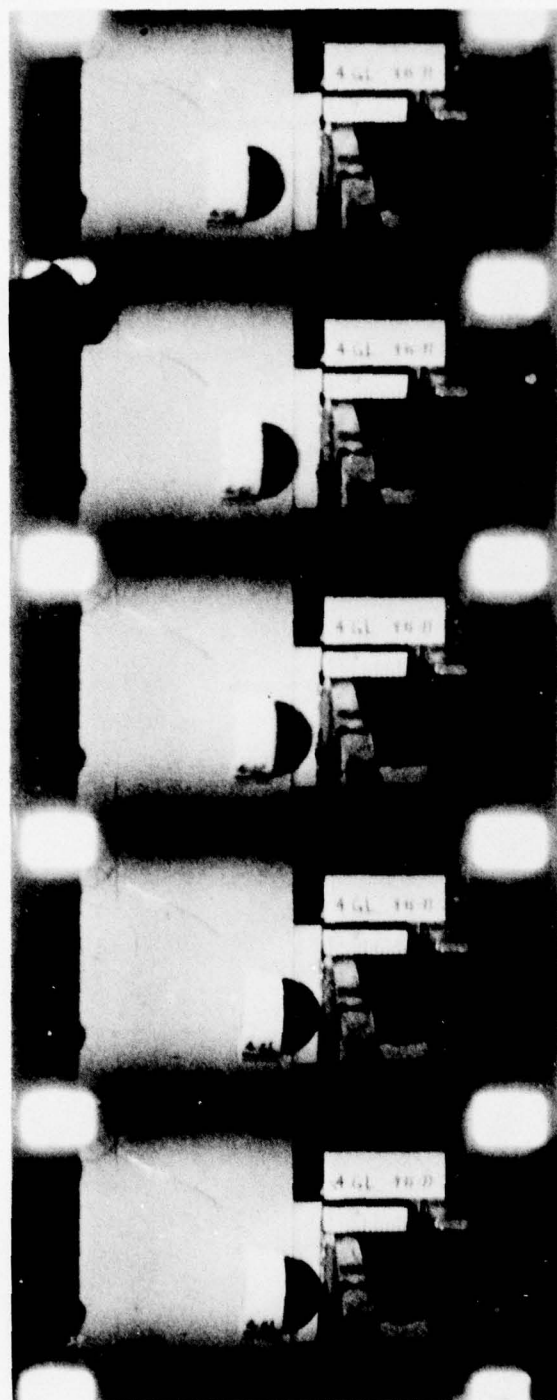
Figure 4-6. Glass Sphere Projectile (4GL) Impacting Beam (Projectile
Velocity 854 in./s, Film Speed 5760 Frames/s) (Sheet 1 of 3)
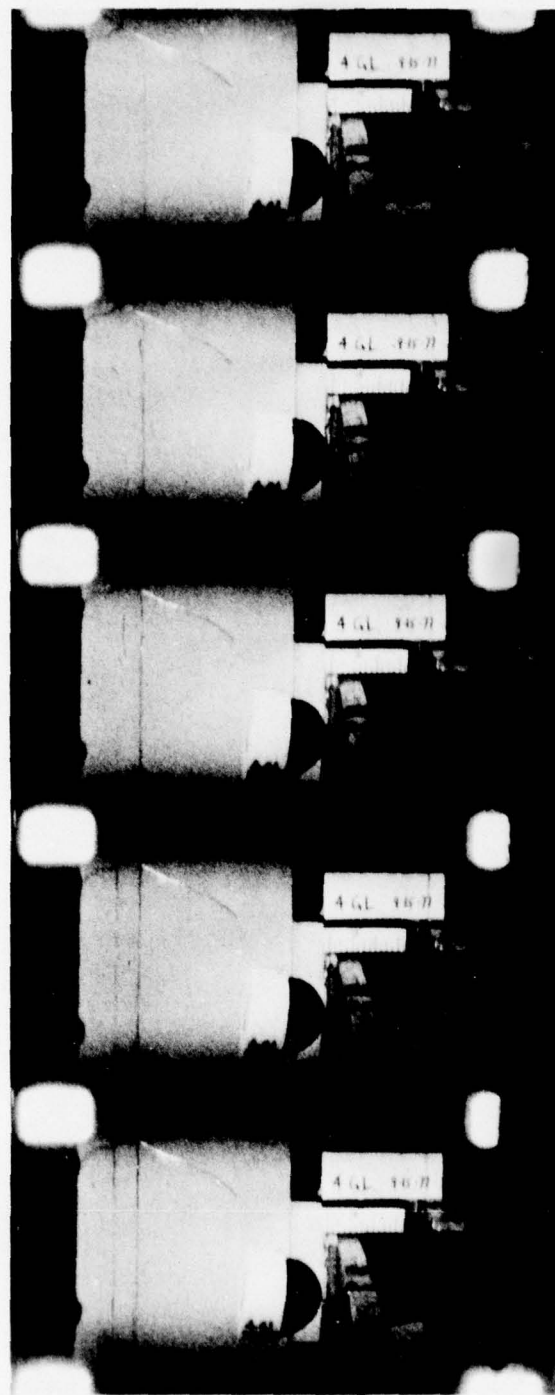
B6061

Figure 4-6. Glass Sphere Projectile (4GL) Impacting Beam (Projectile
Velocity 854 in./s, Film Speed 5760 Frames/s (Sheet 2 of 3)
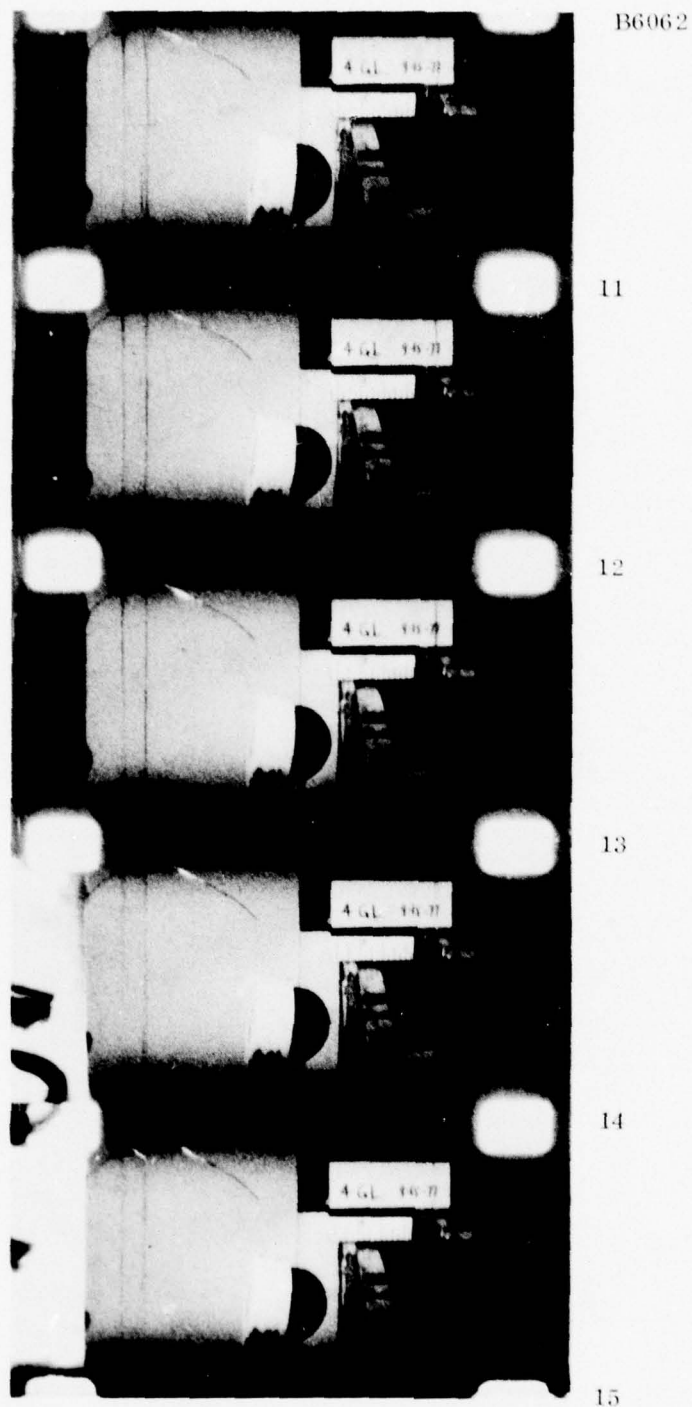
Figure 4-6. Glass Sphere Projectile (4GL) Impacting Beam (Projectile
Velocity 854 in./s, Film Speed 5760 Frames/s (Sheet 3 of 3)
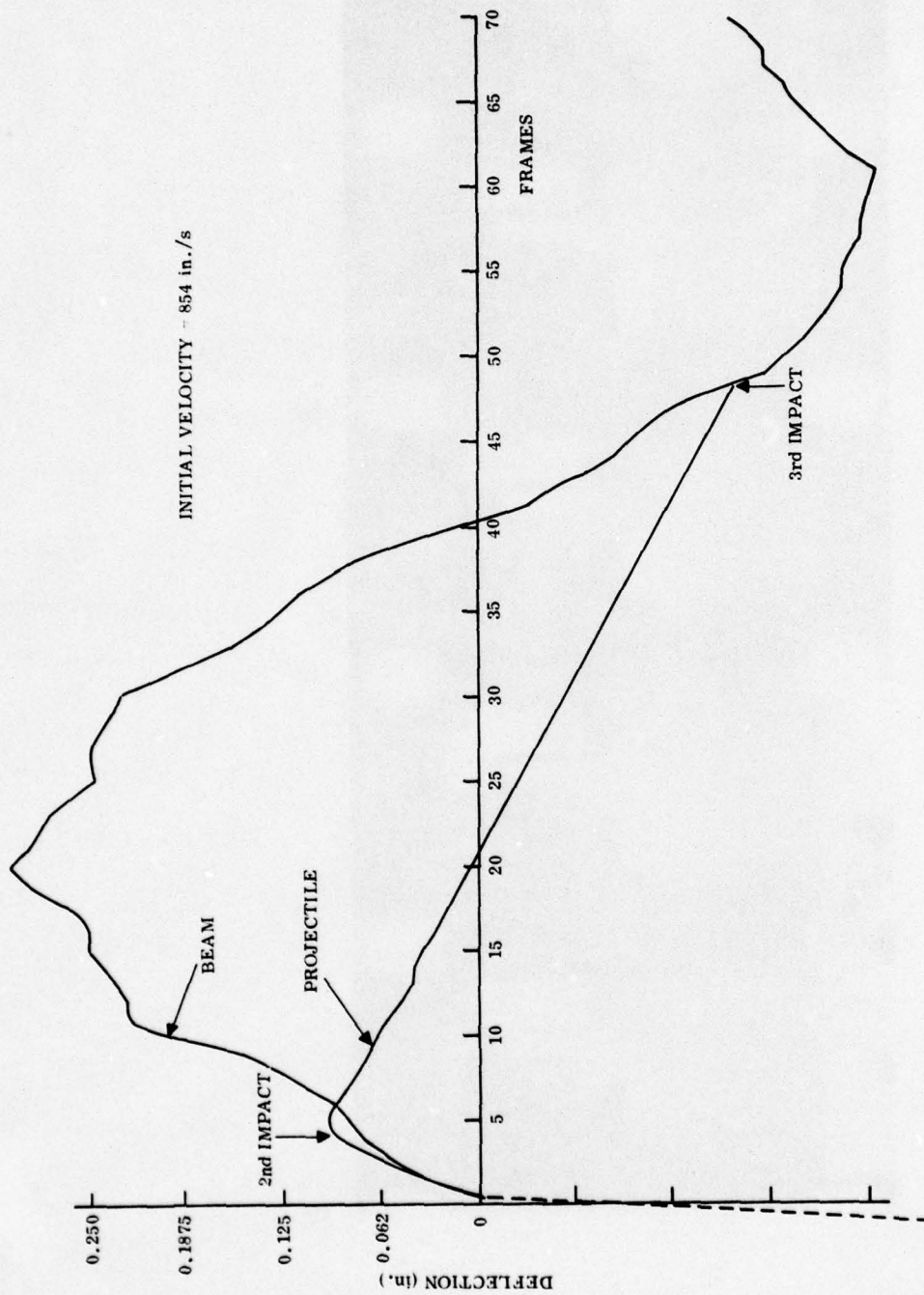
Figure 4-7. Beam Response to Impact with Glass Sphere (4GL)

frame numbers 1-4 the projectile is moving toward the beam at a constant
140 in./s. During this time, the contact point of the projectile is below the
flat surface of the contact; however, it is closing the clearance with the in-
dentation surface formed in the initial contact. A second impact occurs between
frame numbers 4 and 5, where the projectile velocity can be observed to de-
crease. Finally at frame number 6 the projectile departs from the beam at a
velocity of -33 in./s. The projectile continues to move with this horizontal
velocity component until it collides with the beam once again when the beam
is rebounding from its maximum displacement.

4.2   IMPACT BEHAVIOR OF SANDSTONE

The harder sandstones, those having compressive strengths greater than
10,000 psi, exhibit a rather interesting behavior upon impact with an aluminum
beam. This type of sandstone leaves a permanent indentation in the contact
plate. In addition, a conical shaped mound of the rock material remains
permanently embedded in the plate. Figure 4-8 shows rock specimens for 5S
and 6S along with the respective contact plates. Sample 5S exhibits the charac-
teristic fracture that occurs for projectile velocities above 1000 in./s. One
can see the conical shaped cavity at the center of the rock and the cracks which
extend from the cavity both radially and longitudinally through the sample.
Figure 4-8 shows a side view of the contact plate with the embedded conical
rock. This contact plate was potted in a hysol epoxy and sectioned. Enlarged
views of this section are given in Figure 4-9. Figure 4-9a shows good detail
of the indentation profile. The indentation is 0.010 in. deep and has a 0.18-in.
average diameter. The conical mound of sandstone is 0.28 in. in diameter
and is 0.10 in. high. Figure 4-9b is a 50X photomicrograph that shows a partial
section of the permanently deformed surface. The local variations along the

profile are due to the deeper penetration of the hard silica grains of the sand-
stone. At the bottom of each local valley, the impression of individual grains
can be observed. The grains can be identified by the light gray regions and the
cement material by the dark gray areas. Figure 4-8 also shows a mound of
embedded sandstone for 6S. The outline with the plate surface in this case is
triangular. A close examination of the rock indicates a shallow cavity at the
fracture surface. This surface is located just above the center of the specimen
as positioned in Figure 4-8. Although the rock is intact, it does show evidence
of radial cracks from the cavity to the top and right side of the sample.
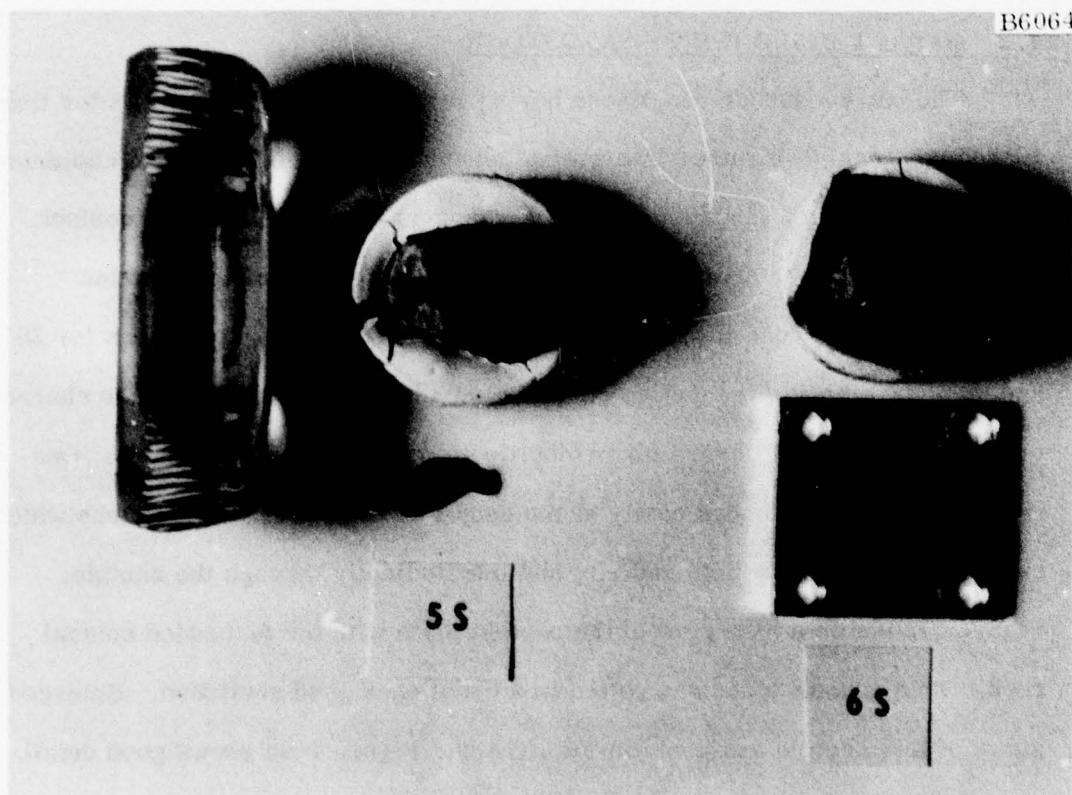
Figure 4-8. High Strength, Fine Grained Sandstone Projectiles Following
Impact (Impact Plate of (5S) Potted and Sectioned)

B6065

50X

(a) Side View of Contact Plate
Showing Embedded Rock
From 5S

(b) Photomicrograph (50X) Showing
Partial Section of Indentation

Figure 4-9. Embedded Rock in Contact Plate

4-17

Static compression tests were conducted on samples of this material in order to gain a better understanding of the fracture process. Two samples A and B shown in Figure 4-10 were loaded to exhibit varying degrees of damage. Sample A was loaded to 710 lb against the contact plate. The contact plate shows a mound of sandstone embedded in the plate. This mound can be identified by (18.24) which is the mass in grams of this specimen and measures 0.12 x 0.21 in. and projects above the surface 0.06 in. View A shows the four large pieces of rock which broke away from the main body upon reaching the 710-lb load. The failed surfaces, appear to be on planes running from the contact region to the nearest edge at the base of the rock. Loading sample B to 540 lb resulted in an indentation which can be identified by (18.92). In this case, sandstone material did not embed itself in the contact plate. The indentation is shown to be elliptical in shape and measures 0.06 x 0.09 in. for the minor and major diameters. The identation is approximately 0.002-in. deep. A closer look at sample B shows the initial crack development. At the center of the rock one can observe a complete elliptical crack which measures 0.08 x 0.12 in. Also, note that this area which was in contact with the plate is slightly larger than the permanent indentation in the plate. Impact tests run on samples having velocities below 700 in./s tend to leave indentations without the permanent ingraining of sandstone.
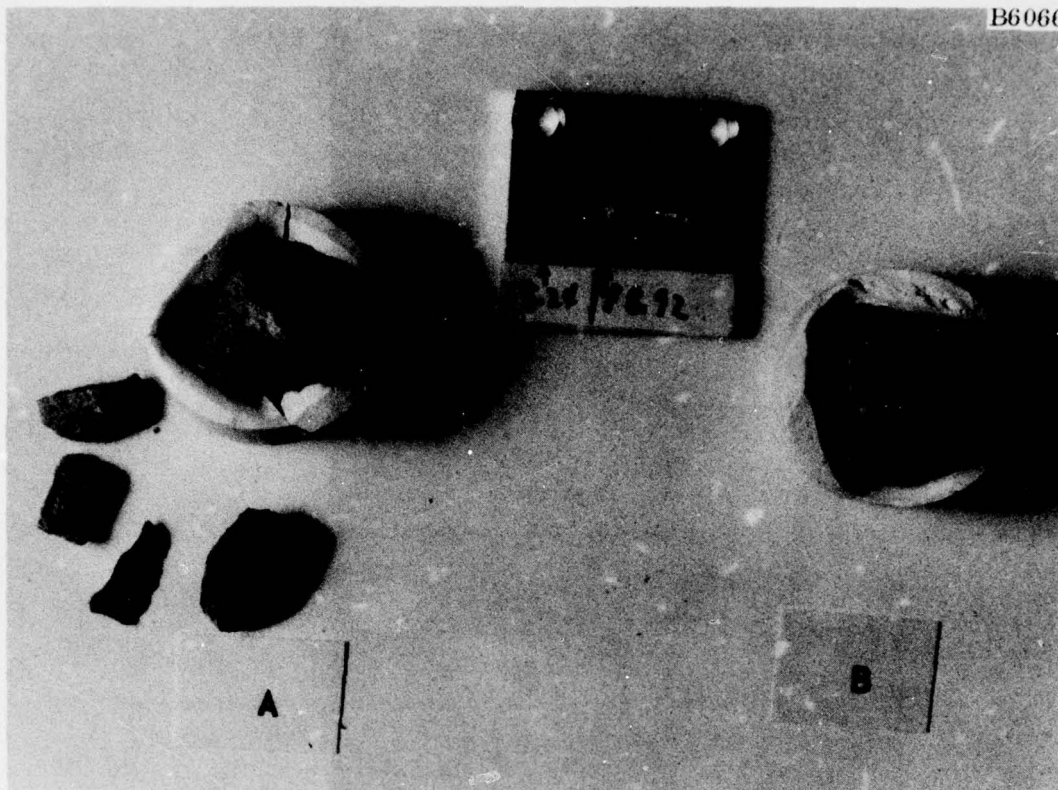
Figure 4-10. Static Compression Test Specimens of High Strength,
Fine Grained Sandstone (A is loaded to 710 lb,
B is loaded to 540 lb)

Figure 4-11 shows five frames of high speed film data for projectile
4S. The rock fracture appeared quite similar to that shown by sample A,
Figure 4-10. The projectile having an initial velocity of 788 in./s is shown
in frame 1 at the moment of contact with the beam. Frame 2 shows the
spreading out of pulverized material across the surface of the beam contact
plate. Frames 3-5 show the growth of the spreading of pulverized material
and portions of the plaster of Paris jacket breaking away from the sample.
Film speed for this test was 2800 frames/s. The dynamic response of the
center of the beam is given in Figure 4-12. The maximum deflection is shown
to be 0.230 in.
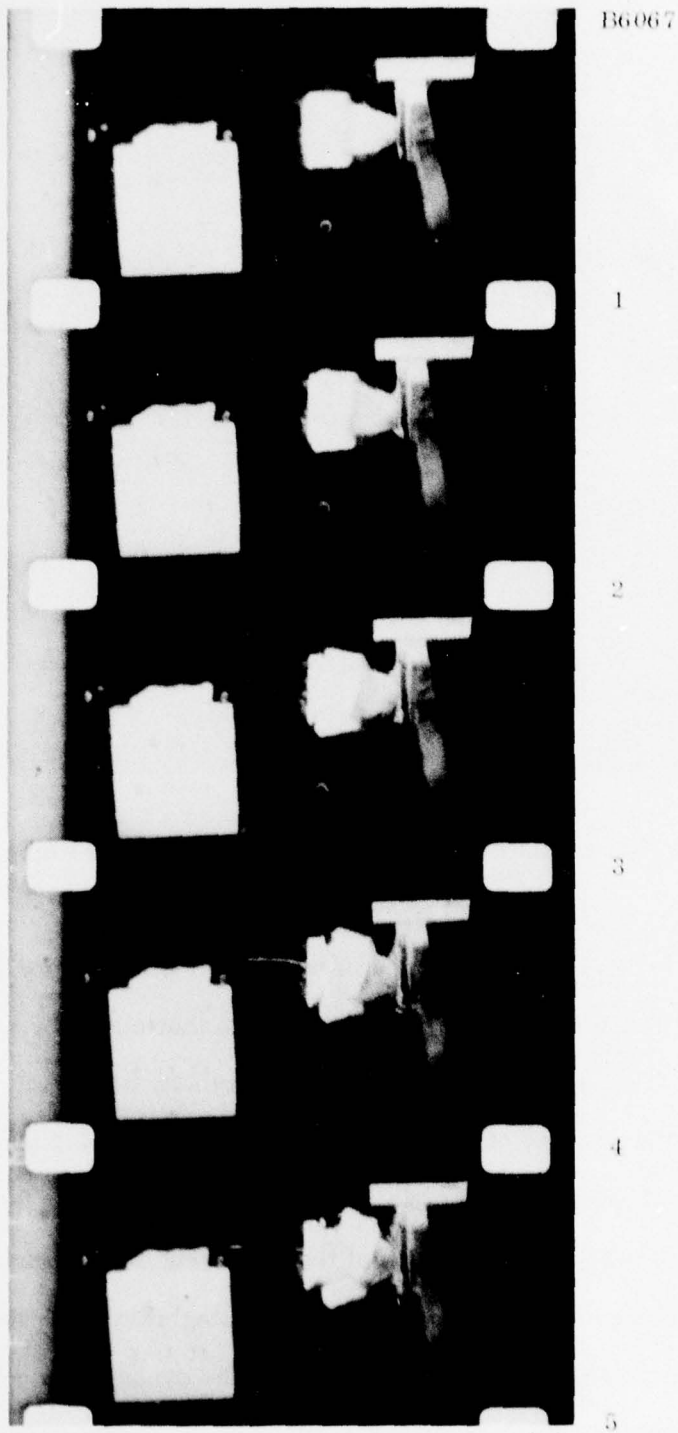
Figure 4-11.   Fine Grained Sandstone (4S) Impacting Beam (Projectile
Velocity 788 in./s, Film Speed 2800 Frames/s)
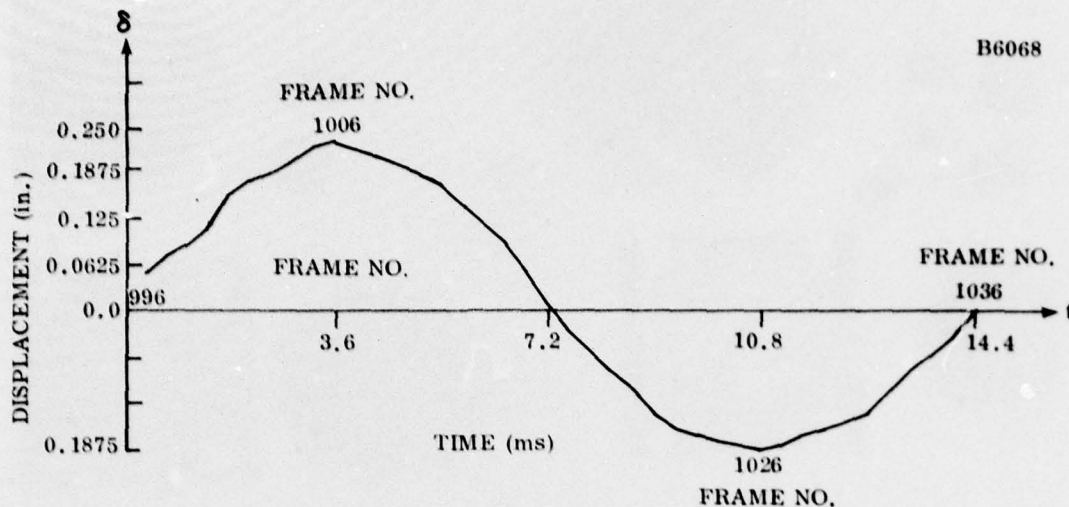
Figure 4-12.   Beam Response to Impact with Fine Grained
Sandstone Projectile (4S)

4.3   IMPACT BEHAVIOR OF INDIANA SANDSTONE

The Indiana sandstone has a fracturing behavior quite different from that
of the higher strength sandstones.   At velocities as high as 1100 to 1200 in./s
the projectile experiences spalling completely around the area of contact.   This
spalling or flaking away at the surface can be seen in Figure 4-13 for test
samples 8 I.S. and 10 I.S.   In addition to the larger flakes of sandstone one
can observe a considerable amount of pulverized material.   A close look at
10 I.S. will show a longitudinal crack at the upper right-hand quadrant of the
projectile.   This crack has formed along the stratum passing through the
contact region.   Because of the greater strength for this rock along the strata,
the final contact area which remains in the intact rock after separation, is
is the form of a straight narrow line.   In the case of 8 I.S., this area is 0.30
x 0.060 in.   The contact plates for 8 I.S. and 10 I.S. show small amounts of
embedded material.   This material can easily be wiped away by lightly rubbing
the surface.

8 I.S.

10 I.S.
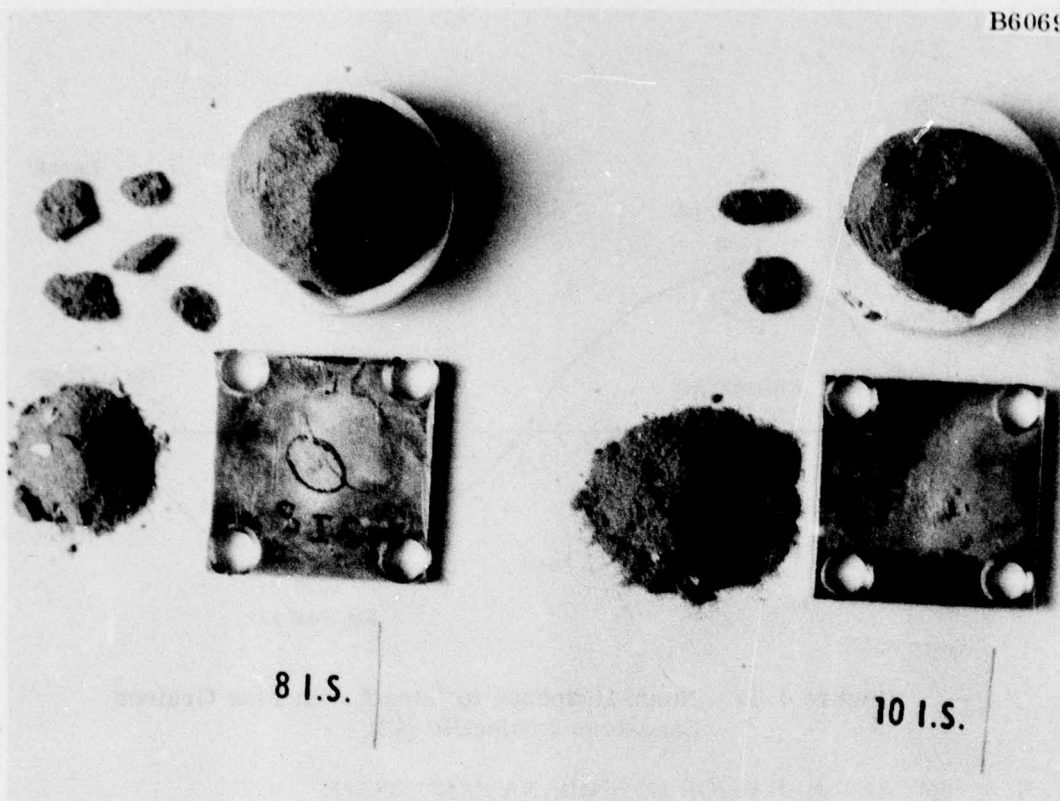
Figure 4-13.   Indiana Sandstone Projectiles Showing Surface Spalling and
Pulverized Material

Figure 4-14 shows severe projectile fracturing for sample 11 I.S.

This projectile had an initial velocity of 1452 in./s at the time of impact.

The main body of the projectile encased in the plaster of Paris was reassem-

bled to show that the major fracturing occurred on planes along the natural

boundary layers for this sedimentary rock.   Two major fracture surfaces

can clearly be observed.   The remaining debris shows considerable spalling

and pulverization.   The contact plate shows a rather large spreadout impact

pattern.   Particle penetration once again was negligible.   Beam displacement

data is presented in Figure 4-15 for sample 11 I.S.   For this test, the maxi-

mum center deflection of the beam was 0.42 in.
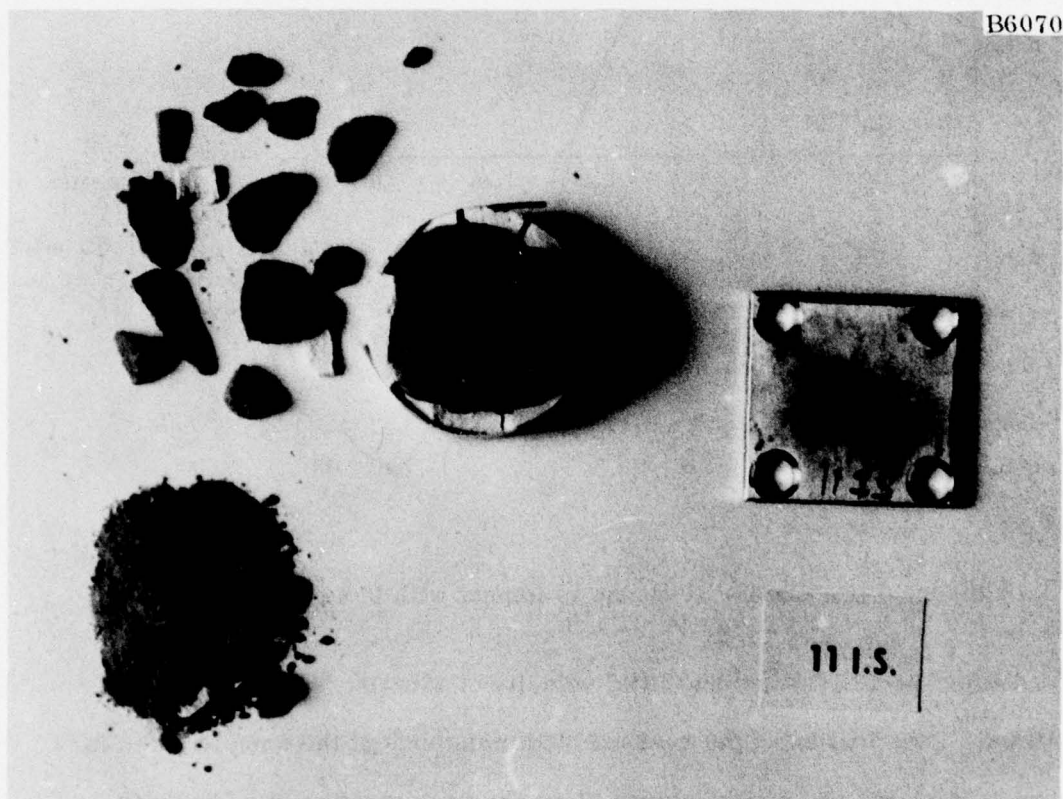
Figure 4-14. Severe Fracturing of Indiana Sandstone Projectile
Following Impact of 1452 in./s

B6071
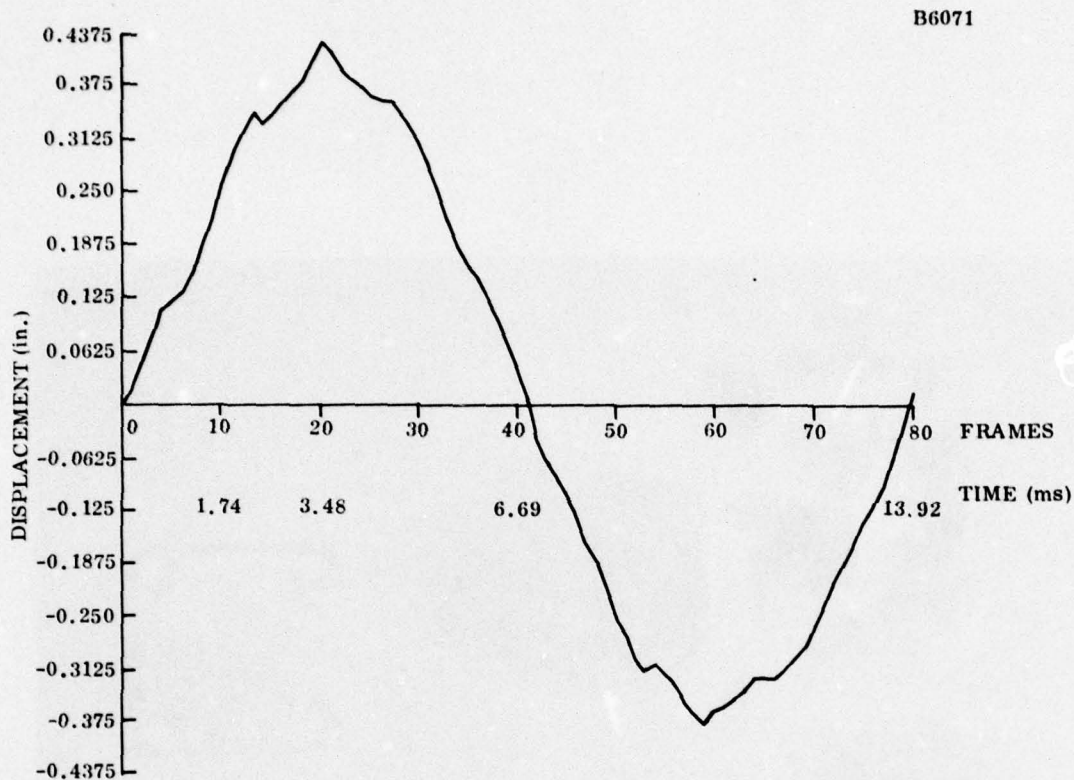
Figure 4-15. Beam Response to Impact with Indiana Sandstone
Projectile (11 I.S.)

Projectile 12 I.S. had an initial velocity of 1658 in./s upon impacting
the beam. Examination of the reassembled main body of the sample given in
Figure 4-16 shows one main fracture along the rock stratum in addition to
some fracturing across the rock layers. This sample shows a lesser amount
of spalling than did sample 11 I.S. A very small amount of material is em-
bedded in the contact plate. The plate was completely covered with fine dust-
like material which is shown partially removed from the top of the plate.
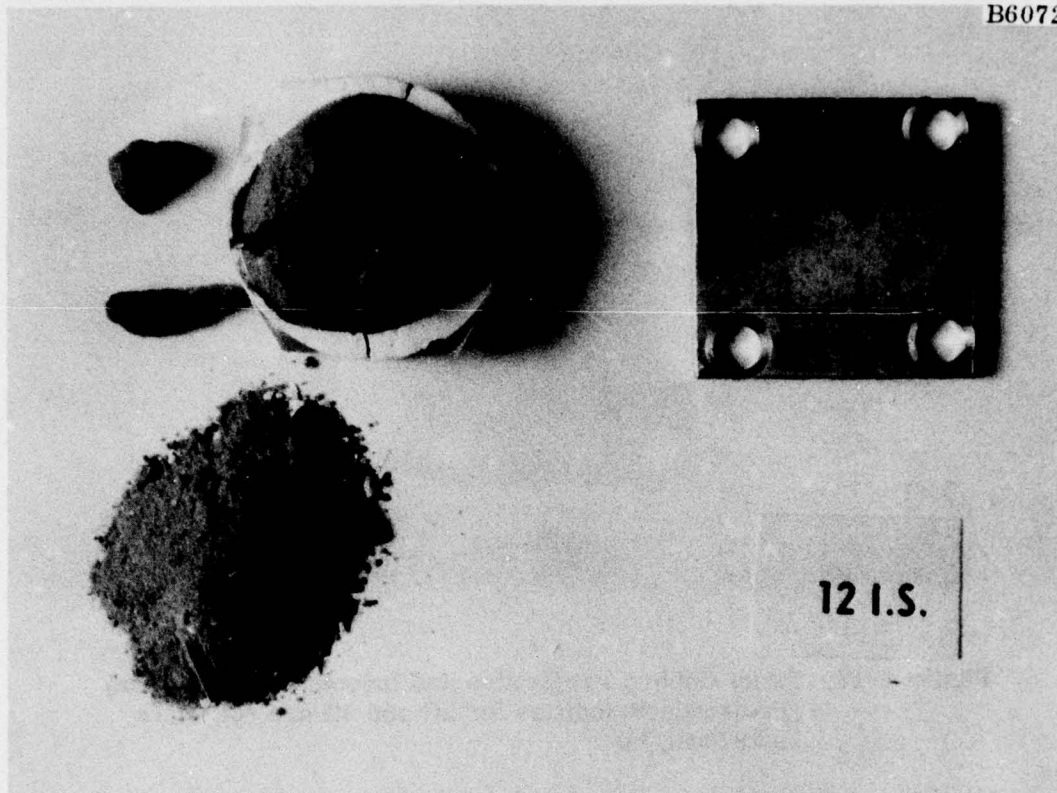
Figure 4-16. Severe Fracturing and Pulverization of Indiana Sandstone
Projectile Following Impact at 1658 in./s

4.4 IMPACT BEHAVIOR OF GABBRO

Representative indentations which resulted from the impact of gabbro

projectiles with the aluminum beam are shown in Figure 4-17. The Cold

Springs Green gabbro projectiles 2G and 3G had initial velocities of 868 and

970 in./s, respectively. Projectile 2G is classified as a B/C shape while

3G is the B shape. The contact plate indentation caused by 2G is elliptically

shaped and measures 0.18 x 0.12 in. while that associated with 3G is D-

shaped, measuring 0.18 x 0.15 in. The maximum crater depths are 0.013 in.

and 0.016 in. respectively for 2G and 3G. The indented surface which resulted

from 3G clearly shows a replica of the undulations of the contact surface of the

projectile. A close examination of the projectiles following the test show no

evidence of fracturing.   4-25

B6073
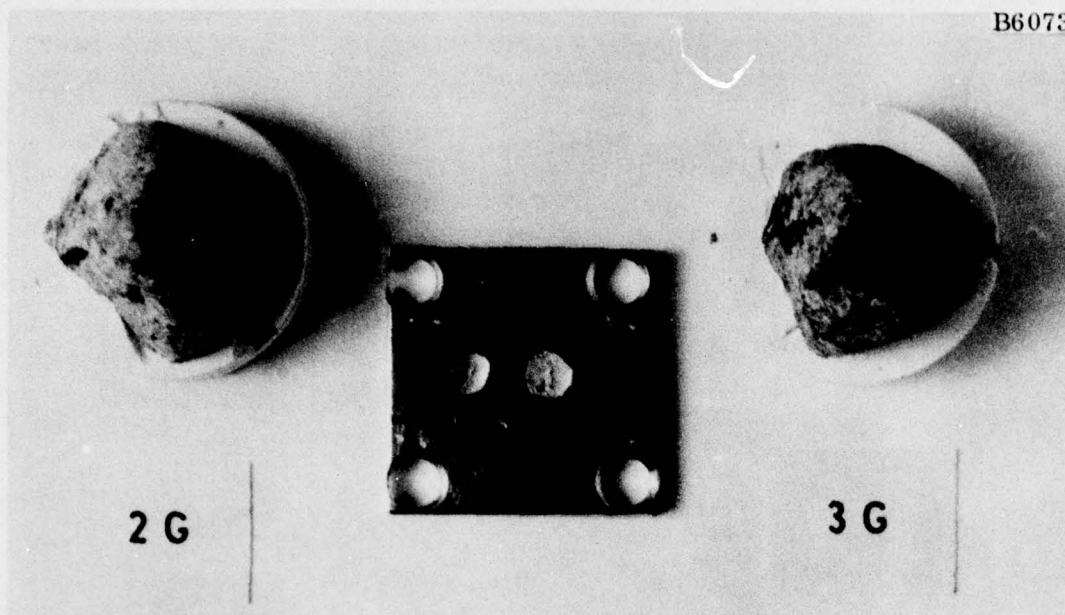
Figure 4-17. Intact Gabbro Projectiles and Indented Contact Plate
(Projectile Velocities for 2G and 3G are 868 in./s
and 970 in./s)

All of the tests involving gabbro were limited to velocities below 1000 in./s. At this time, it is not known what threshold velocity is required to cause grain boundary fracturing for projectiles having masses between 0.00009 and 0.000011 $lb/s^2/in$.

Both projectiles experienced secondary impacts upon rebound of the beam. These caused slight indentations measuring approximately 0.030 in. in diameter. They are located in Figure 4-17 just to the left and also above the 3G indentation. These secondary impacts have the effect of reducing the maximum negative displacement of the beam which occurs at frame number 60 in Figures 4-18 and 4-19. These figures show the maximum displacement of 2G to be 0.29 in. and 3G, 0.32 in. Both curves show significant 3rd mode contribution to the total displacement as well as evidence of 5th mode participation. A 5th mode peak can be observed at frame 26 in Figure 4-19.
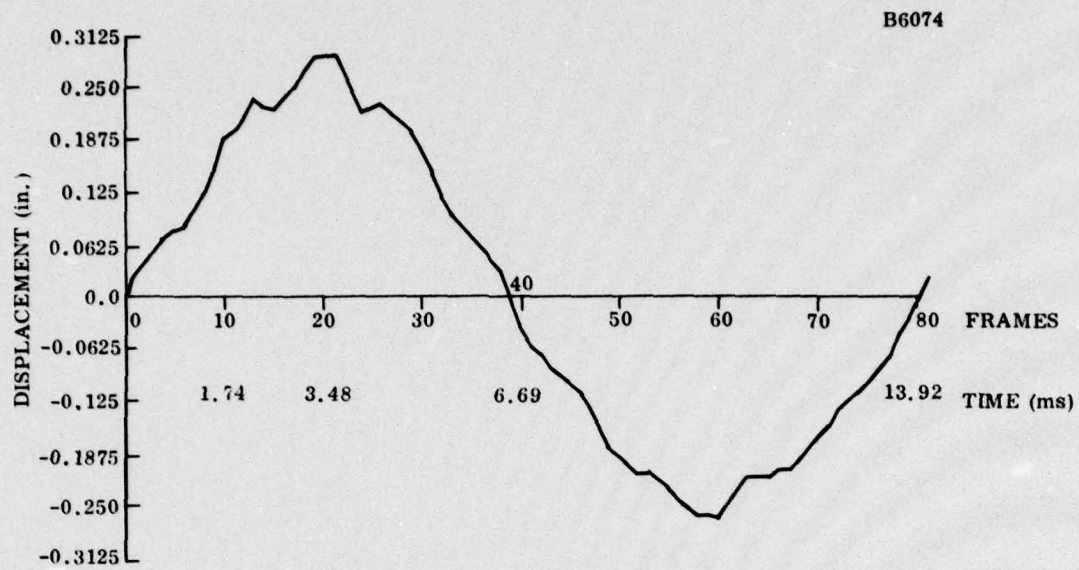
Figure 4-18. Beam Response to Impact with Gabbro Projectile 2G
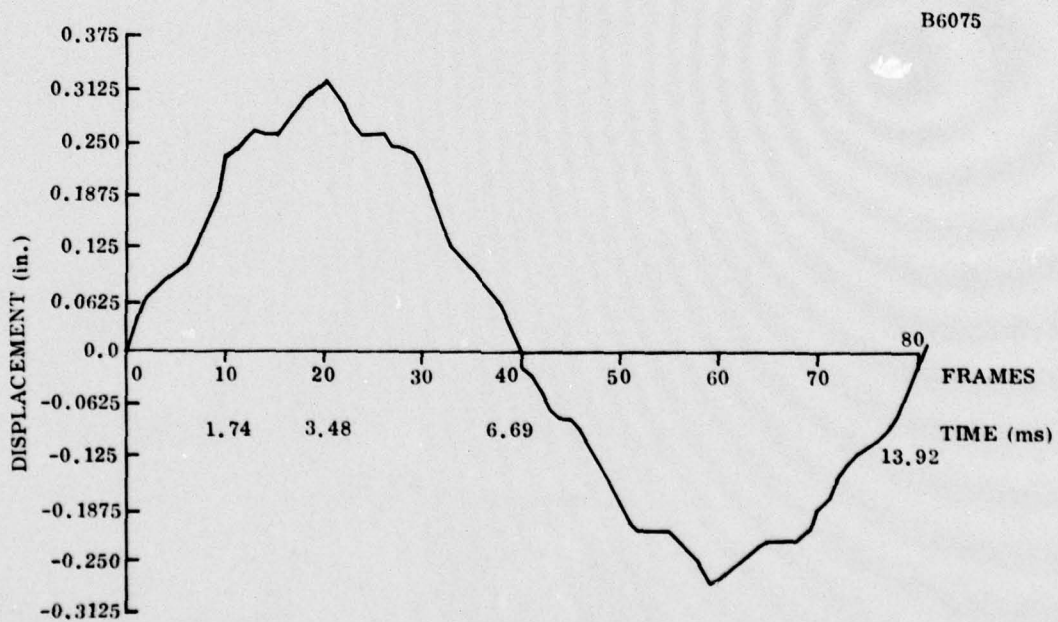
Figure 4-19. Beam Response to Impact with Gabbro Projectile 3G

SECTION V

MECHANICAL SIGNATURES OF SANDSTONE AND GABBRO

5.1 MECHANICAL SIGNATURES

Numerous experiments were conducted on sandstone and gabbro projectiles having masses in the general range of 0.000085 to 0.000097 lb-s^2/in. For the Indiana sandstone projectiles, velocities as high as 1658 in/s were achieved without inducing plastic deformation of the beam. For the high strength sandstone, gabbro and glass spheres, velocities were limited to 1000 in./s.

In addition to the extremely valuable 16-mm high speed film data, strain gage data was obtained for each impact experiment. Strain data at the center of the beam is equally as important, since it provides additional information that cannot be deduced from the film data. For example, high strain levels may be experienced by the beam within 0.200 ms following an impact. At this time, the center displacement of the beam may be only 0.010 in.

After collecting strain data for each material treated in this investigation it became apparent that each material exhibited its own characteristic dynamic strain response, or mechanical signature. A comparison of beam strain response, to each type of rock material tested, is presented in Figures 5-1 and 5-2. The strain response to Indiana sandstone projectile 8S is given for approximately 7.0 ms, which is one-half the fundamental period of the beam. The periods associated with the 1st, 3rd, 5th and 7th normal modes of vibration of the beam are 14.2, 1.58, 0.56 and 0.289 ms respectively. The first few milliseconds for each

B6076
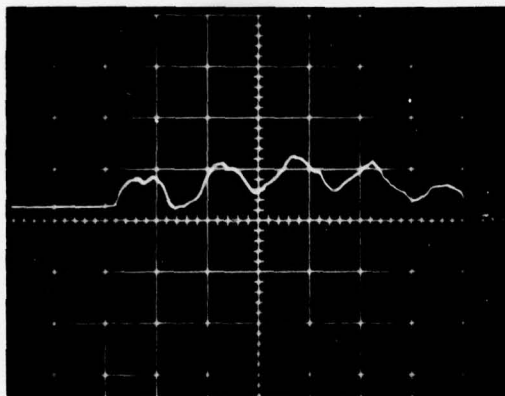
TEST (8 S)

STRAIN: 2000 μSTRAIN/DIV
TIME: 1.0 ms/DIV
MASS: 0.000087 lb-s^2/in.
VELOCITY: 1330 in/s

STRAIN

TEST (1 G)

STRAIN: 1000 μSTRAIN/DIV
TIME: 1.0 ms/DIV
MASS· 0.000109 lb-s^2/in.
VELOCITY: 720 in./s

TEST (4 G L)

STRAIN: 1444 μSTRAIN/DIV
TIME: 1.0 ms/DIV
MASS: 0.000097 lb-s^2/in.
VELOCITY: 854 in./s

TIME $\longrightarrow$

Figure 5-1. Beam Strain Response due to Impact with Indiana Sandstone
(8 S), Gabbro (1 G) and Glass Sphere (4 GL)

TEST (4 S)
STRAIN: 1000 μSTRAIN/DIV
TIME: 1.0 ms/DIV
MASS: 0.000097 lb-s^2/in.
VELOCITY: 788 in/s^2

(a)   Short-Time Beam Strain Response
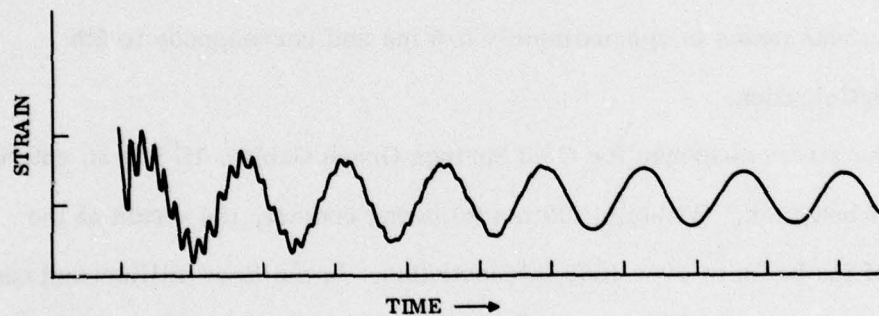
STRAIN: 1000 μSTRAIN/DIV   TIME: 10.0ms/DIV

(b)   Long-Time Beam Strain Response

Figure 5-2.   Responses Due to Impact with Fine Grained Sandstone (4S)

response is the zero-strain reference, which commences when the cross wires in the path of the projectile touch thereby triggering the time sweep of the oscilloscope. The strain record for 8S indicates a rather-slow increase in strain during the first 0.4 ms following contact. This behavior is characteristic of all Indiana sandstone projectiles tested. It is the result of an impulse upon impact, which has a small peak contact force and a long-time duration of loading. The response primarily exhibits 1st and 3rd mode participation. Modal participation can be deduced from the strain-time response by observing the time interval between major peak values. For 8S in Figure 5-1, the major peak spacing at approximately every 1.60 ms corresponds to the period of the 3rd mode. During the first millisecond of response, two peak strains of equal magnitude can be observed. The time between these peaks is approximately 0.5 ms and corresponds to 5th mode participation.

The strain response for Cold Springs Green Gabbro 1G has an entirely different behavior. Within 0.100 ms following contact, the strain at the center of the beam is over 1500 microstrains. In the first millisecond one can observe significant 5th mode participation as well as some evidence of 7th mode. This response, with considerable high frequency content, is due to an impulse with a large peak force having a short time of contact. The maximum strain for 8S is 2000 microstrains, compared with 1700 microstrains for 1G. However, note that the initial kinetic energy of the projectile for 8S was almost 3 times that of 1G.

The beam response, upon impact with the glass sphere 4GL is also shown in Figure 5-1. The strain record is quite similar to that of 1G. There appears to be somewhat more 5th mode content however. The response is expected to be similar since both projectiles have similar hardness and did not fracture upon impact. The strain curve for 4GL shows an initial point of strain of 2890 microstrains within 0.100 ms of contact. The oscilloscope trace for rapid rise in strain is intermittent due to the rise time limitations of the strain gage amplifiers.

Figure 5-2a gives strain response of the beam upon impact with sandstone projectile 4S. This material exhibits an early time behavior similar to the gabbro. After an initial period of 0.60 ms, the strain behavior appears quite similar to that of the Indiana sandstone. Although this material is not as hard or strong as the gabbro, it has a compressive strength of three times that of the Indiana sandstone. It should therefore be able to develop a fairly-high contact force upon impact before fracturing. Secondary impacts occur once fracturing begins. Significant pulverization takes place along the circumferential edges surrounding the embedded mound of sand. These secondary impulses tend to be of longer time duration with a significantly reduced magnitude. The maximum strain of 1400 microstrains occurs within 0.200 ms. The maximum strain which occurs at approximately 3.5 ms was found to be 1100 microstrains. This lower beam strain value is the result of significant energy loss of the higher frequency vibration modes. Figure 5-2b gives the beam response for approximately 100 ms. This response obtained from the oscillograph recorder

shows the overall damping behavior of the beam. Here one can observe the natural decay in amplitude of the fundamental mode having a period of 14.2 ms along with the decay of the third mode (T = 1.58 ms), which is riding on the fundamental. Evidence of third mode contribution ceases to exist after 60.0 ms.

Beam strain response is strongly influenced by projectile strength and hardness. Projectile shape appears to have only minor effect on the beam vibration and its associated mechanical signature. Regardless of projectile shape in a given material type, the mechanical signatures are similar over a range of velocity. The mechanical signatures are for the most part a function of the time duration of contact between the projectile and the beam. The major difference is that strain amplitudes naturally will increase with increased projectile velocity. It has been observed that the blunt shaped projectiles (3/8 A) of a given mass in Indiana sandstone require greater velocity to fracture than those of equivalent mass having an A- or B-shape. In any event, regardless of whether or not the projectile completely fractures or remains intact following some material loss, the mechanical signatures of Indiana sandstone are quite similar. Figures 5-3 and 5-4 show the results of six beam responses for impact with Indiana sandstones for projectile velocities ranging from 556 to 1658 in/s. Test 1 I.S. shows the strain record for a projectile with an initial velocity of 556 in./s. The velocity for this test was determined from the photocell response traces shown at the bottom of the figure. The photocells for this test were separated by a distance of 1.50 in. Projectiles of the same mass and shape were used for test 3 I.S. and 4 I.S. The initial kinetic energies varied by approximately 10%, however. The first 2-ms of response are essentially
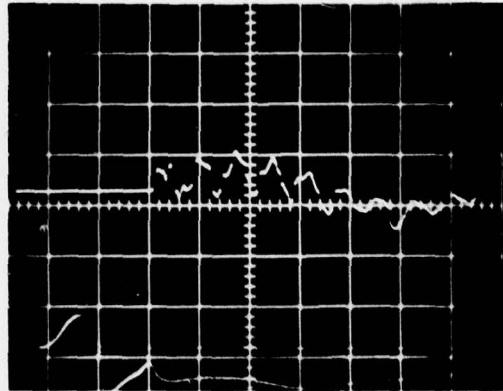
TEST (1 IS)

STRAIN: 1000 μSTRAIN/DIV
TIME: 2.0 ms/DIV
MASS: 0.000087 lb-s^2/in.
VELOCITY: 556 in/s
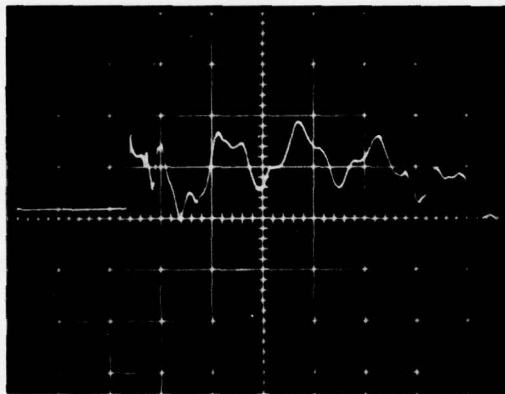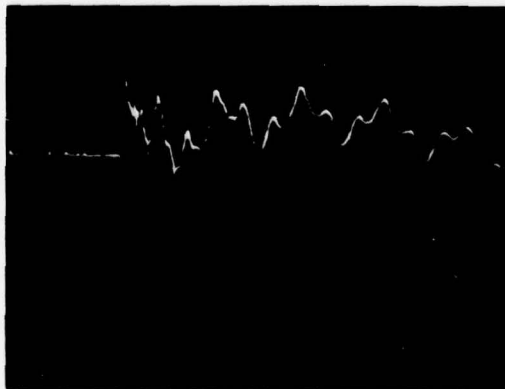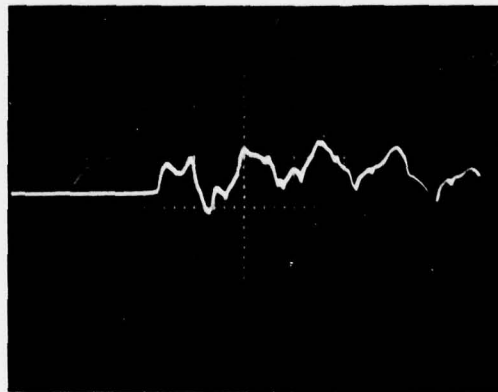
TEST (3 IS)

STRAIN: 1000 μSTRAIN/DIV
TIME: 1.0 ms/DIV
MASS: 0.000086 lb-s^2/in.
VELOCITY: 833 in./s
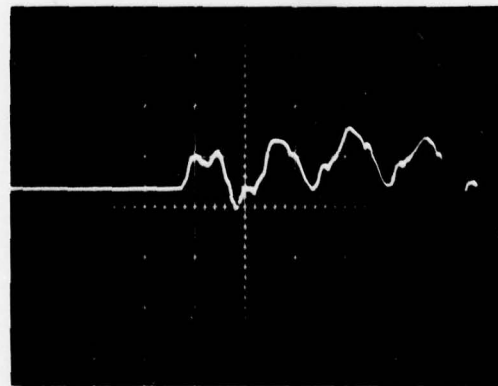
TEST (4 IS)

STRAIN: 1000 μSTRAIN/DIV
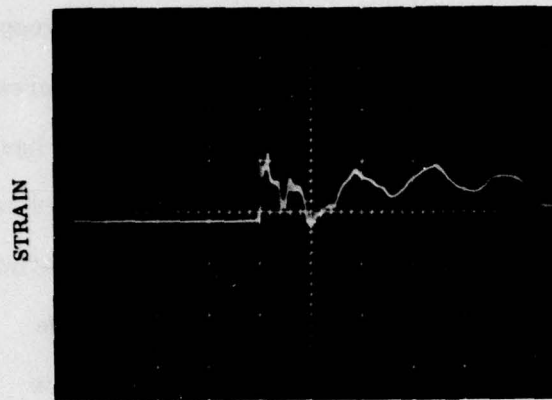TIME: 1.0 ms/DIV
MASS: 0.000086 lb-s^2/in.
VELOCITY: 882 in./s

STRAIN

TIME ⟶

Figure 5-3. Beam Strain Response Due to Impact with Indiana Sandstone
Projectiles Having Initial Velocities < 900 in./s
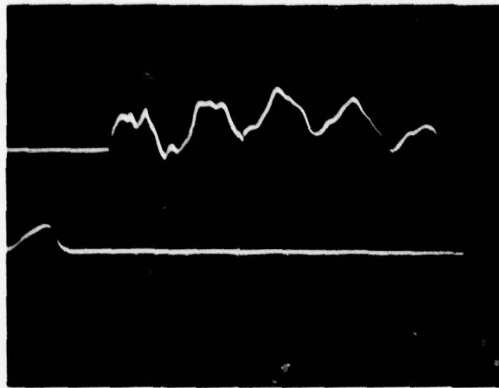
TEST (8 IS)
STRAIN: 1286 μSTRAIN/DIV
TIME: 1.0 ms/DIV
MASS: 0.000088 lb-s^2/in.
VELOCITY: 1184 in./s
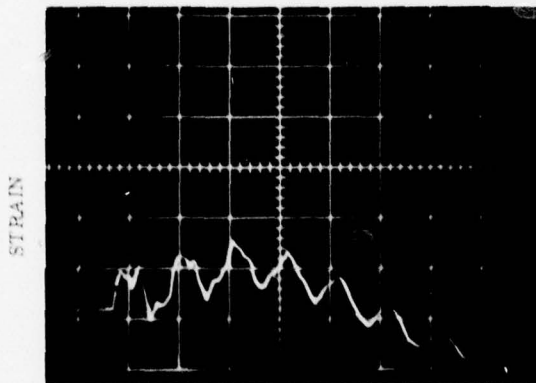
TEST (10 IS)
STRAIN: 1211 μSTRAIN/DIV
TIME: 1.46 ms/DIV
MASS: 0.000084 lb-s^2/in.
VELOCITY: 1128 in./s
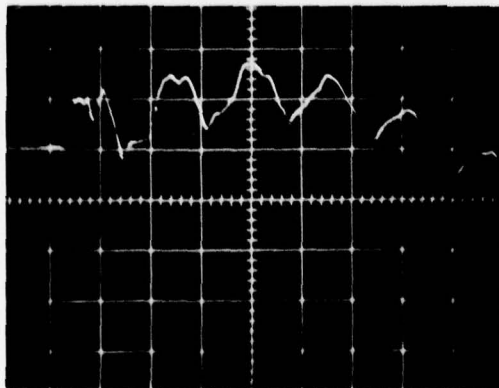
TEST (12 IS)
STRAIN: 1211 μSTRAIN/DIV
TIME: 1.0 ms/DIV
MASS: 0.000090 lb-s^2/in.
VELOCITY: 1658 in./s

STRAIN

TIME ——▶

Figure 5-4.   Beam Strain Response Due to Impact with Indiana Sandstone
Projectiles Having Initial Velocities > 1100 in./s

identical. Indiana sandstone test in the high velocity range is shown in Figure 5-4. Projectiles 8 I.S. and 10 I.S. remained intact after impact while 12 I.S. experienced severe fracturing. The initial kinetic energy of projectile 12 I.S. was twice 8 I.S. and 10 I.S. However, a close comparison of the strain response traces once again shows the basic mechanical signature of Indiana sandstone.

5.2 PROJECTILE INITIAL KINETIC ENERGY VS BEAM STRAIN ENERGY

The deflection of a simply supported beam which experiences central impact can be obtained by the superposition of the normal modes of vibration. The deflection of the beam at a time of maximum displacement in the first mode is given by,

$$y = A_1 \sin \frac{n \pi x}{\ell} \tag{5-1}$$

where A_1, is the modal amplitude of the first mode, and l is the length of the beam. Strain energy U_1, associated with this mode is given by,

$$U_1 = \int_0^1 \frac{M^2 dx}{2EI} = \int_0^1 \frac{EI}{2} \left(\frac{d^2 y}{dx^2}\right)^2 dx \tag{5-2}$$

Substituting Equation (5-1) into Equation (5-2) gives,

$$U_1 = \frac{\pi^4 EI}{4\ell^3} A_1^2 \tag{5-3}$$

For the beam used for the experimental work U_1 is found to be:

$$U_1 = 54.28 \, A_1^2 \tag{5-4}$$

Modal amplitude A_1 and extreme fiber strain ϵ_1 are related by:

$$\frac{d^2y}{dx^2} = \frac{\epsilon_1}{C} \qquad (5\text{-}5)$$

The distance from the neutral axis to the extreme fiber is given by C.

Substituting Equation (5-1) into Equation (5-5) and using the properties of the beam used in the experiment gives:

$$A_1 = 263.2\,\epsilon_1 \qquad (5\text{-}6)$$

Using Equations (5-4) and (5-6), strain energies associated with the 1st mode of beam vibration were obtained and plotted as a function of initial projectile kinetic energy. Figure 5-5 shows plot for Indiana sandstone, high strength sandstone, Cold Spring Green Gabbro and the glass sphere 4 GL. The high-speed film displacement data was used to obtain A_1 for projectiles 1G, 2G, 3G, 4GL, 4S, 8S, 11 I.S. and 12 I.S.

The oscilloscope strain records were used to obtain ϵ_1 for projectiles 5S, 6S, 7S, 1 I.S., 2 I.S., 3 I.S., 4 I.S., 6 I.S. and 8 I.S. Although 3rd and 5th mode strain energies are a significant part of the total beam strain energy, these are not included here because of the difficulty in separating them. The intent of data presented in Figure 5-5 is to show relative beam strain energies for impact of the different materials, at least for 1st mode contribution.

For Indiana sandstone projectiles having initial kinetic energies up to 40 in.-lb, only 5% of the energy is absorbed by the beam in the 1st mode. At the higher projectile energies, the energy absorbed almost doubles. For the gabbro projectiles and 4GL, the beam strain energy
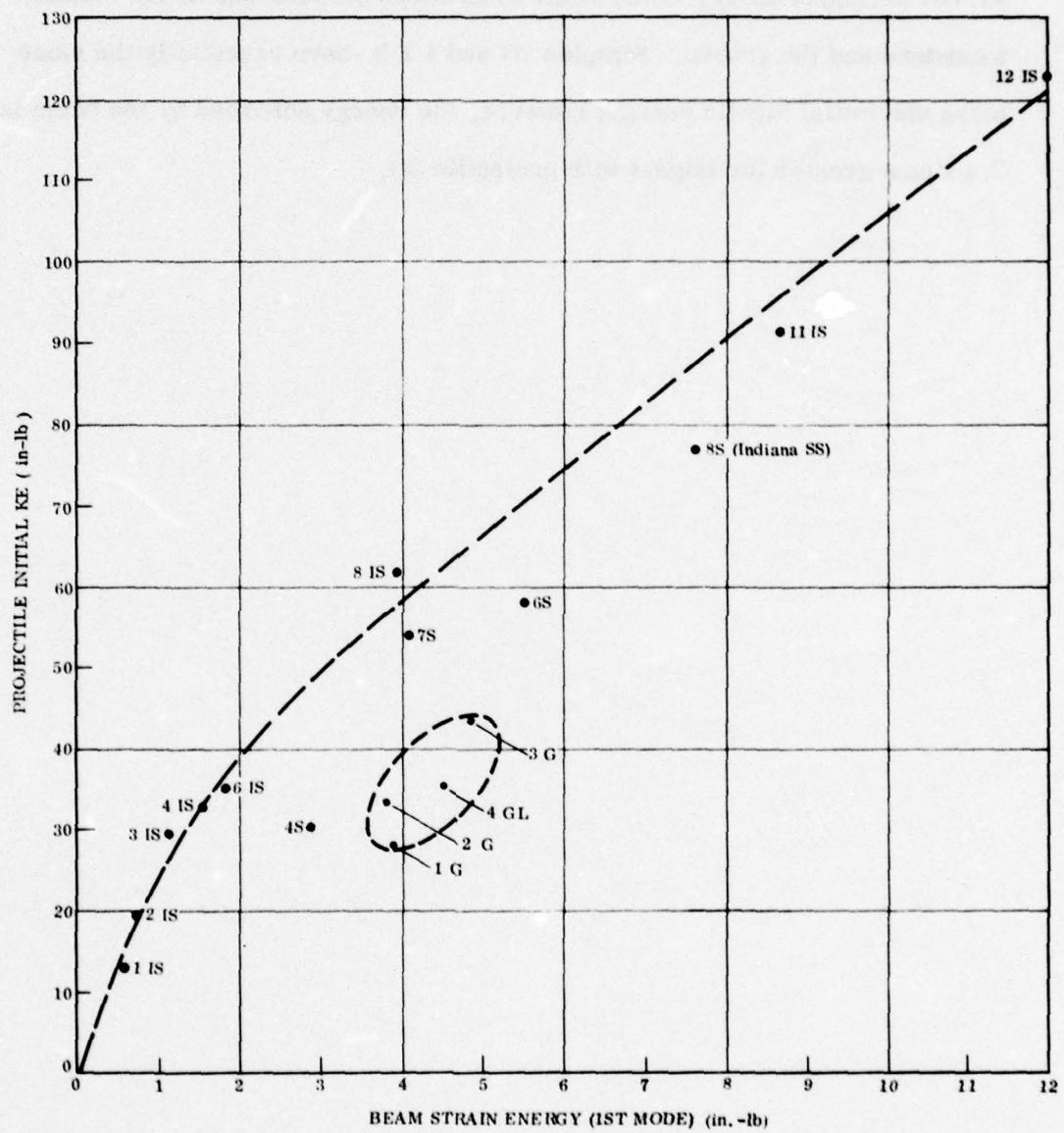
Figure 5-5. Projectile Initial Kinetic Energy vs First Mode, Beam
Strain Energy

is approximately 13%. The high-strength sandstone projectiles can be observed to impart energy to the beam somewhere between that of the Indiana sandstone and the gabbro. Samples 2G and 4 I.S. have essentially the same mass and initial kinetic energy; however, the energy absorbed by the beam is 2.4 times greater for impact with projectile 2G.

SECTION VI

ANALYTICAL MODEL FOR IMPACT OF ROCK DEBRIS WITH A SIMPLY SUPPORTED BEAM

The two preceding chapters, which present experimental data and results, provide some direction in which to proceed in obtaining a force deformation relationship. The mechanical strain signature of the glass sphere 4GL appears to be quite similar to the gabbro 1G, 3G. These projectiles are dissimilar in shape at the impact point; however, they have similar hardnesses and did not fracture as a result of the impact. During the first 100 μs from the initial contact both have extremely large strains. For projectiles having the same initial kinetic energy, the localized craters appear to be similar with regard to size. Undoubtedly, a significant amount of energy goes into the localized permanent deformation of each contact plate.

The Hertz Law of Contact[10] is a force deformation relation which was developed to describe the static deflection of two elastic bodies having regular shapes (spheres, cylinders, plane surface). This force deformation law is given by $F = k_2 a^{3/2}$, where a is the approach of two bodies and represents the maximum relative compression of the bodies. Other laws have been developed in an effort to account for plastic contact indentation. One such law is the Meyers Law,[10] given by $F = \bar{N} a^{\bar{n}}$, where (a) is the permanent crater radius and $\bar{N}$ and $\bar{n}$ are constants which depend on the radius of a contacting sphere and the material properties of the contacting bodies.

---

[10]Goldsmith, Werner, Impact, the Theory and Physical Behavior of Colliding Solids, (London: Edward Arnold Ltd., 1960), pp. 82-92.

The development of a load indentation law that can readily treat a variety of projectile shapes must be based on experimental test data for each shape of interest. The impact behavior of an irregular-shaped rock projectile with a simply supported beam can be determined if one can model the impact by means of a nonlinear contact spring at the point of impact between the two bodies. The question of impact plate strain rate sensitivity must be addressed in determining the acceptability of static load indentation data which can readily be obtained. Hot-rolled mild steel is known to be highly strain rate sensitive. However, the material used in this investigation, 6061T6 aluminum, is believed to be essentially strain rate insensitive.[11]

The work which follows will describe procedures which have been developed for predicting impulse, localized permanent deformation and dynamic response of a beam impacted with both nonfracturing and fracturing projectiles.

6.1 COMPUTER MODEL FOR IMPACT OF A NONFRACTURING PROJECTILE WITH AN ALUMINUM SIMPLY SUPPORTED BEAM

A simply supported beam can be described as a distributed mass system having an infinite number of degrees of freedom. If one can determine the mode shapes and frequencies of a beam with given boundary conditions, then the system can be considered as being equivalent to a discrete mass system. Modal superposition analysis which has been applied to discrete parameter systems can also be applied to distributed mass systems, because the

---

[11] Jones, Norman, A Literature Review of the Dynamic Plastic Response of Structures, "The Shock and Vibration Digest", Vol. 7, No. 8, August 1975, pp. 89-105.

generalized coordinates of a system are the amplitudes of the modal masses.[12]
For a simply supported beam, the generalized coordinate for each mode of
vibration is usually taken at the center of the beam. The total motion of the
beam center at any time is the sum of the modal contributions.

The "component element method" computer program,[13] entitled
"Dynamics of a Many Degree of Freedom System," was used to determine the
dynamic response of a simply supported beam due to impact of rock debris
projectiles. This finite difference program can compute the dynamic re-
sponse of a system having up to 65 degrees of freedom.

The basic elements of any dynamic system are the mass or inertial
properties, the internal force elements and the generalized coordinates.
In a dynamic system, the generalized mass could be a point mass, an inertia
or a modal mass. The component elements in this program are the springs,
dampers, stops and frictional elements which connect the generalized masses
to one another or to a support. Each element has a coupling ratio which
facilitates the connection to each generalized mass. The component elements
provide for setting up equations of motion for each generalized mass that are
uncoupled. The generic name "component element" is derived from the man-
ner in which the elements are selected and the means of developing the equa-
tions of motion by the use of coupling ratios.

[12]Clough, Ray W., Penzien, Joseph, Dynamics of Structures, (New
York: McGraw-Hill Book Co., Inc., 1975), p. 328.
[13]Levy, Samuel, Wilkinson, John P.D., The Component Element Method
in Dynamics, (New York: McGraw-Hill Book Co., Inc., 1976), pp. 139-147.

The characteristic mode shape for a simply supported beam is given by: [12, 13, 14]

$$\phi_n(x) = \sin \frac{n \pi x}{\ell} \tag{6-1}$$

where

ℓ = the length of the beam

$n = 1, 2, \ldots, \infty$

The associated natural frequency is given by:

$$\omega_n = \frac{n^2 \pi^2}{\ell^2} \sqrt{\frac{EI}{m}} \tag{6-2}$$

where EI is the flexural rigidity of the beam and m is the mass intensity.

The total deflection of the beam can be obtained by modal superposition as:

$$y(t, x) = \sum_{n=1}^{\infty} A_n(t) \phi_n(x) \tag{6-3a}$$

where $A_n(t)$ is the modal amplitude or generalized displacement of the nth mode. In the case of a simply supported beam

$$y(t, x) = \sum_{n=1}^{\infty} A_n(t) \sin \frac{n \pi x}{\ell} \tag{6-3b}$$

[12] Clough, Ray W., Penzien, Joseph, Dynamics of Structures, (New York: McGraw-Hill Book Co., Inc., 1975), p. 328.

[13] Levy, Samuel, Wilkinson, John P. D., The Component Element Method in Dynamics, (New York: McGraw-Hill Book Co., Inc., 1976), pp. 139-147.

[14] Biggs, John M., Introduction to Structural Dynamics, (New York: McGraw-Hill Book Co., Inc., 1964), p. 154.

From the Lagrange equation it can be shown, that for an undamped beam acted upon by an external dynamic force $p(t, x)$, the modal equation of motion is given by:[12]

$$\ddot{A}_n(t) \int_0^{\ell} m(x)\, \phi_n^2(x)\, dx + A_n(t) \int_0^{\ell} \phi_n(x)\, \frac{d^2}{dx^2} \left(EI\, \frac{d^2 \phi_n}{dx^2} \right) dx$$

$$= \int_0^{\ell} \phi_n(x)\, p(x,\, t)\, dx \qquad\qquad\qquad (6\text{-}4)$$

This equation of motion has exactly the same form as that of a one degree of freedom system.

The coefficients can be expressed as generalized parameters of the system as follows:

$$M_n = \int_0^{\ell} m(x)\, \phi_n^2(x)\, dx \qquad \text{(Generalized Mass)} \qquad (6\text{-}5)$$

$$P_n(t) = \int_0^{\ell} p(x,\, t)\, \phi_n(x)\, dx \qquad \text{(Generalized Force)} \qquad (6\text{-}6)$$

$$K_n = \int_0^{\ell} \phi_n(x)\, \frac{d^2}{dx^2} \left(EI\, \frac{d^2 \phi_n}{dx^2} \right) dx \qquad \text{(Generalized Spring)} \qquad (6\text{-}7)$$

[12]Clough, Ray W., Penzien, Joseph, Dynamics of Structures, (New York: McGraw-Hill Book Co., Inc., 1975), p. 328.

Figure 6-1 shows a schematic or computer model for the central impact of a simply supported beam. The model illustrated is that of a six degree of freedom system; one degree of freedom for the projectile and the first five odd modes of the beam. The projectile motion is given by the generalized displacement Z_1. The projectile mass is connected to all beam modal masses by means of a series of "stop" component elements. This series of stop elements $K_1(Z)$, constitutes a nonlinear spring at the contact point. Generalized masses M_2 through M_6 are the 1st, 3rd through 9th modal masses respectively of the beam. Even mode participation does not exist for the case of central beam loading. The generalized spring stiffness is given by K_2 through K_6 along with C_2 through C_6, the associated viscous damping coefficients. The total deflection at the center of the beam is given by:

$$y = \sum_{i=2}^{6} Z_i \tag{6-8}$$

6.2 MODEL OF NONLINEAR CONTACT SPRING FOR INCREASING LOADING PHASE

A glass sphere projectile 4GL was used as the test case in the development of a computer model. Sample 4GL was selected because its symmetrical shape facilitates the measurement of contact plate indentations. In addition the excellent quality of the 16-mm high speed film, from the impact experiment, provides the accurate measured data with which the analytical model can be compared and evaluated. The impact plate indentation from the 0.859 in. diameter projectile 4GL was 0.0065 in. deep and 0.160 in. diameter. Results of a preliminary static compression test, using the Instron Universal Testing machine, revealed that a maximum compressive force of approximately 3000 lb could produce the same size indentation.
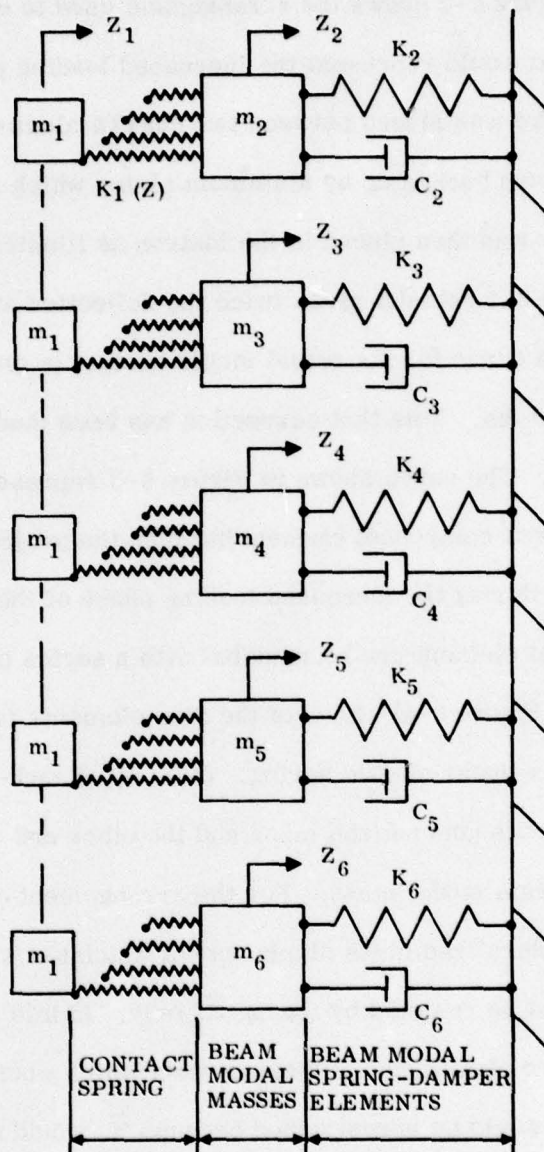
Z_1 : GEN DISP OF PROJECTILE
Z_2 : GEN DISP OF 1st MODE OF VIBRATION OF BEAM
Z_3 : GEN DISP OF 3rd MODE OF VIBRATION OF BEAM
Z_4 : GEN DISP OF 5th MODE OF VIBRATION OF BEAM
Z_5 : GEN DISP OF 7th MODE OF VIBRATION OF BEAM
Z_6 : GEN DISP OF 9th MODE OF VIBRATION OF BEAM

Figure 6-1. Computer Model for Impact of Nonfracturing Projectile
With Aluminum Simply Supported Beam

Figure 6-2 shows the arrangement used to develop a force-deflection curve that would represent the increased loading phase of the actual impact. The sphere was placed between two 6061T6 aluminum contact plates which were in turn backed up by aluminum plates which simulate the beam. This assembly was then placed in the Instron as illustrated. The arrangement shown in Figure 6-2 actually gives twice the deflection at any given load. The force deflection curve for the actual single contact is given Figure 6-3 for loading up to 3000 lbs. Note that correction has been made for the effect of machine stiffness. The curve shown in Figure 6-3 represents the resistance function or nonlinear component element between the projectile and the impact plate of the beam during the increased loading phase of the impact. This nonlinear component element can be modeled with a series of four stop elements as shown in Figure 6-4. Each of the stop elements is characterized by a clearance and a linear elastic spring. One end of each stop element is connected to the projectile generalized mass and the other end of each element is connected to each beam modal mass. For the arrangement of stop elements in Figure 6-4, a generalized mass displacement which tends to compress the elements would first be resisted by spring $\overline{K}_1$ only. In this case, spring $\overline{K}_1$ has an initial zero clearance. A displacement which would tend to elongate the elements would be unrestrained because $\overline{K}_1$ would now develop a clearance.

0.250 in. X 1 in. X 2 in. PLATE

0.125 in. X 1 in. X 1 in. CONTACT PLATE

0.859 in. DIA GLASS SPHERE

INSTRON MACHINE HEAD

BED
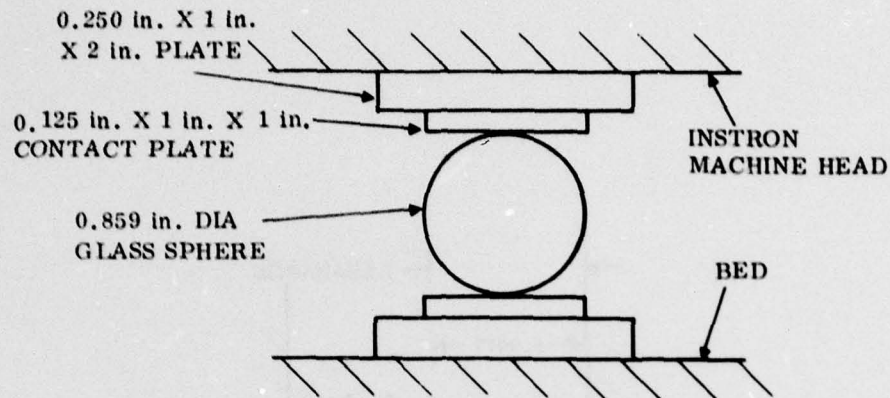
Figure 6-2.   Experimental Configuration Used in Compression Test to Develop Force-Deflection Data
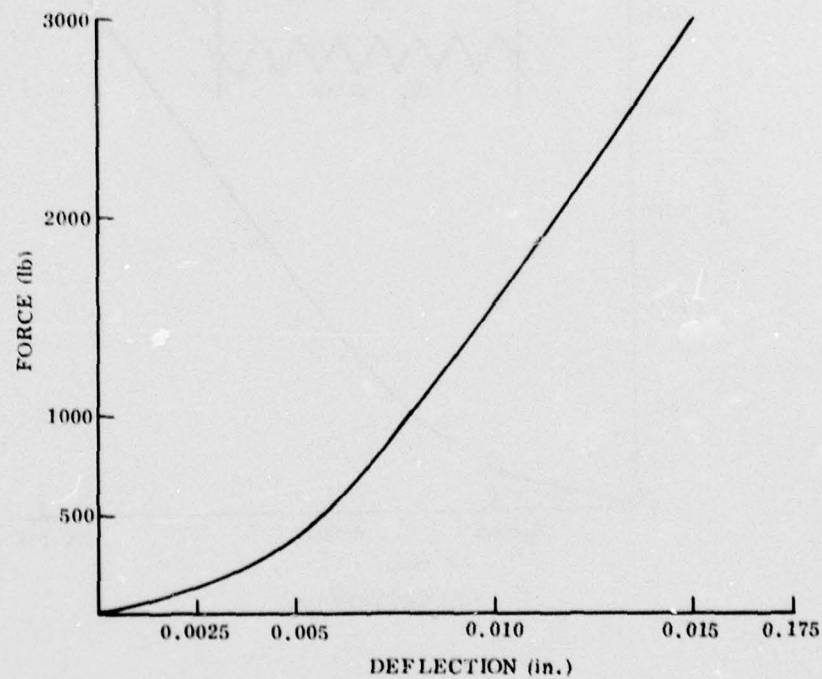
Figure 6-3.   Loading Phase of Glass Sphere Compressed Between 6061T6 Aluminum Plates
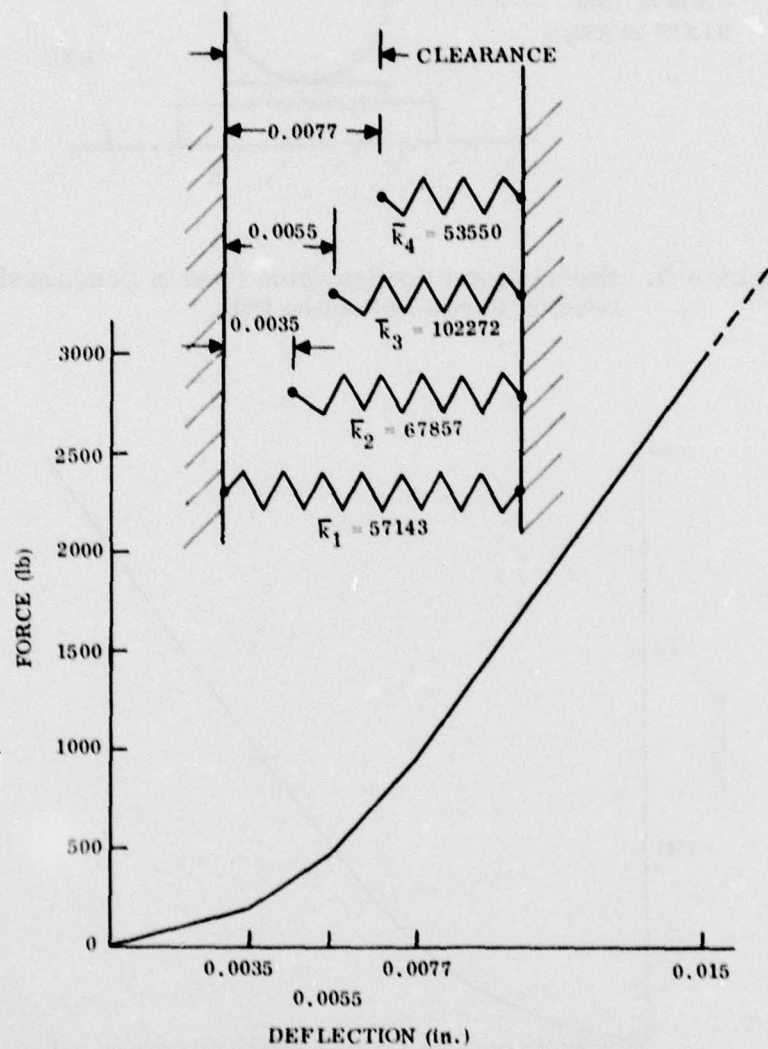
Figure 6-4. Model of Nonlinear Contact Spring for Loading Phase

6.3 COMPUTER INPUT DATA

Input data to the Levy/Wilkinson computer program is given in the appendix for the impact of glass sphere projectile (4GL) with an 18-in. simply supported beam. The computer model for this system is given in Figure 6-1. The input requires specification of the following functions; mass description, time specification, excitation description, initial conditions and force element description.

The mass description includes specification of the projectile mass and each of the beam modal masses. The time variables are the time step for the numerical analysis, total time of the computer run and the desired time step for printing the output data.

In this program, it is possible to impose a number of different excitations on the system including displacement-time histories, force-time histories, as well as sinusoidal forcing and displacement functions.

The initial conditions function provides for specification of initial displacement and initial velocity of each generalized coordinate. For the computer model in Figure 6-1, the projectile was given an initial velocity of 854 in./s.

The force element description enables one to specify "spring-damper" elements which in this case are the generalized springs associated with each modal mass. The damping coefficients were determined from vibration decay data obtained from the 16-mm film. Decay of peak amplitude is shown in Figure 6-5. The masses to which force elements are connected are also specified within this description.
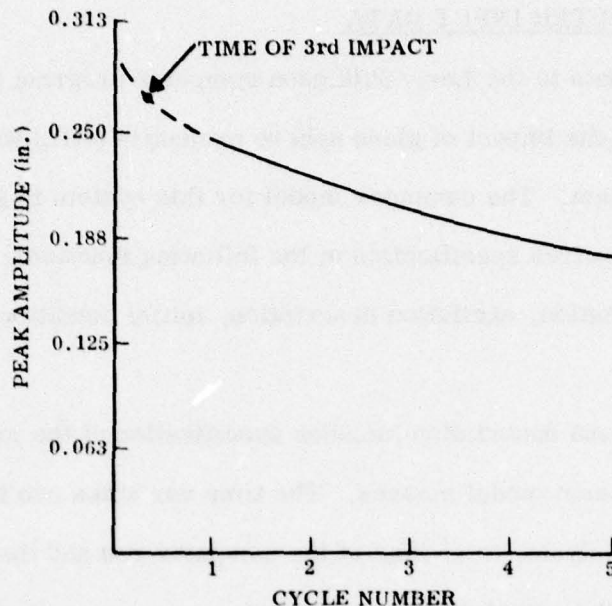
Figure 6-5. Natural Decay of Peak Amplitude of Beam Vibration From
Film Data of (4GL) (Logarithmic Decrement $\delta = 0.0889$,
Damping Factor $\zeta = 0.0141$)

The nonlinear contact spring connecting the projectile with the beam is
specified using "stop" force elements. Each "stop" element is defined by
specifying a clearance and a spring stiffness.

6.4 SYSTEM RESPONSE AT TIME OF MAXIMUM CONTACT FORCE BETWEEN PROJECTILE AND BEAM

The maximum contact force between the projectile and beam is 3219 lb,
and occurs at time $t = 0.027$ ms. The increasing load profile, starting from
the time of initial contact, is illustrated in Figure 6-6. The contact force
time curve was obtained from the computer output data. At time $t = 0.027$ ms,
the projectile and beam have reached the same velocity. During this loading
phase or approach period, the velocity of the projectile is reduced from 854 to

378 in./s. A summary of generalized coordinate displacement and velocity is given in Table 6-1. The total displacement at the center of the beam is 0.003098 in. This is the algebraic sum of the displacement of the separate modal masses.
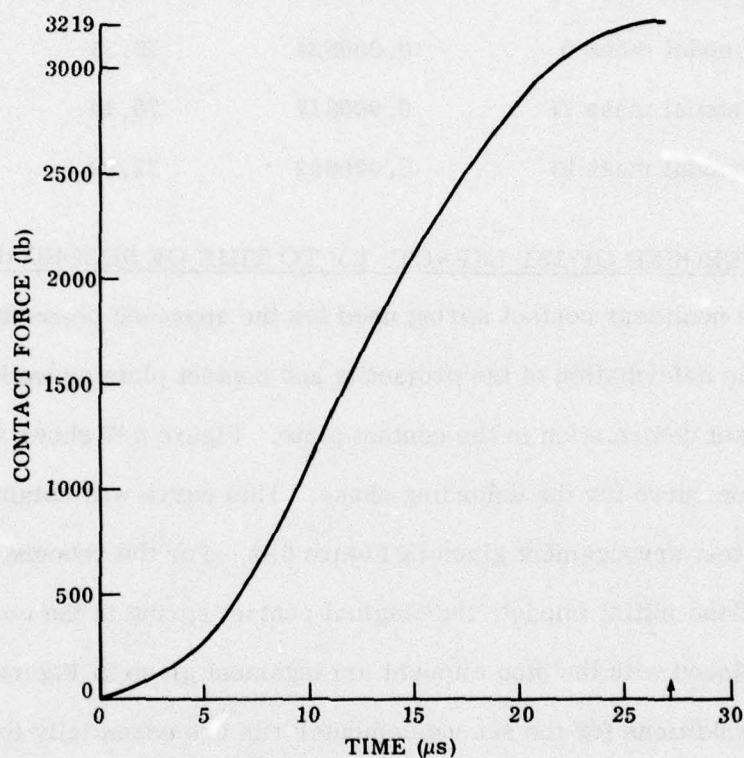
Figure 6-6. Contact Force vs Time During Impact Loading Phase

TABLE 6-1. SYSTEM RESPONSE AT TIME t = 0.027 ms

Generalized Coordinate	Displacement (in.)	Velocity (in./s)	Contact Force (lb)
1 (projectile)	0.018879	378.11	
2 (modal mass 1)	0.000628	77.25	
3 (modal mass 3)	0.000627	77.12	3219
4 (modal mass 5	0.000624	76.61	
5 (modal mass 7)	0.000617	75.14	
6 (modal mass 9)	0.000602	71.99	

6.5 REBOUND OF 1ST IMPACT, UP TO TIME OF SECOND IMPACT

The nonlinear contact spring used for the approach phase included the effect of elastic deformation of the projectile and contact plate as well as the localized permanent deformation in the contact plate. Figure 6-7 shows the load-deflection curve for the unloading phase. This curve was obtained from the Instron test arrangement given in Figure 6-2. For the rebound or unloading phase of the initial impact, the original contact spring in the computer model was replaced with the stop element arrangement given in Figure 6-8. The initial conditions for the second computer run are essentially those given in Table 6-1. The one exception is that the projectile generalized displacement was changed to 0.010768 in. This initial displacement is the sum of the modal mass displacements in Table 6-1 and initial compression required in the stop elements to develop a contact force of 3219 lb.
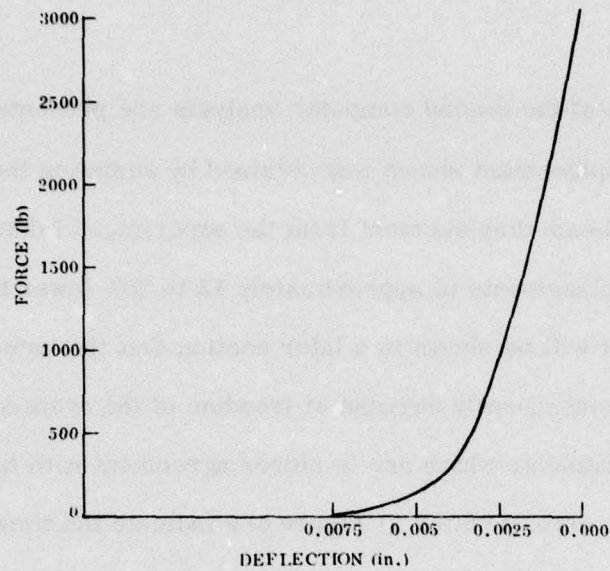
Figure 6-7. Unloading Phase of Glass Sphere Initially Compressed Between 6061T6 Aluminum Plates
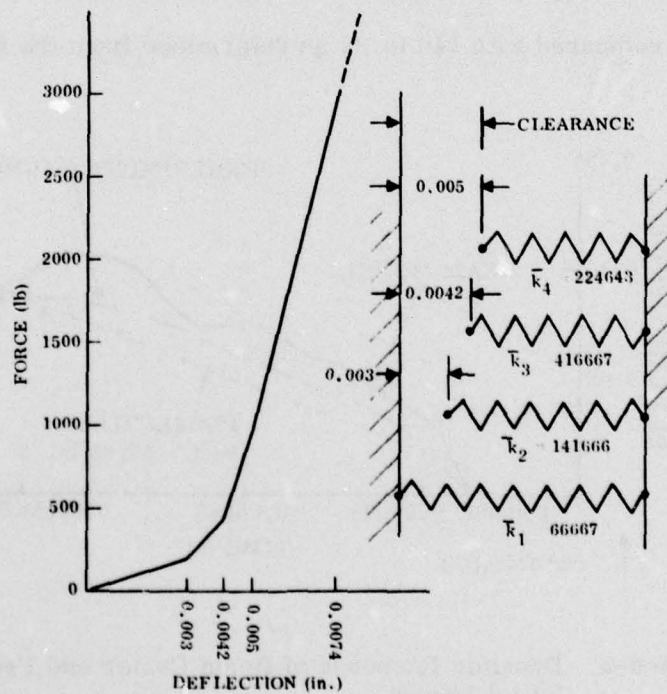
Figure 6-8. Model of Nonlinear Contact Spring for Unloading Phase

Results of the second computer analysis are presented in Figure 6-9. The beam displacement shown was obtained by summing the modal displacements. The beam displacement from the experimental data for sample 4 GL indicates displacements of approximately 15 to 20% lower than those given by the model. It will be shown in a later section that the inclusion of more modal masses and consequently degrees of freedom of the system will give computer model displacements which are in closer agreement with the measured results. The arrows shown in Figure 6-9 indicate the time at which a second impact occurs. One can observe that the impact times between experiment and model are fairly close. The starting time of second impact is mainly influenced by the constant velocity of the projectile following the initial impulse. The projectile velocity from the computer model is 96 in./s compared with 140 in./s as determined from the film data.
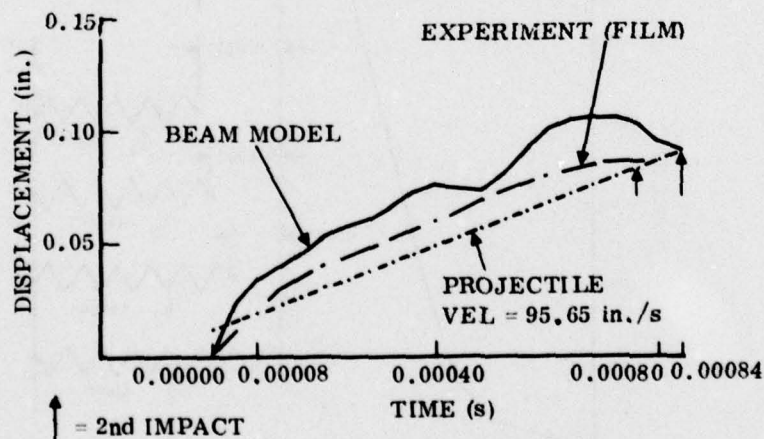
Figure 6-9. Dynamic Response of Beam Center and Projectile Following Initial Impact

Contact between the projectile and beam lasted for 20 μs during the
rebound phase. The rebound time is considerably shorter than the approach
time of 27 μs. The energy dissipated during the first impact is given by the
area enclosed between approach and rebound force-deflection curves given
in Figure 6-10. The energy which went into contact plate identation was
calculated from Figure 6-10 and found to be 11.5 in.-lb. This dissipated
energy is approximately 33% of the initial kinetic energy of the system.
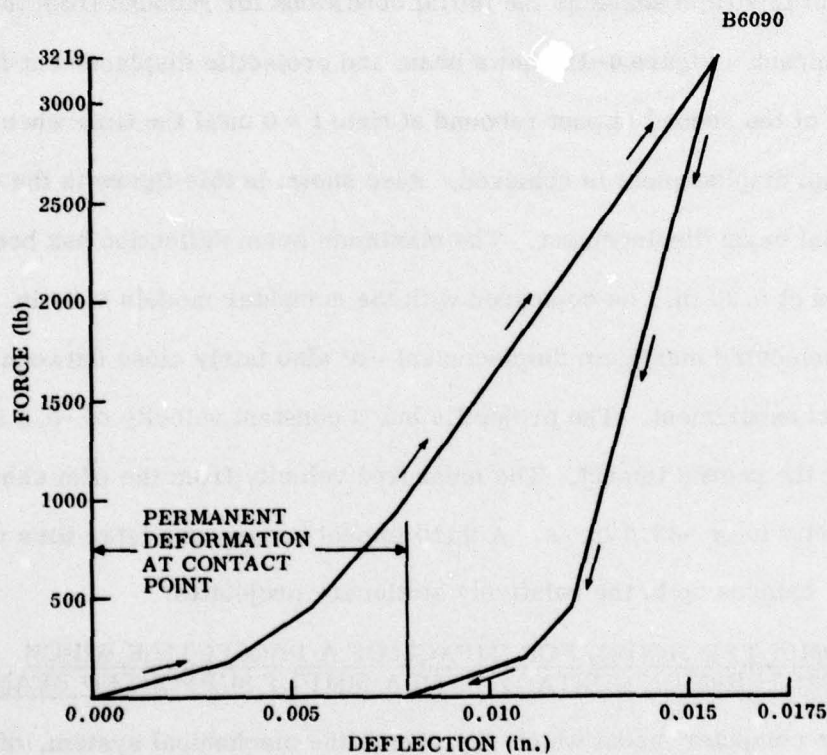
Figure 6-10. Contact Spring Force Deflection During Loading and Unloading
Phase for Computer Model Initial Impact

6.6 SECOND IMPACT RESPONSE

Initial conditions at the start of a second impact are given in Table 6-2. The impulse during the loading phase of this impact is presented in Figure 6-11. The curve given in Figure 6-11 was obtained from a third computer run for this impact problem. Time $t = 0.0$ s in Figure 6-11 is the starting time of the second impact and corresponds to a system response time $t = 0.84$ ms. The maximum contact force from Figure 6-11 is 262 lb and occurs some $32 \mu s$ after initial contact. Projectile and modal mass displacement and velocity at this time serve as the initial conditions for rebound from the second impact. Figure 6-12 shows beam and projectile displacement from the start of the second impact rebound at time $t = 0$ until the time when maximum beam displacement is achieved. Also shown in this figure is the experimental beam displacement. The maximum beam deflection has been measured at 0.30 in., as compared with the computer models 0.34 in. The time of achieving maximum displacement are also fairly close between the model and experiment. The projectile has a constant velocity of -5.0 in/s following the second impact. The measured velocity from the film shows this velocity to be -33.0 in./s. A third impact occurs at a later time when the beam catches up to the relatively stationary projectile.

6.7 COMPUTER MODEL FOR IMPACT OF A PROJECTILE WHICH FRACTURES ON CONTACT WITH A SIMPLY SUPPORTED BEAM

The computer model which represents the mechanical system, of a projectile which fractures on impact with a beam, is essentially the same model that was presented in Figure 6-1 for a nonfracturing projectile. The only change is that an entirely different contact spring is required to represent the resistance function between the colliding bodies.

TABLE 6-2. SYSTEM RESPONSE AT TIME t = 0.84 ms

Generalized Coordinate	Displacement (in.)	Velocity (in./s)	Contact Force (lb)
1 (projectile)	0.092276	95.65	
2 (modal mass 1)	0.101920	115.50	
3 (modal mass 3)	−0.006329	−117.90	0
4 (modal mass 5)	0.001010	−91.27	
5 (modal mass 7)	−0.002300	13.3	
6 (modal mass 9)	−0.002025	−47.7	
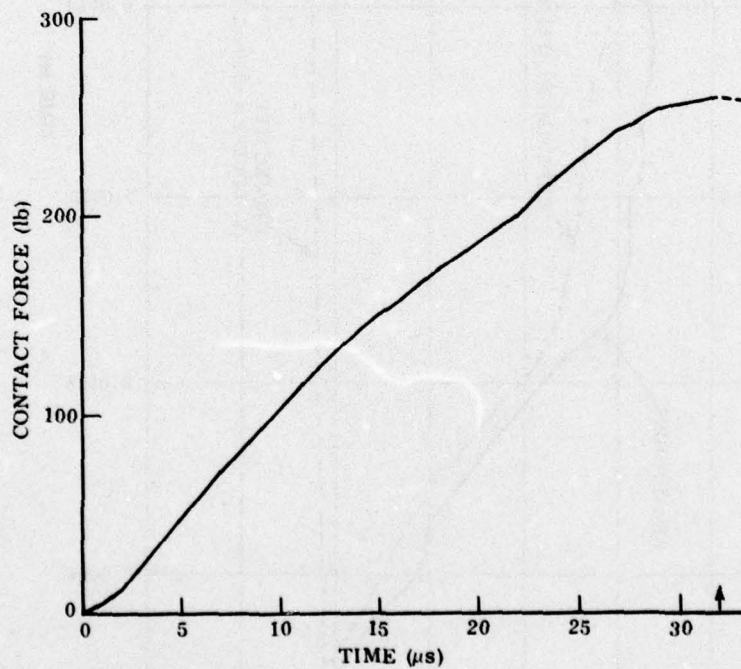
Figure 6-11. Contact Force vs Time During Second Impact Loading Phase
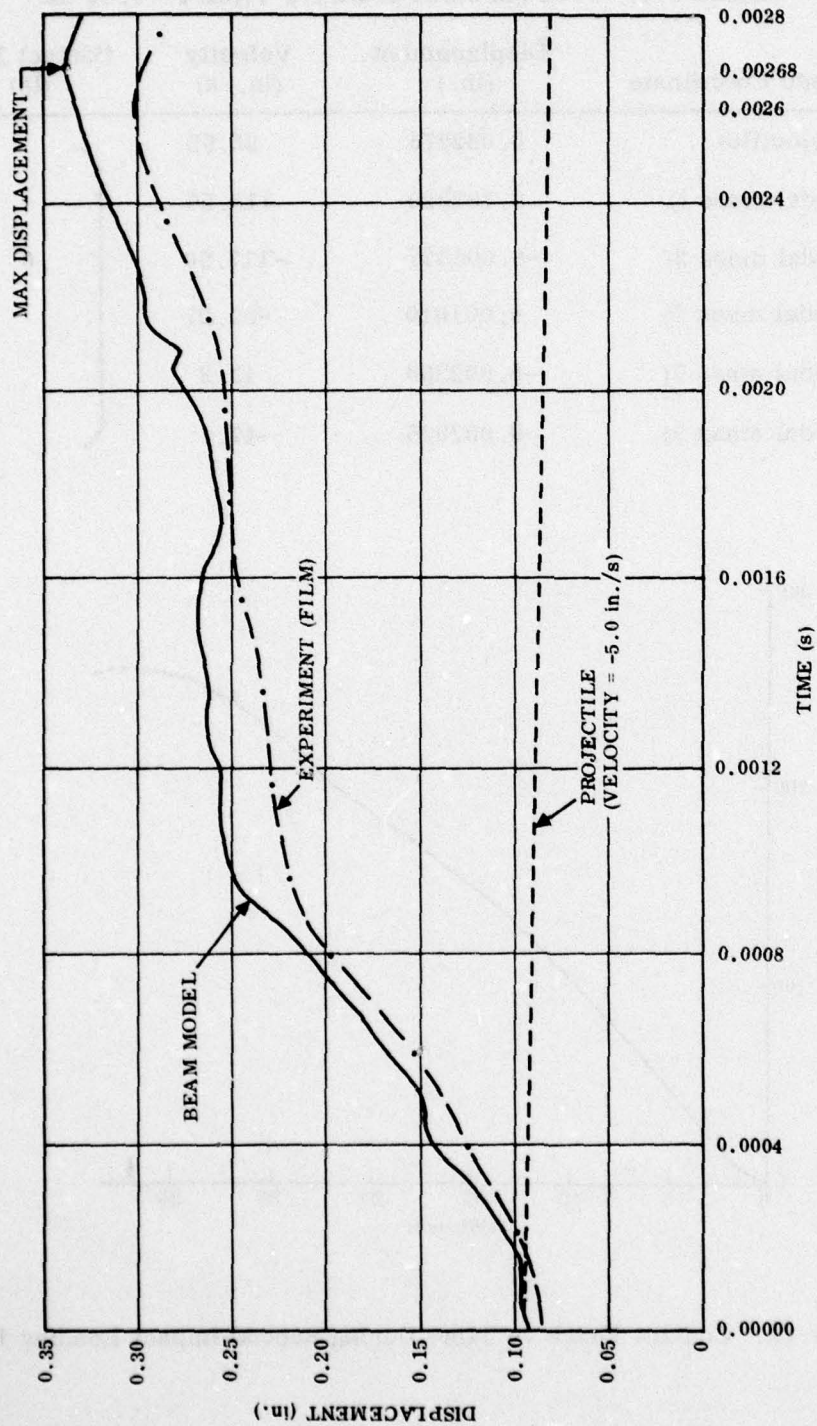
Figure 6-12. Dynamic Response of Beam Center and Projectile Following Second Impact

Load displacement data, from static tests on samples of Indiana sandstone, are given in Figure 6-13. Both samples had essentially the same size and shape. The mass of samples A and B were 15.45 and 15.39 gms respectively. These samples and the damage imposed on them are illustrated in Figure 6-14. The compression tests were run using the Instron. Each specimen encapsulated in plaster of Paris was placed in the machine with its cylindrical base in contact with the bed and the 0.125-in. contact plate bearing against the machine head. Referring to Figure 6-13a, one can observe that the projectile upon initial loading has a uniformly increasing resistance until reaching a load of approximately 75 lb. For the next 20 mils of displacement there is essentially no change in load carrying capacity, while the localized material in the contact region is being pulverized. During the next 10 mils of displacement, the projectile attains a load carrying capability of 150 lb. Further compression of the sample results in sudden steps of unloading. As compression of the sample continues, one can observe the cyclic nature of loading and unloading. When the sample is loaded to 300 lb at a displacement of 120 mils, a major longitudinal crack forms. This is followed by an unloading to 200 lb and an increase load phase to 375 lb. At this time major fracturing occurs and two large pieces of rock break away from the sample. The pieces are shown at the lower half of the reconstructed sample in Figure 6-14a.

Figure 6-13b shows load displacement data for the sample in Figure 6-14b. This test was conducted to obtain test data with limited displacement, in addition to the minor fracturing experienced during initial phase of loading. Again one can observe the cyclic nature of the loading. Although the load profiles are not the same upon comparison of Figures 6-13a and b, one can observe that the average load during the first 120 mils of displacement is approximately 75 lb in each case.
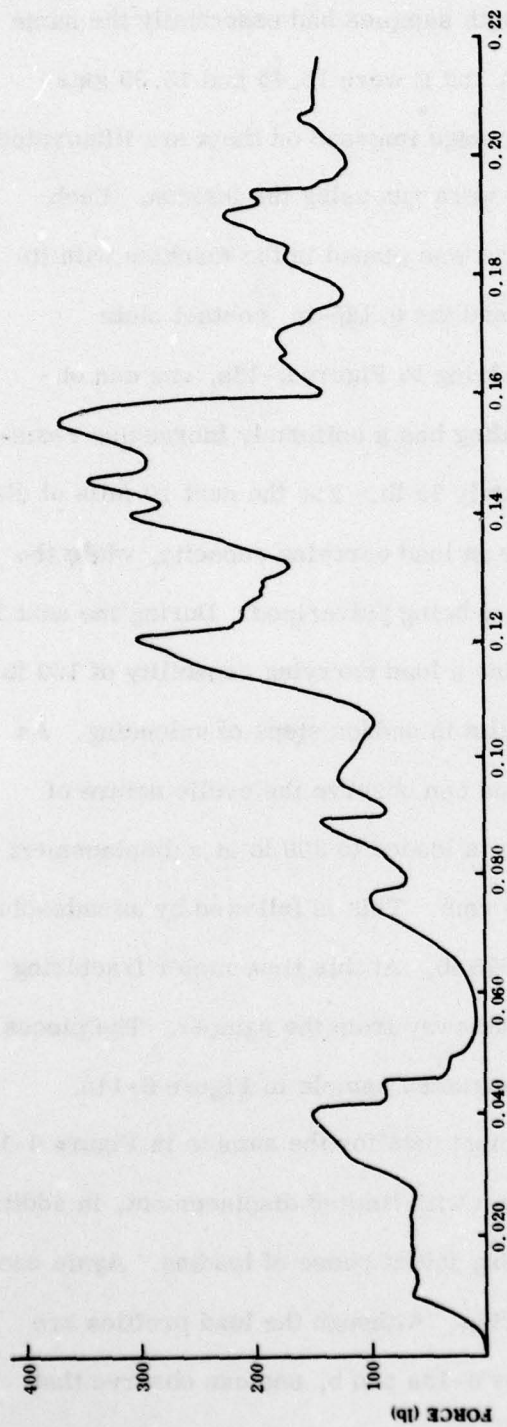
(a) Force Displacement Curve from Static Compression Test on Indiana Sandstone Projectile Sample A
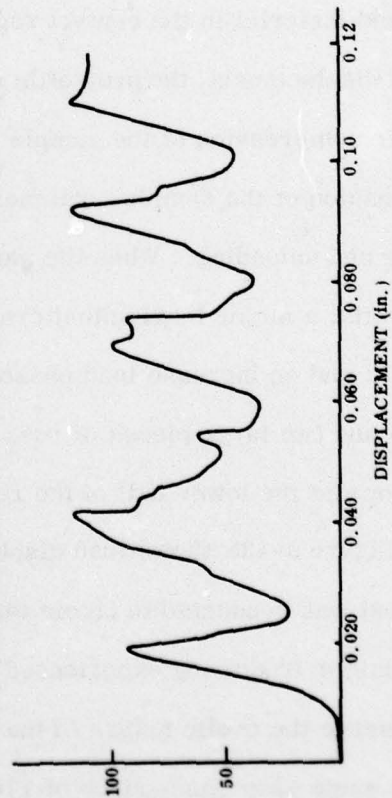
(b) Force Displacement Curve for Projectile Sample B

Figure 6-13. Force Displacement Curves
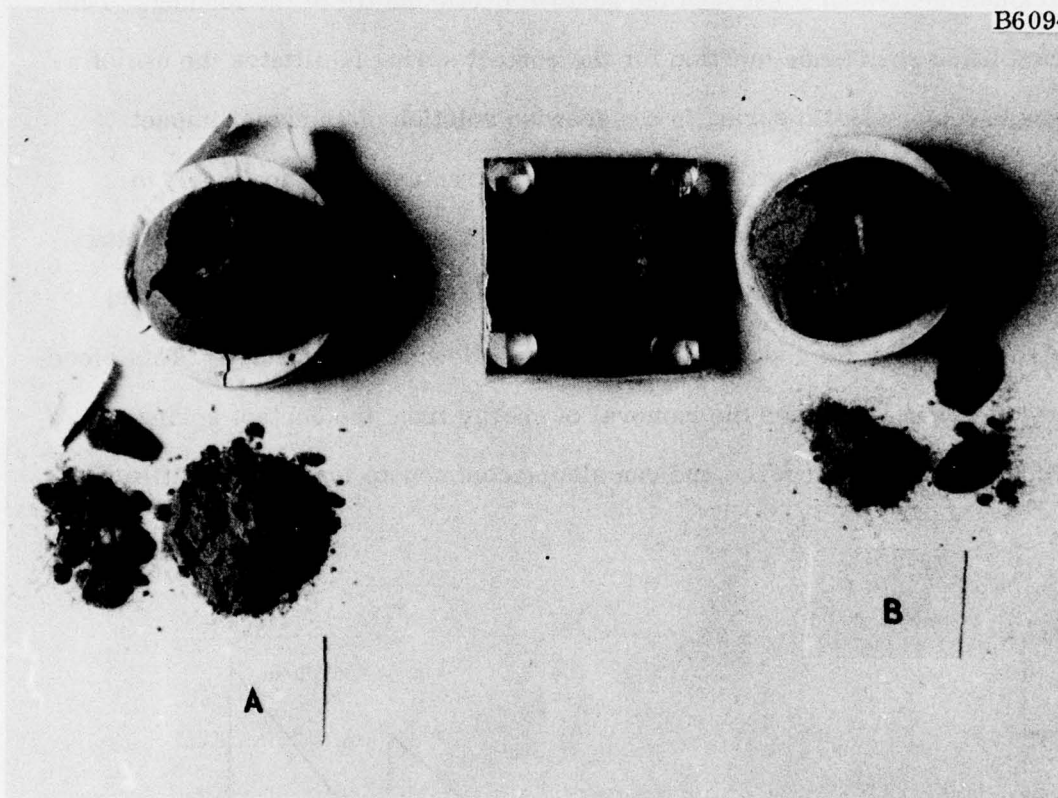
Figure 6-14. Indiana Sandstone Projectiles A and B Following Static
Compression Against 6061T6 Aluminum Plate

A simplified resistance function for the contact spring of Figure 6-13a
is given in Figure 6-15. Although this curve is an approximation, it charac-
terizes the function in that it contains major peak load values at corresponding
displacements and possesses the general cyclic nature of the loading. This
simplified resistance function for the contact spring facilitates the use of a
single linear elastic spring in a piecewise solution of an actual impact
problem. Upon the occurrence of the first fracture indicated by (1) in
Figure 6-15, the energy stored in the contact spring is removed. During
the next phase (1) to (2), the contact spring stiffness can be changed and
also preloaded if a contact force remains following the fracture. This piece-
wise method facilitates the removal of energy from the contact spring,
reduction in contact force and can also accommodate loss of projectile mass.
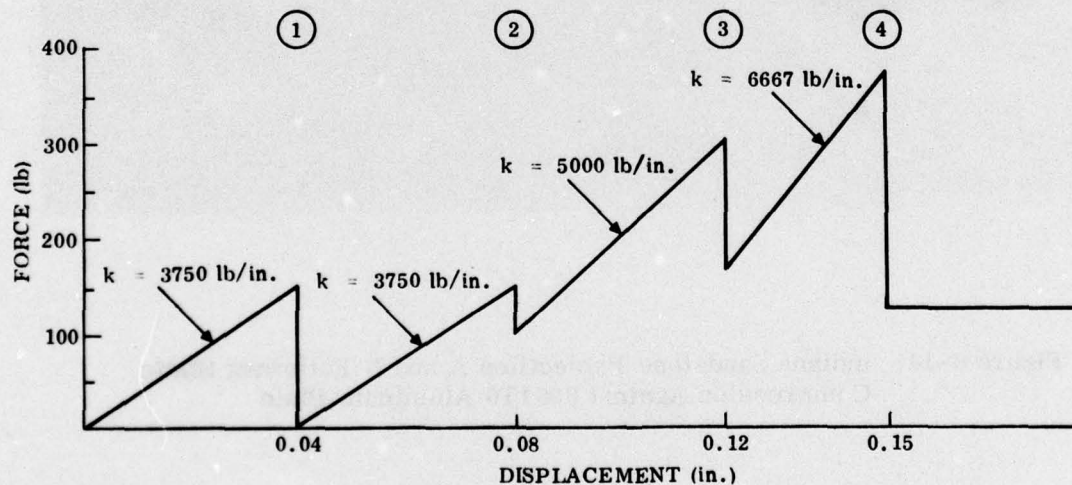
Figure 6-15. Simplified Resistance Function for Indiana Sandstone
Projectile A

6.8 RESULTS OF COMPUTER ANALYSIS FOR IMPACT OF INDIANA SANDSTONE PROJECTILE

A computer analysis was made for the impact of Indiana sandstone with a simply supported beam using the projectile-beam model of Figure 6-1, and the contact spring resistance function given in Figure 6-15. A sandstone projectile having an initial mass of 0.000087 $lb-s^2/in.$ and initial velocity of 900 in./s was selected as a representative model for this analysis. The initial projectile kinetic energy of 35.24 in.-lb is the same as experimental test sample 6 I.S., and can thereby facilitate a comparison. In addition, comparisons can be made with test sample 4 GL which had an initial kinetic energy of 35.37 in.-lb.

Six separate computer runs were required to handle the numerous loading and fracturing phases during the contact period. After each portion of this piecewise solution the mass of the projectile was slightly reduced to compensate for material loss. This reduction was based on data obtained from static load displacement tests. Figure 6-16 shows a system energy balance which includes projectile kinetic energy, beam strain and kinetic energy, contact spring strain energy and contact spring energy loss. This figure summarizes the energy exchanges which take place during the impact process. At time zero the initial KE of the projectile is 35.24 in.-lb, and is the total energy of the system. At station 1 the contact spring strain energy of 2.85 in.-lb is suddenly removed due to rock fracturing. Also, at this time the projectile KE is reduced to 32.33 in.-lb and the beam energy only increases to 0.05 in.-lb. This loading and partial unloading process continues as the contact spring displacement increases. Station 4 shows a number of interesting results. Immediately following the contact spring unloading, the
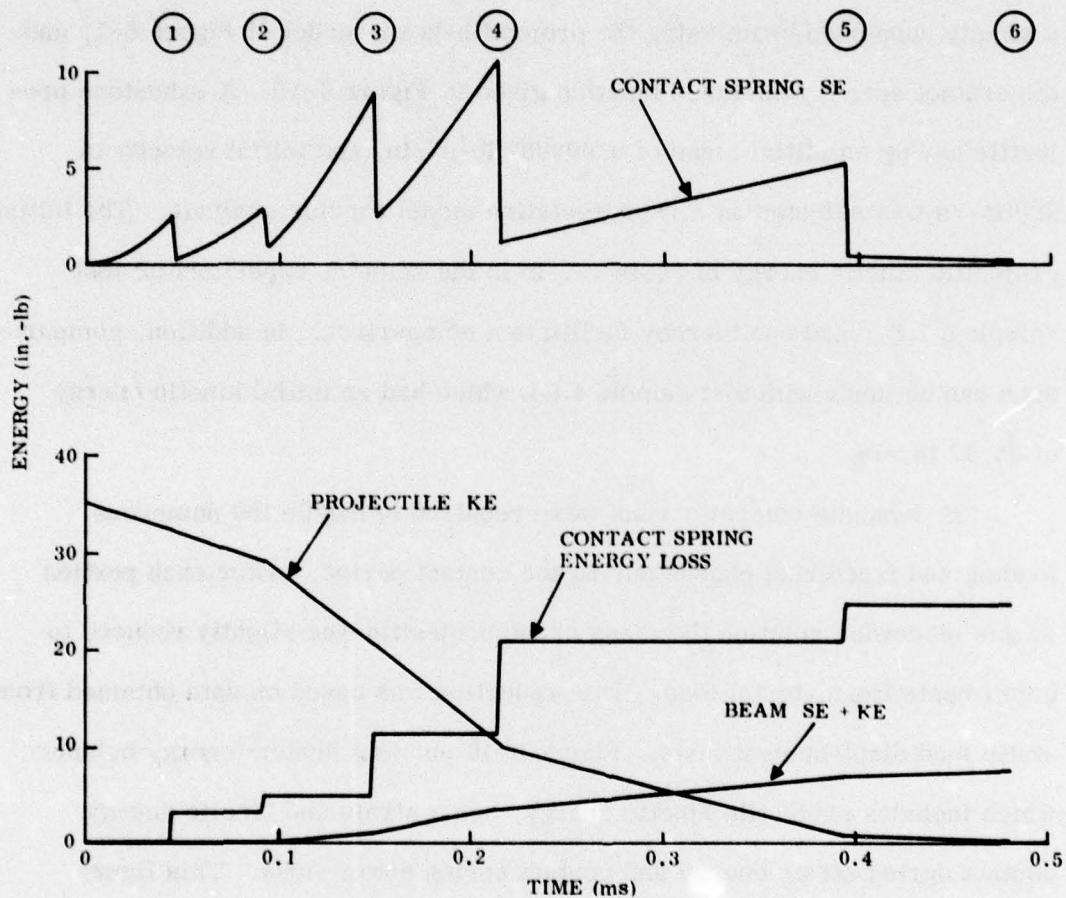
Figure 6-16. Energy Balance for an Indiana Sandstone Projectile and
Simply Supported Beam During Impact Process

energy loss in this spring, which is the system energy loss, has reached

20.74 in.-lb. The total energy of the beam, however, is only 3.42 in.-lb

while the projectile KE has been reduced to 10.0 in.-lb. At this time less than

10% of the system energy has been gained by the beam while almost 60% has

been lost by the system. From station 4 to 6, the force in the contact spring

varies from a maximum of 120 lb to minimum of 0 lb when separation occurs. During this time the beam experienced a large energy increase from 3.42 to 7.77 in.-lb, while the contact spring energy only increased from 20.74 to 24.42 in.-lb.

At the time of projectile-beam separation, the system energy distribution from this analysis indicates that 69.3% is in contact spring energy loss, 22.0% in beam vibrational energy, 0.03% in projectile KE and 8.67% in KE of particles which broke away from the projectile. The contact spring energy loss consists of rock fracturing and permanent deformation of the contact plate. Examination of the contact plate used in developing the resistance function in Figure 6-13 shows negligible indentation. This should be expected since the maximum contact force was only 370 lb. It is reasonable to suggest therefore that the major system energy loss can be attributed to the rock fracturing processes.

Figure 6-17a gives the strain response of the beam for test 16 I.S. The test projectile has exactly the same initial kinetic as the projectile in the computer model. Figure 6-17b presents the strain response which was derived from the generalized displacement from the six computer runs. Note that stations (1) through (6) corresponds to those identified in Figure 6-16. A comparison between the measured dynamic strain response with that obtained from the six degree of freedom model shows fairly good agreement. The peak strain values that occur within the first 1.0 ms following contact agree to within 20% while those that occur at 3.7 ms are within 30%. These differences between the measured and modeled results could be decreased by adding more modal degrees of freedom to the system. A comparison of the general characteristic shape between the measured and modeled response is excellent.

6-27
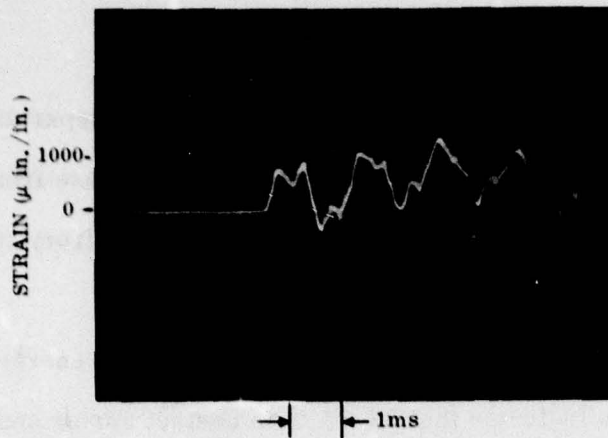
(a) Experimental Strain Response
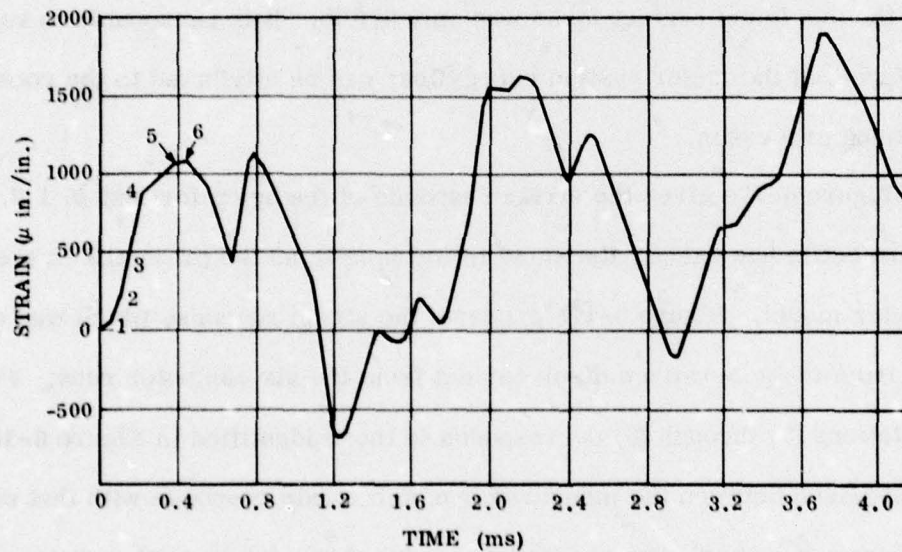
(b) Computer Model Strain Response

Figure 6-17. Comparison Between Experimental and Analytical Strain Response

SECTION VII

DISCUSSION AND CONCLUSIONS

7.1 EXPERIMENTAL WORK

The experimental investigation has provided both expected and un-expected results. Some rock projectiles fracture on impact and impose negligible damage on the beam contact surface. Some fracture and leave material embedded in the beam, while others remain intact and cause localized permanent deformation.

What "impact" does the rock debris study have on the design of a hardened radar structure? This question can be answered by simply summarizing the behavior of each of the three rock materials treated in this investigation. Of all the rock materials investigated in this study, Indiana sandstone having a compressive strength of approximately 4000 psi will impose minimal damage on the structure. For the projec-tile size and initial velocities achieved in the experimental work with this material , superficial-surface deformation can be expected with minimum energy imparted to the structure. The fine grained sandstone with a com-pressive strength of 11400 psi does, however, pose a potential problem. A conical mound of embedded sandstone 0.28-in. in diameter pro-jecting 0.01-in. above the beam surface resulted from an impact with projectile 5S. This projectile had an initial velocity of 1104 in/s prior to impact. A greater build up of embedded material is expected from rocks larger than 1 in. size used in the experiment and having an equivalent or greater velocity. Mounds of this material, known to be almost pure quartz, in effect can be thought of a dielectric material embedded in an electrical

ground plane. The dielectric constant of this sandstone $(S_i O_2)$ is 3.8. A build up of this material between antenna elements, which are attached to the ground plane, will tend to reduce the maximum scan angle of the array due to the formation of grating lobes or secondary beams. This dielectric material may also degrade the impedance matching of the antenna elements, which would result in a reduction of the range capability of the radar.

Gabbroic rock projectiles having initial kinetic-energies comparable with the sandstones, imposed the greatest mechanical damage on the beam. The effect of deeper indentations and more energy imparted to the structure, may be of secondary importance in comparison to the embedding of the fine grained, high strength sandstone.

The test apparatus developed for the experimental study performed extremely well. The air gun is capable of firing 1 in. projectiles at velocities greater than 4000 in./s. The projectile velocities were, however, limited to 1640 in./s, because of the strength capability of the 0.250 x 1.00 x 18.00 in., 6061T6 aluminum beam used in the experiment. The apparatus can accommodate beams up to 30.00-in. in length. If such beams are used in future work, the protective enclosure would have to be modified to facilitate larger beam displacements.

Encapsulation of rock projectiles in plaster of Paris appears at this time to be the best scheme for controlling projectile velocity and trajectory. For the majority of rocks encapsulated, the plaster of Paris represented approximately 20% of the total projectile mass. For future testing, attempts should be made to further reduce the encapsulating material. This could be accomplished by making cylindrical cores having a 0.90-in. diameter and then cutting the desired shape at the impact end of each cylinder.

The storage oscilloscope, which contained a Type 3A74 four-trace amplifier, was used to record one channel of strain gage data and two channels of photocell data. This method of data recording was used when testing without high speed filming. The strain gage output was somewhat discontinuous, as shown in Figure 5-3 for test 1 I.S. Strain response is best when using a single channel. It is therefore recommended that future testing be performed using two oscilloscopes, one for the photocell data and another for a single channel of strain response.

7.2 COMPUTER IMPACT MODELS

The component element method computer program provided the means of treating this complex impact problem. A six degree-of-freedom model was developed which considered the first five odd modes of vibration. A second model which contained six modes of beam vibration was also evaluated. The additional mode was added to study the system response and show that a larger number of normal modes of vibration would give results which would be in closer agreement with the experimental results.

The ability of the computer model to adequately represent the actual impact process is greatly dependent on the specification of the nonlinear stop element parameters. This contact spring is the critical element in the computer model of the dynamic system. The nonlinear contact spring between the projectile and beam was based on static load-deflection data. The use of four stop elements in parallel provided the mechanism of approximating the nonlinear resistance function for the case of nonfracturing irregular shaped projectiles.

Results of computer output were compared in Section VI and found to be in reasonable agreement with experimental results. In all cases, beam displacement response from the computer model was always greater than the measured response.

Maximum displacement variations between experiment and model were approximately 15 to 20% for the glass sphere 4 GL. This difference could possibly be decreased by including more degrees-of-freedom of the beam in the model. However, if one intends to use the results for design purposes, a conservative approach might be to say that the six degree of freedom model is adequate.

A comparison made between a six and seven degree of freedom model showed some rather interesting results. The initial conditions were those for 4 GL. Model 1 included beam modes 1, 3, 5, 7, 9 while model 2 contained beam modes 1, 3, 5, 7, 9, 11. Beam damping was taken as 2.0% of critical. This damping factor was obtained from oscillograph recorder data. A comparison of contact force for both models is given in Figure 7-1. The maximum impact force for model 1 was found to be 3221 lb while that of model 2 was only 3088 lb. The time to peak of model 2 is shown to be 1-μs less than that of model 1. One can observe that the effect of adding one more mode of vibration reduces the impulse a small amount. Also note that the peak force for model 2 seems to more closely approach 3000-lb static force observed to cause the same size indentation in the contact plate. Beam displacements for both models are given in Figure 7-2. From time t = 0 to t = 0.0004 s, the center displacement of model 2 has decreased in

B6098
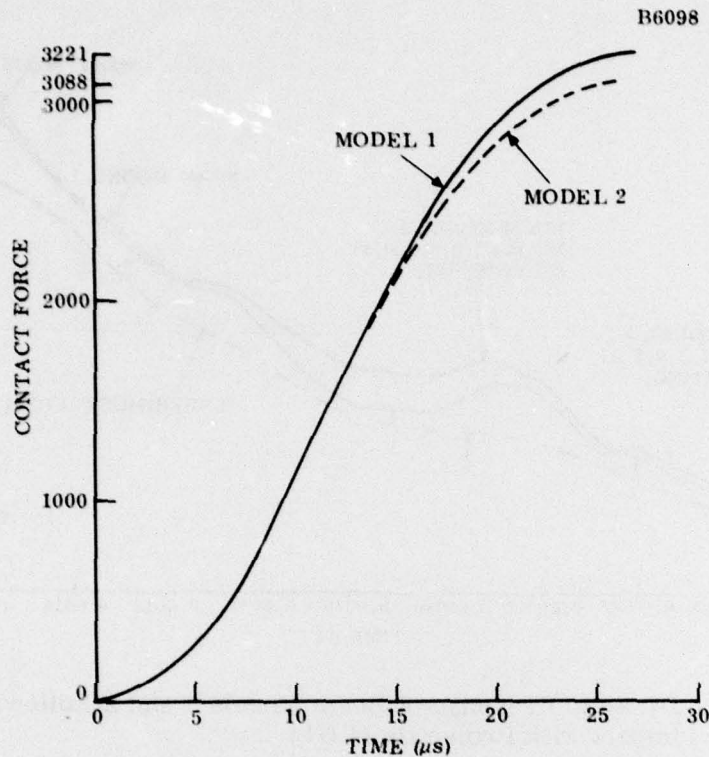
Figure 7-1. Contact Force vs a Time During Impact Loading Phase for
Beam Models 1 and 2 (Modes 1, 3, 5, 7, 9, 11)

the direction of the experimental displacement. This is expected since the
beam was subjected to a smaller impulse. The second impact at time
t = 0.0004 s was however unexpected. The actual time of second impact
from the experiment was 0.00076 s as determined from film data. One
explanation for this premature collision is that between the end of the first
impact and the start of the second the projectile is moving at a constant
velocity of 152 in./s. The actual velocity is known to be only 140 in/s.
Perhaps if a smaller time increment were used in the analysis, model 2
would be found to peak at 26.5 μs rather than 26.0 μs.
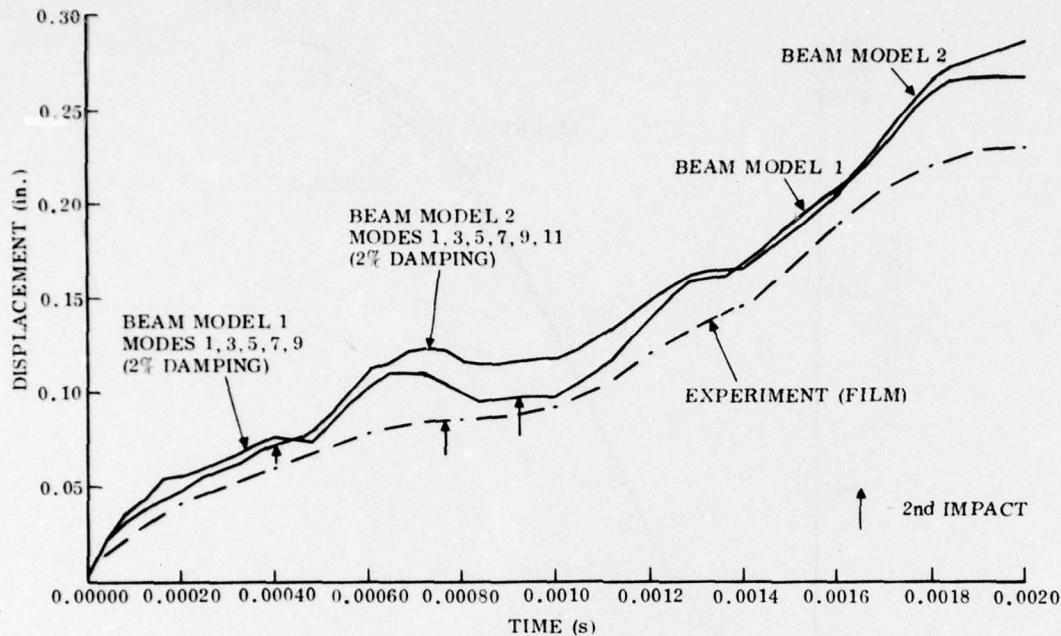
Figure 7-2. Dynamic Response of Beam Models 1 and 2 Following Initial Impact with Projectile (4 GL)

Such a change would result in slightly more energy input to the beam, a small reduction in projectile velocity and a second impact occurring at approximately 0.80 ms.

Figures 7-3 and 7-4 show the strain response for models 1 and 2 respectively. The strain profiles for the first millisecond of beam strain response were obtained from the computer output data for each model. The initial peak strain at t = 0.080 ms is 2750 microstrain for model 1 and approximately 3100 microstrain for model 2. Figure 7-5a shows the measured strain response for approximately 7.0 ms. The recorded data does give an initial data point at 2890 microstrain. The maximum strain is at least this value and probably somewhat greater. Upon further comparison of Figures 7-3 and 7-4 , with Figure 7-5a one can conclude that model 2 in

B6101

STRAIN (μ in./in.)

TIME (ms)

Figure 7-4. Beam Strain Response for Model 2
Following Initial Impact with
Projectile (4GL)

B6100

STRAIN (μ in./in.)

TIME (ms)

Figure 7-3. Beam Strain Response for Model 1
Following Initial Impact with
Projectile (4 GL)

B6102

STRAIN (μ in./in.)

TIME (ms)
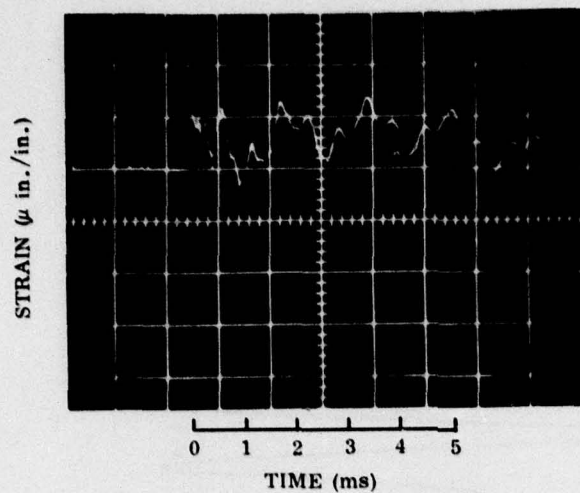
(a) Strain Response of Beam Upon Impact with Projectile (4GL)
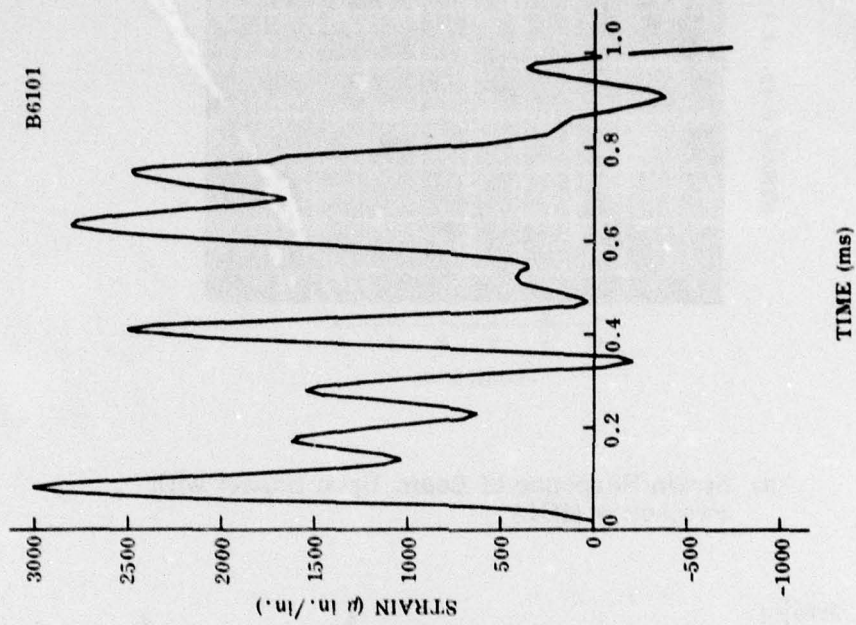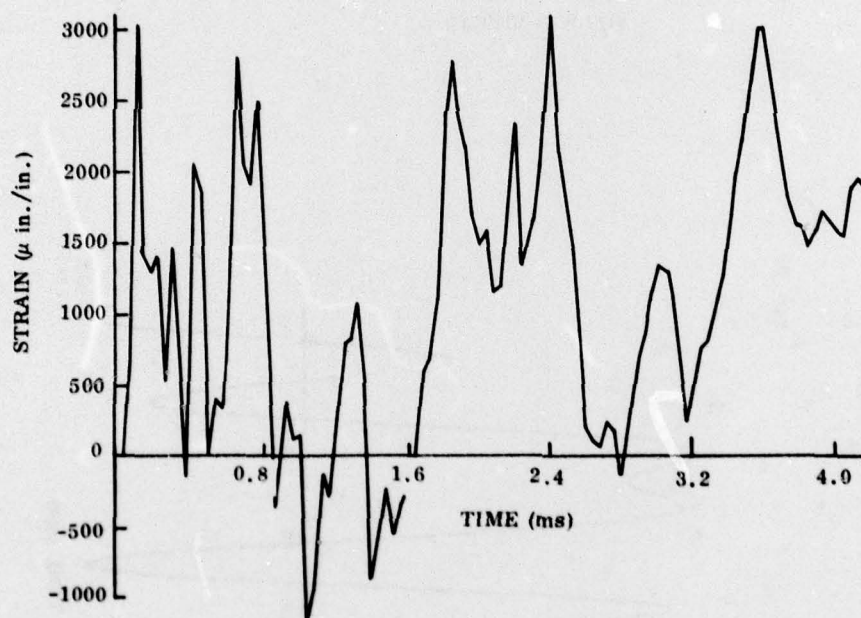

STRAIN (μ in./in.)

TIME (ms)

(b) Strain Response of Beam Model 2

Figure 7-5. Comparison of Experimental and Analytical Beam Strain Response

Figure 7-4 is in better agreement with the measured data. The addition of the 11th mode of vibration in model 2 had the effect of pulling up the -1200 microstrain value at t = 0.5 ms given for model 1. Figure 7-5b gives 4.0 ms of strain response for model 2. Comparing the general shape of the measured and computed strain, one can see good agreement. However, there is a relative increase in magnitude of the calculated peak strain values at later times. One reason for this is that strain associated with the higher frequencies of the actual beam vibration have significantly damped out, whereas model 2 does not contain frequencies greater than 8530 Hz, the 11th mode natural frequency.

At t = 3.6 ms, the time of maximum beam displacement, the strain energy associated with the first mode was 4.6 in.-lb. This value was developed and presented in Section V. The strain energy associated with the first mode for model 1 was found to be 5.28 in.-lb. This computed value is expected to be slightly greater than the actual and does appear to be in fairly good agreement. Also note that the strain energy of the first mode at the time of maximum beam displacement was 62% of the total beam energy. The 3rd and 5th modes accounted for 26% and 8%, respectively. Although the strain associated with the 7th and 9th mode was 16% of the total strain, the strain energy for these modes accounted for only 4% of the total beam energy.

The initial impulse time for representative nonfracturing high-strength rock projectiles having a mass of approximately 0.0001 lb s^2/in. and initial kinetic energy of 30 to 40 in.-lb is approximately 0.050 ms. Weak rock

projectiles, such as those from Indiana sandstone, have contact times of 0.50 ms. The corresponding maximum impact forces also vary approximately by an order of magnitude. The maximum contact force for the glass sphere 4 GL was 3220 lb while that of 6 I.S. was approximately 370 lb, both having essentially the same initial kinetic energy.

7.3 RECOMMENDATIONS FOR FUTURE WORK

A viable procedure has been developed for determining impact behavior of a rock projectile with a simply supported beam. The component element method computer program provided the means of modeling and analyzing the projectile-beam system. However, a number of changes should be made to the program to make it more suitable for rock impact problems. A scheme could be developed to change the contact spring for rebounding from the first impulse without having to evaluate initial conditions for a second computer run. In addition to having a tabulation of only separate modal displacements, a total displacement should be added at each printed time step. It would be advantageous to have the program compute strain corresponding to each mode of beam displacement as well as total displacement. A scheme should be developed so that a contact spring could handle the total resistance function for projectiles which fracture on impact.

For nonfracturing rock such as gabbro, a set of contact spring resistance functions should be developed for each shape given in the classification as shown in previous Figure 3-4. This set of resistance functions would effectively be standard design curves to be used in the computer program.

The range of projectile velocity should be extended from 1650 in./s to 2500 in./s. This can be accomplished by reducing the projectile mass and using the existing 6061T6 aluminum beam. An alternative would be to change the beam material to 7075T6 aluminum which has a higher yield strength.

The rock material used for projectiles in this investigation are representative of typical rock found throughout the country. These materials, however, may be significantly differently than those found at a particular hardened structure site. It is therefore recommended that rock borings be taken at each site location. Specifically the borings should be taken at the expected location (ground zero) of a surface burst. The sample borings can be prepared as debris projectiles and evaluated using the impact test apparatus.

SECTION VIII
SUMMARY

The subject work treated a variety of rock materials which might be expected in the form of debris fragments from crater ejecta as a result of a nuclear weapon surface burst. Regular as well as irregular shaped rocks were used in a series of impact tests. Sedimentary and igneous rocks were prepared as 1.0-in. projectiles. The sedimentary rocks included both weak and strong materials. The velocity range was controlled such that some projectiles experienced severe fracturing while others remained intact.

The experimental work was extremely valuable and provided a major part of the understanding of the impact process. High speed films of sufficient quality facilitated plotting beam displacement as a function of time. It was possible to plot 82 frames of beam displacement for one cycle of first-mode beam vibration. For projectiles which did not fracture on impact, it was possible to track their motion, detect multiple impact and determine time of second and third impact. For those which fractured it was possible to measure projectile shortening as material spalled away from the surface in contact with the beam. Strain gage time-response data revealed that each rock projectile of a given material exhibits its own unique characteristic shape or mechanical signature. The response was not significantly affected by the initial shape of the projectile.

A procedure was developed for predicting impulse, localized permanent deformation and dynamic response of a beam upon impact with both fracturing and nonfracturing rock projectiles. A finite difference computer program was used to determine the dynamic behavior of

the projectile-beam system. A six degree of freedom model was developed. One generalized coordinate described the motion of the projectile while the remaining coordinates described the motion of the first five odd modes of the beam vibration. Total beam motion was obtained by the superposition of the modal amplitudes. The projectile was connected to the beam modal masses by means of nonlinear "stop elements". These "stop elements" are essentially nonlinear springs which provide the means of modeling a contact resistance between the projectile and the beam. Resistance functions were developed for both fracturing and nonfracturing projectiles. Experimental and analytical results from computer models were compared and found to be in fairly good agreement. In general, the analytical results show beam displacement and associated strain to be approximately 15 to 20% greater than the experimental values.

APPENDIX

COMPUTER INPUT DATA

Input data, which represents the initial conditions at the moment of contact between a projectile 4GL and a 0.25 x 1.00 x 18.0 in. 6061T6 aluminum simply supported beam is presented below.

1. $ LIST/NZ = 6, DEL = 0.0000005, TTL = 0.00003,

2. TSTP = 0.0000005, ZM (1) = 0.000097, ZM (2) = 0.00058,

3. ZM (3) = 0.00058, ZM (4) ≈ 0.00058, ZM (5) = 0.00058

4. ZM (6) = 0.00058, Z DOT (1) = 854.0 $

5. $ LIST/INDX = 1, C1 = 0.007, C2 = 114, NG = 1, NC = 2, CC = -1 $

6. $ LIST/INDX = 1, C1 = 0.068, C2 = 9211, NG = 1, NC = 3, CC = -1 $

7. $ LIST/INDX = 1, C1 = 0.180, C2 = 71062, NG = 1, NC = 4,
   CC = -1 $

8. $ LIST/INDX = 1, C1 = 0.350, C2 = 273714, NG = 1, NC = 5,
   CC = -1 $

9. $ LIST/INDX = 1, C1 = 0.567, C2 = 747954, NG = 1, NC = 6,
   CC = -1 $

10. $ LIST/INDX = 3, C1 = 0.0000, C2 = 57143, NG = 6, NC = 1, 2, 3, 4,
    5, 6

11. CC = -1, 1, 1, 1, 1, 1 $

12. $ LIST/INDX = 3, C1 = 0.0035, C2 = 67857, NG = 6, NC = 1, 2, 3, 4,
    5, 6

13. CC = -1, 1, 1, 1, 1, 1 $

14. $ LIST/INDX = 3, C1 = 0.0055, C2 = 102272, NG = 6, NC = 1, 2, 3,
    4, 5, 6,

15. CC = -1, 1, 1, 1, 1, 1 $

16. $ LIST/INDX = 3, C1 = 0.0077, C2 = 53550, NG = 6, NC = 1, 2, 3,

      4, 5, 6,

17.   CC = -1, 1, 1, 1, 1, 1 $

The computer program[13] uses NAMELIST for data input. With this FOR-
TRAN option one need only input the variables required for a given problem.
For the Levy/Wilkinson program, variables are input using the name list
called LIST. Lines 1-4 give the time, generalized mass and initial conditions
at time zero.

NZ: Number of generalized coordinates.

DEL: Time step for the numerical analysis.

TTL: Total time of computer run.

TSTP: Time step for printing output data.

ZM (1): Projectile Mass

ZM (2)-(6): 1, 3, 5, 7, 9 modal mass of the beam.

Z DOT (1): Initial velocity of coordinate 1.

Lines 5-9 give the beam stiffness parameters associated with each of the five
modal masses.

INDX = 1: Identifies spring damper force element.

C1: Damping coefficient

C2: Spring constant

NG: Number of generalized coordinates acted upon by the force element.

NC: Identifies masses acted upon by force element.

CC: Coupling ratios.

---

[13]Levy, Samuel, Wilkinson, John P.D., The Component Element Method
in Dynamics, (New York: McGraw-Hill Book Co., Inc., 1976), pp. 139-147.

The damping coefficients were based on a damping factor $\zeta = 0.014$. This factor was determined from vibration decay data obtained from the 16 mm film. Decay of peak amplitude is shown in Figure 6-5. Lines 10-15 contain the parameters for each of the stop elements illustrated in Figures 6-1 and 6-4.

    INDX = 3: Identifies stop force element

        C1: Element clearance

        C2: Spring constant

    NC = 1, 2, 3, 4, 5, 6: The stop element is acted upon by the projectile mass 1, and modal masses 2 through 6.